Dissertation zur Erlangung des Doktorgrades

der Fakultät für Chemie und Pharmazie

der Ludwig-Maximilians-Universität München

Structural studies of ribosome stalling

and translocation complexes

Birgit Seidelt

aus

Strausberg

2010

TABLE OF CONTENTS

SUMMARY

In this study, cryo-electron microscopy (cryo-EM) and single particle reconstruction were used as a main technique to investigate the involvement of bacterial ribosomes in two crucial cellular processes: the regulation of gene expression and the biogenesis of membrane proteins. Whereas most nascent chains are thought to transit passively through the ribosomal exit tunnel during translation, a number of regulatory peptide sequences, such as TnaC and SecM, have been proposed to specifically interact with tunnel components, causing the ribosome to stall which in turn regulates the expression of downstream gene products. In the first part of this study, a 5.8 Å resolution cryo-EM reconstruction of an *Escherichia coli* 70S ribosome stalled during translation of the TnaC leader peptide could be determined. The high quality of the map allowed the visualization of the TnaC nascent chain within the exit tunnel of the ribosome, making contacts with ribosomal components at distinct sites. At the peptidyl transferase center (PTC), the universally conserved nucleotides A2602 and U2585 adopt conformations that are incompatible with co-habitation of the termination release factors. Moreover, a model could be proposed where interactions within the tunnel are relayed back to the PTC, leading to its inactivation. In addition, a foundation for the elucidation of the SecM-stalling mechanism could also be established.

The membrane protein insertase YidC is the prokaryotic member of the conserved YidC/Oxa1/Alb3 protein family. It assists in the assembly and folding of membrane proteins in conjunction with the Sec translocase as well as on its own. *E. coli* YidC is a hexaspan protein with a large, non-conserved periplasmic domain between the first and second transmembrane (TM) segment. In contrast, YidC2 from the Gram-positive bacterium *Streptococcus mutans* contains five TM segments and an extended C-terminal region akin to the C-terminal ribosome binding domain of the mitochondrial YidC homolog Oxa1. In the second part of this study, programmed 70S ribosomes carrying the YidC-specific nascent chain MscL could be generated, and visualized in a preliminary low-resolution cryo-EM structure in complex with *E. coli* YidC. Furthermore, purified *S. mutans* YidC2 was reconstituted into proteoliposomes and the formation of a ribosome-YidC2-proteoliposome complex could be demonstrated. Thus, the foundations have been laid for the visualization of YidC2 in the membrane environment. Improvement of the preliminary RNC-YidC structure together with determination of an RNC-YidC2 complex are expected to provide insights into the molecular mechanism of YidC mediated membrane protein biogenesis.

I INTRODUCTION

1.1 Cryo-electron microscopy and single particle reconstruction

Three-dimensional (3D) structure determination of macromolecules and macromolecular assemblies is essential for the understanding of complex biological processes, such as mRNA transcription, protein translation and folding. The dynamic nature and the large size of these macromolecular machines, as well as the involvement of multiple ligands, have made the elucidation of their structures difficult, when using conventional methods, like X-ray crystallography or nuclear magnetic resonance (NMR).

X-ray crystallography covers small molecules as well as very large assemblies. But the limiting factor, especially for dynamic multi-component complexes, is the requirement of ordered crystallization of molecules. Structure determination by NMR, on the other hand, still has size limitations of around 100 kDa (Tugarinov et al., 2005). In recent years cryo-electron microscopy (cryo-EM) in combination with single particle reconstruction turned out to be a powerful tool, providing two advantages over the other methods: There are no upper size limitations, and crystallization is not required.

Cryo-EM uses transmission electron microscopy (TEM) in order to visualize a specimen in a thin layer of vitreous ice at very low temperature (Dubochet et al., 1983; Lepault et al., 1983). Therefore, the entire molecule is in a fully hydrated state under near physiological conditions. In combination with the single particle approach, where 3D reconstructions out of two-dimensional (2D) EM images of single particles are obtained, this method is optimally suited for visualizing macromolecular machines in different functional states or with a variety of ligands bound.

The procedure of structure determination by cryo-EM and single particle reconstruction is as follows (Fig. 1.1). The first and very decisive step is the preparation of a homogeneous sample which is then placed on an electron microscope grid. In order to increase the amount of adherent specimen, the holey carbon grid should be glow discharged beforehand (Ruprecht and Nield, 2001). Excess sample is blotted away with filter paper. The specimen is then rapidly frozen by plunging the grid into a bath of liquid ethane at liquid nitrogen temperature (- 196 °C). This rapid freezing causes the water to turn into non-crystalline, vitreous ice which has properties comparable to those of liquid water (Frank, 2002). As a result of this vitrification step the single particles are embedded in a thin layer (30-100 nm) of vitreous ice in random orientation.
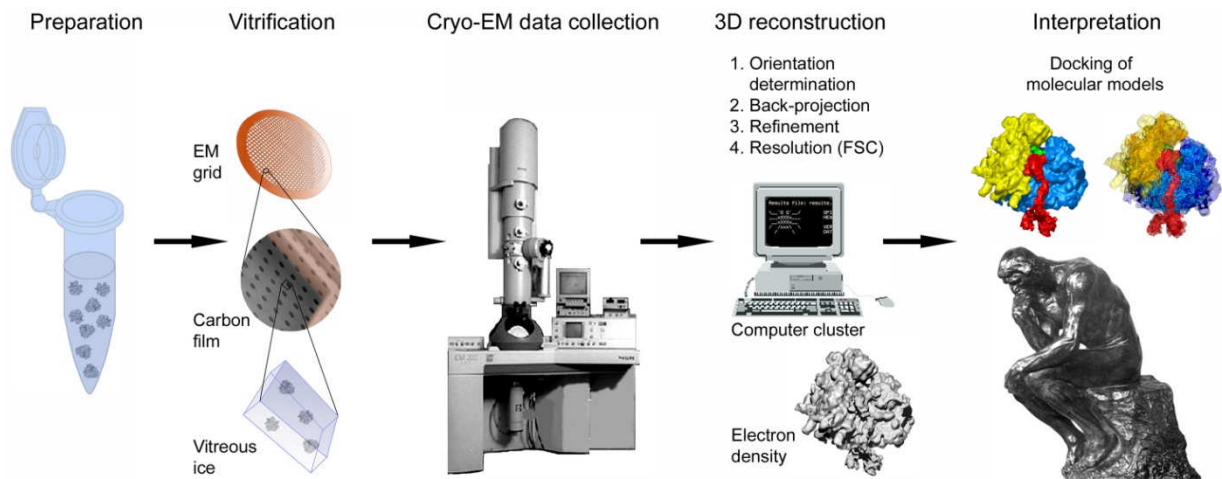
Figure 1.1: Schematic representation of structure determination by cryo-EM and single particle reconstruction. Details are described in the text (graphic by Roland Beckmann).

In the next step, data collection is carried out on a cryo-electron microscope where the grid is inserted into a stage which is kept under vacuum and cooled by liquid nitrogen. In order to reduce beam damage to the specimen, micrographs are taken under conditions in which the electron dose is minimized to approximately 10-20 electrons per $Å^2$ (Stark et al., 1996). The hence resulting low signal-to-noise ratio (SNR) in the images can be circumvented by averaging signals from many single particles. The desired area of the grid is exposed only once to the electron beam so that the final image is recorded unsighted and the quality can only be assessed after the micrograph has been taken. Since there is no contrast when the image is in focus, data are collected below the true focus of the objective lens. This leads to a distortion of the images which is described in real space by a point spread function or in reciprocal space by a contrast transfer function (CTF). In order to restore the correct structural information, the images have to be corrected for the CTF during the image-processing procedures (Saibil, 2000). Furthermore, micrographs are collected at a range of different defocus values due to the zeros in the CTF whose positions vary with the defocus, *i.e.* the distance of the specimen from the true focus.

In the next step, a 3D model of the macromolecular complex is reconstructed computationally from the 2D projection images obtained on the micrographs. Single particle reconstruction assumes that all particles embedded within the vitreous ice layer are identical but in different orientations. Therefore, one of the most important steps of the 3D reconstruction is the determination of the exact relative orientation of each particle. This process is called alignment and is performed after micrographs are digitized, quality assessed and single

particles were selected. The orientation of each particle is described by x-/ y-translation in the plane and three projection angles (Euler angles). For the determination of these parameters several methods exists. If the structure is known, at least as a first approximation, reference alignment can be performed using the so-called "projection matching" method (Penczek et al., 1994). In this approach, computationally generated projections of a previously obtained structure, used as reference, are compared with the actual electron microscopy images. On the other hand, if the structure of the molecule is unknown, two *ab initio* methods can be used for orientation determination. (a) In the "random conical tilt" approach pairs of micrographs of a tilted and a non-tilted specimen are used to assess the geometrical relation between particles which reside on the grid in the same orientation (Radermacher et al., 1986). (b) The "common line" method is based on the central projection theorem which states that in reciprocal space two 2D projections of the same 3D object share a common line (Crowther, 1971; Penczek et al., 1996). These common lines can be located and used for computations of the relative orientations between those two particles.

Following orientation determination, all of these individual 2D projection images are combined in order to reconstruct the first 3D structure by a process called back-projection. This first reconstruction serves then as a new reference for the next round of alignment which is now performed using the projection matching method. The iterative cycle of alignment and back-projection is called refinement. Refinement continues until the orientation parameters are determined accurately or until no further improvement in the 3D structure is observed.

In order to assess the resolution of the computed 3D model, the Fourier shell correlation (FSC) between two independent 3D reconstructions is measured (van Heel and Schatz, 2005). Therefore, the dataset is randomly divided into two halves. The FSC measures the degree of similarity between the two resulting reconstructions as a function of spatial frequency in reciprocal space. The most commonly used criterion for determining the resolution is to take the reciprocal of the spatial frequency when the correlation coefficient equals 0.5. This cutoff-value corresponds to a SNR of 1. Another, more optimistic criterion is the so-called 3σ threshold criterion. Here, the resolution is determined by taking the reciprocal of the spatial frequency at the intersection of the FSC function with the 3σ curve which represents three times the standard deviation of random noise.

In the last step, structural interpretation of the obtained 3D reconstruction is performed in order to answer specific biological questions. An efficient approach is to place available atomic structures (X-ray- or NMR-structures) or molecular models of individual components into the cryo-EM density of multi-component complexes. Therefore, a medium-resolution

cryo-EM reconstruction can be interpreted at the molecular level, exceeding the experimental obtained resolution manifold.

1.2 Structure and function of the prokaryotic ribosome

The ribosome is a macromolecular machine that is responsible for the synthesis of proteins in all living cells. It consists of two ribonucleoprotein subunits which work together to translate the information that is encoded in the messenger RNA (mRNA) into specific proteins.

Back in 1955, George Palade obtained the first negatively stained images of ribosomes in the cell. Therefore, ribosomes were initially called Palade particles (Palade, 1955). The term "ribosomes" was finally coined by Dick Roberts for "ribonucleoprotein particles in the size range 20 to 100S" (Roberts, 1958). 20 years later, the overall shape of the ribosome could be determined by electron microscopy (Lake and Kahan, 1975). Owing to the rapid progress in ribosome biochemistry and macromolecular crystallography, complete atomic-resolution structures for both subunits of archaeal and bacterial ribosomes were solved in 2000 (Ban et al., 2000; Schluenzen et al., 2000; Wimberly et al., 2000). These crystal structures as well as the first structure of the complete 70S ribosome (Yusupov et al., 2001) were the beginning of revolutionizing the understanding of the structural basis for ribosomal function.

In prokaryotes, the ribosome has a molecular weight of approximately 2.5 MDa with approximately two-thirds of the mass consisting of ribosomal RNA (rRNA) and one-third of ribosomal proteins. The larger of the two subunits sediments at 50S and comprises two rRNA molecules (the ~2900 nucleotides long 23S rRNA and the 120 residues long 5S rRNA) and 34 ribosomal proteins. The smaller subunit sediments at 30S and contains a single rRNA strain (the ~1500 nucleotides long 16S rRNA) as well as 21 ribosomal proteins (Erlacher and Polacek, 2008).

Each subunit has three binding sites for transfer RNA (tRNA) molecules that are in three different functional states: an A-site which is responsible for the recognition of aminoacyl-tRNAs (aa-tRNAs), a P-site that binds peptidyl-tRNAs and an E (exit)-site which holds the deacylated tRNA before it dissociates from the ribosome. Both subunits perform different functions during protein synthesis. The 30S ribosomal subunit contains the decoding center and mediates the correct base pairing between anticodons of the aa-tRNAs and codons in the mRNA which determine the order of the amino acids of the growing peptide chain. The 50S ribosomal subunit contains the peptidyl transferase center (PTC), which catalyzes peptide

bond formation between the incoming amino acid on A-site tRNA and the nascent peptide chain attached to the P-site tRNA.

1.2.1 Protein synthesis

The synthesis of proteins involves initiation, elongation and termination steps. In each of these steps additional protein factors are required, many of which are GTPases activated by the ribosome itself.

During initiation, a complex composed of the 30S ribosomal subunit and an initiator tRNA binds the initiation codon (AUG) of an mRNA. This ternary complex then associates with the large ribosomal subunit to form an initiation complex of translation. The three initiation factors IF1, IF2 and IF3 are involved in this process (reviewed in (Gualerzi and Pon, 1990)). At the end of the initiation step, an aminoacylated initiator tRNA resides in the P-site of the ribosome and the A-site is empty.
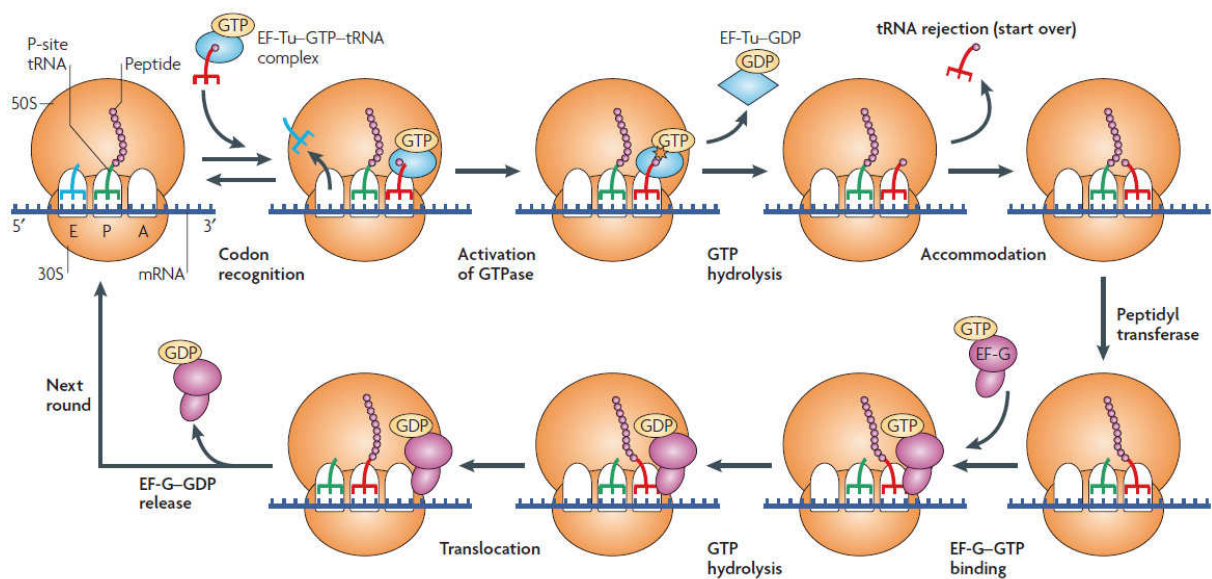
Figure 1.2: Schematic overview of the elongation cycle of protein synthesis. An incoming tRNA in complex with elongation factor (EF)-Tu-GTP is delivered to the A-site. Correct codon-anticodon pairing leads to GTP hydrolysis and release of the aminoacyl end of the tRNA from EF-Tu. It also induces conformational changes in ribosomal RNA that optimally orientates the peptidyl-tRNA and aminoacyl-tRNA for the peptidyl-transferase reaction which involves the transfer of the peptide chain onto the A-site tRNA. In the following step the ribosome shifts in the 3' mRNA direction so that it can decode the next mRNA codon. This translocation is facilitated by the GTPase EF-G, which after GTP hydrolysis causes the deacylated tRNA at the P-site to move to the E-site and the peptidyl-tRNA at the A-site to move to the P-site. The deacylated tRNA in the E-site is released when the next aminoacyl-tRNA reaches the A-site for the next round of elongation. Elongation finally ends when a stop codon appears in the A-site of the decoding center (Steitz, 2008).

The elongation cycle of protein synthesis (Fig. 1.2) starts with the delivery of the correct aa-tRNA to the A-site of the ribosome in a ternary complex with elongation factor Tu (EF-Tu) and GTP. Correct codon-anticodon interactions induce conformational changes in the ribosome which stabilize tRNA binding and promote GTP hydrolysis by EF-Tu. This causes the release of EF-Tu from the tRNA and ribosome so that the aminoacyl end of A-site tRNA swings into the PTC in a process called accommodation (Ramakrishnan, 2002). Peptide bond formation, where aa-tRNA in the A-site reacts with peptidyl-tRNA bound to the P-site, then followes rapidly. Consequently, the ribosome has a deacylated tRNA in the P-site and an A-site peptidyl tRNA that is extended by one amino acid. The subsequent movement of the tRNAs and associated mRNA from their positions in the A-site and P-site to the P-site and E-site, respectively, is facilitated by the elongation factor G (EF-G), a GTPase. As a result of this movement, which is called translocation, the ribosome is ready for the next round of elongation, with deacylated tRNA in the E-site, peptidyl-tRNA in the P-site and an empty A-site where a new codon is exposed for the interaction with the next ternary complex.

Termination of translation occurs when one of the three stop codons (UAA, UAG or UGA) reaches the A-site in the decoding center of the small ribosomal subunit. In contrast to sense codons, which are decoded by aa-tRNAs, stop codons are recognized by class I release factor proteins (RF). In bacteria, there are two such factors with overlapping codon specificity: RF1 recognizes UAG, whereas RF2 is specific for UGA, but both factors recognize UAA (Scolnick et al., 1968; Youngman et al., 2008). Upon stop codon recognition, class I RFs promote the hydrolysis and the release of the completed polypeptide chain from the P-site tRNA. This functions as a signal to recruit class II RFs (RF3 in bacteria), which accelerate the dissociation of class I RFs from the ribosome once the peptide release reaction is complete (Youngman et al., 2008). Consequently, the ribosome is left with mRNA and a deacylated tRNA in the P-site. In order to prepare the ribosome for a new round of protein synthesis, this complex needs to be disassembled. Therefore, the ribosome recycling factor (RRF) binds together with EF-G to the complex which leads after GTP hydrolysis to the dissociation of the ribosome into subunits (Karimi et al., 1999). Furthermore, initiation factor IF3 is required for removal of the deacylated tRNA from the P-site (Ramakrishnan, 2002).

1.2.2 The ribosomal peptidyl transferase center

The ribosomal peptidyl transferase center is part of the large ribosomal subunit and is located at the bottom of a deep cleft at the interface side of the large subunit underneath the central

protuberance (Ban et al., 2000; Harms et al., 2001). The peptidyl transferase cavity is densely packed and decorated with universally conserved nucleotides of the central loop of domain V of 23S rRNA. The high-resolution crystal structure of the 50S subunit from the archaeon *Haloarcula marismortui* revealed that protein side chains from ribosomal proteins are absent within a radius of approximately 18 Å of the active center (Nissen et al., 2000). This finally confirmed the peptidyl transferase as an ribozyme (Doudna and Cech, 2002).

The inner core of the PTC is comprised of the universally conserved nucleotides C2063, A2451, U2506, U2585 and A2602 of 23S rRNA. In the case of a non-translating large ribosomal subunit, the cavity is empty except for the bases of nucleotides A2602 and U2585, which bulge into its center (Polacek and Mankin, 2005). The orientation of these two flexible residues can vary depending on the functional state of the ribosome and the nature of the bound substrate. The acceptor arms of A- and P-site tRNA substrates reach deep into the cleft of the 50S ribosomal subunit on the side facing the 30S subunit. Their universally conserved CCA ends are locked in a proper orientation by forming Watson-Crick interactions with 23S rRNA nucleotides (Yusupov et al., 2001). Although the PTC is composed of RNA only, long "tails" of ribosomal proteins L2, L3, L4 and L16, as well as the flexible N-terminus of protein L27 are quite close to the PTC (Nissen et al., 2000). Since it was shown that at least two of them (L2 and L3) are essential for the peptidyl transferase activity (Hampl et al., 1981; Khaitovich et al., 1999), these long, positively charged extensions may serve to hold together the rRNA components of the PTC (Nissen et al., 2000).

The PTC is the catalytic center of the ribosome. Its primary function is to covalently link amino acids via peptide bonds into polypeptide chains through the proper alignment of the reaction components. During peptidyl transferase reaction, the nucleophilic α-amino group of the aa-tRNA in the A-site attacks the carbonyl carbon of the P-site bound peptidyl-tRNA (Fig. 1.3). As a result, the peptidyl-tRNA at the A-site is elongated by one amino acid whereas the tRNA at the P-site is deacylated. Peptide bond formation is precisely catalyzed by the ribosome with a speed of ~ 15 to 50 peptide bonds per second (Katunin et al., 2002).

The second principal chemical reaction of the PTC is peptidyl-tRNA hydrolysis, which is required for the release of the fully assembled polypeptide from the ribosome during termination of translation. In this reaction, an activated water molecule attacks the ester carbonyl carbon of P-site tRNA which leads to the transfer of the nascent peptide to the water molecule (Fig. 1.3). Since water is a relatively weak nucleophile the catalytic rate constant of peptide release has been estimated to 0.5 to 1.5 per second (Zavialov et al., 2002), which is clearly slower than peptide bond formation.
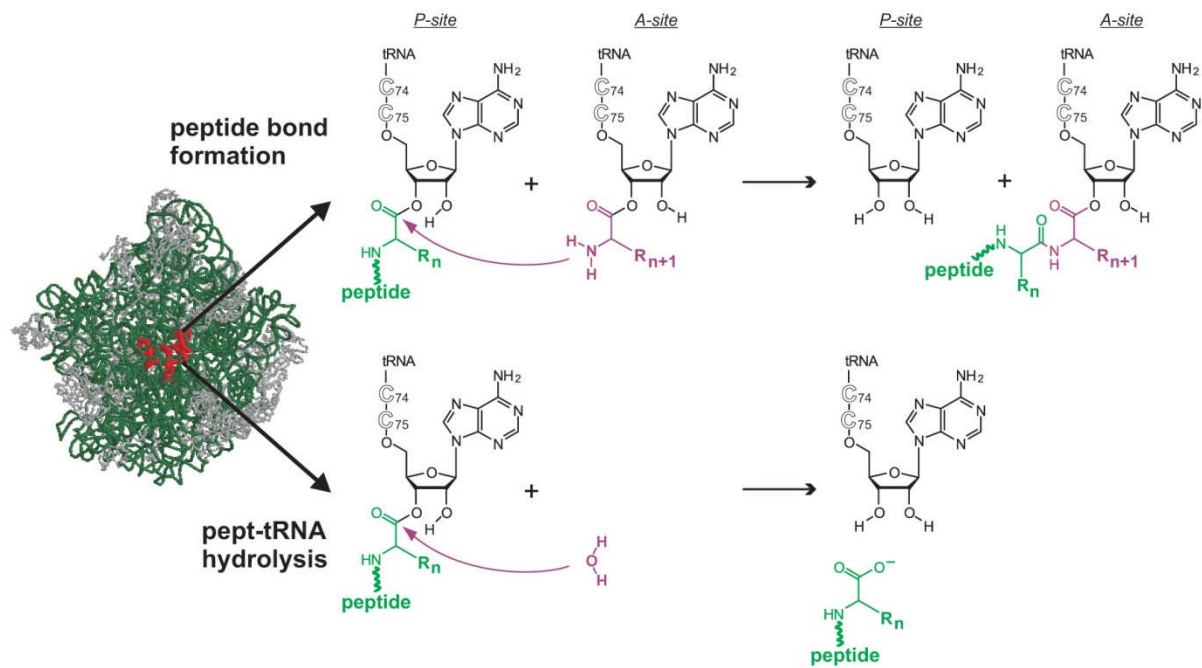
Figure 1.3: The two principal chemical reactions of protein synthesis: peptide bond formation and peptide release. The ribosomal PTC is composed of highly conserved nucleotides of domain V (red) of 23S rRNA (dark green). Ribosomal proteins are shown in grey. During peptide bond formation, the α-amino group of aminoacyl-tRNA in the A-site (purple) attacks the carbonyl carbon of P-site bound peptidyl-tRNA (green). As a result, the tRNA at the P-site is deacylated and the peptidyl-tRNA at the A-site is elongated by one amino acid. During translation termination, the nascent peptide (green) of P-site tRNA is transferred to an activated water molecule (purple) which leads to peptidyl-tRNA hydrolysis and peptide release (Erlacher and Polacek, 2008).

The switch of the PTC from peptide bond formation to peptidyl-tRNA hydrolysis is triggered by the binding of class I RFs to the ribosomal A-site in response to the presence of a stop codon in the decoding center. Thereby, it has been suggested that the nucleotide A2602 plays an important role in the regulation of the PTC activity (Erlacher and Polacek, 2008).

1.2.3 The ribosomal peptide exit tunnel

After peptide bond formation in the PTC, the nascent polypeptide chain leaves the ribosome via the ribosomal polypeptide exit tunnel, which spans the entire large subunit of the ribosome. In 1982, Unwin and coworkers first observed a tunnel-like feature in EM images (Milligan and Unwin, 1982). About the same time, it was reported that nascent peptides first become accessible to antibodies on the exit site of the large ribosomal subunit, roughly 100 Å away from the subunit interface (Bernabeu and Lake, 1982). This observation suggested that the large ribosomal subunit might contain an internal tunnel which connects the PTC to the

site where polypeptides emerge. The existence of such an exit tunnel was then finally confirmed by cryo-EM in 1995 (Frank et al., 1995).

The ribosomal peptide exit tunnel shows the same size and shape in isolated 50S subunits as well as in assembled 70S ribosomes at different functional states (Voss et al., 2006). It is an unbranched tube with a length of 80-100 Å and a diameter of around 10 Å at its narrowest and 20 Å at its widest part (Kramer et al., 2009). The tunnel can accommodate peptides up to 30 amino acids in extended conformation or, assuming that formation of secondary structure is possible, up to 60 amino acids in α-helical conformation (Malkin and Rich, 1967; Picking et al., 1992; Voss et al., 2006). The tunnel wall, which is formed predominantly by 23S rRNA, has a nonsticking Teflon-like character: its surface largely consists of hydrophilic noncharged groups (Nissen et al., 2000). Only 18% are nonglobular parts of the ribosomal proteins L4, L22 and L23, which protrude into the tunnel lumen. Approximately 30 Å from the PTC, there is a pronounced constriction. At this narrowest part of the tunnel, a conserved β-hairpin loop of L22 comes into close proximity to an extended loop of L4.

In some electron microscopy reconstructions of the ribosome, the tunnel appears to branch near its exit end (Gabashvili et al., 2001). This has led to the proposal that nascent peptides might leave the ribosome by two different routes, one used by membrane proteins and the other by cytoplasmic proteins. However, a detailed analysis of the tunnel using the crystal structure of the large ribosomal subunit from *Haloarcula marismortui* shows that there is only one tunnel that is large enough to accommodate polypeptide chains (Voss et al., 2006). In fact, it was found that ribosomal protein occupies the space assigned to the proposed branch. By contrast, water and other small molecules can diffuse into and out of the tunnel along many different interconnected channels which permeate the entire structure of the large ribosomal subunit.

Since the existence of the tunnel was known, people have speculated about the conformation adapted by nascent chains as they pass through the tunnel. Several studies, including protease digestion (Malkin and Rich, 1967), Förster resonance energy transfer (FRET) (Woolhead et al., 2004) and PEGylation experiments (Lu and Deutsch, 2005), support the view that nascent peptides can adopt α-helical conformation within the tunnel. While similar studies propose that even tertiary folding might occur within the last 20 Å of the tunnel, where it widens up (Kosolapov and Deutsch, 2009), other analysis strongly suggest that protein folding beyond the level of an α-helix is extremely unlikely (Bhushan et al., 2010; Steitz, 2008).

1.3 Translational stalling in prokaryotes

Most nascent chains are thought to transit passively through the exit tunnel when they emerge from the PTC. However, recent results indicate that some nascent peptides establish specific interactions with tunnel components which might affect the rate of translation (Lu and Deutsch, 2008) or even induce translational stalling. Such sequence-specific interactions between the exit tunnel and nascent chains assume that the ribosome can recognize amino acid sequences of nascent peptides. The feedback modulation of ribosome activity allows the regulation of expression of genes engaged in different cell functions, such as secretion (Nakatogawa and Ito, 2002), amino acid metabolism (Gong and Yanofsky, 2002a) or antibiotic resistance (Weisblum, 1995). In most cases, the regulation of gene expression involves nascent chain-dependent ribosome stalling. However, the ribosome stalling of a number of inducible antibiotic resistance genes is additionally dependent on the presence of a protein synthesis inhibitor (Ramu et al., 2009).

The inducible expression of the erythromycin resistance genes was the first described example of drug-dependent ribosome stalling (Gryczan et al., 1980; Horinouchi and Weisblum, 1980). The *ermC* cassette is often found in antibiotic resistant pathogens. It consists of the resistance methyltransferase gene (*ermC*) which is preceded by a 19-codon open reading frame (ORF) encoding the regulatory leader peptide ErmCL. In the absence of an inducing antibiotic, *ermC* expression is repressed because its ribosome binding site is coverted in a stem-loop structure of the mRNA. Sub-lethal concentrations of erythromycin or similar macrolide antibiotics bind in the peptide exit tunnel near the PTC and cause the ribosome to stall at the ninth codon of the *ermCL* ORF (Vazquez-Laslop et al., 2008). This promotes a conformational change in the mRNA that exposes the *ermC* ribosome binding site, and thus activates the expression of the resistance methyltransferase gene (Horinouchi and Weisblum, 1980; Narayanan and Dubnau, 1985).

The two best-characterized examples of nascent chain-dependent ribosome stalling in prokaryotes however, are those that control the expression of the *tryptophanase* (*tna*) and *secretion* (*sec*) operons.

1.3.1 Ribosome stalling on the TnaC nascent peptide

The *tna* degradative operon of *Escherichia coli* (*E. coli*) contains two major structural genes, the promoter proximal gene, *tnaA*, and a distal gene, *tnaB* (Deeley and Yanofsky, 1981;

Edwards and Yudkin, 1982). *tnaA* encodes the enzyme tryptophanase, which catalyze the degradation of tryptophan (Trp) to indole, pyruvate, and ammonia by a reversible reaction. The pyruvate and ammonia provide sources of carbon and nitrogen, and the indole has been shown to serve as a signaling compound in quorum sensing (cell-to-cell communication), and biofilm formation (Ren et al., 2004; Winzer et al., 2002). *tnaB* encodes a low-affinity, high-capacity, Trp-specific permease that transports this amino acid into the cell (Deeley and Yanofsky, 1981). The leader transcript of this operon, which precedes the two structural genes, contains three segments: a coding region for a 24-residue leader peptide, TnaC; followed by a RNA *Rho utilization* (*rut*) binding site for the termination factor Rho; and RNA pause sites (Stewart and Yanofsky, 1985).

1) Termination in the absence of inducing levels of Trp

mRNA — AUG — UGG — boxA — UGArut — ATP → ADP+Pi — Rho — RNAP — DNA template

30S — 50S — TnaC — Ribosome releases — Pause structure — **Termination**
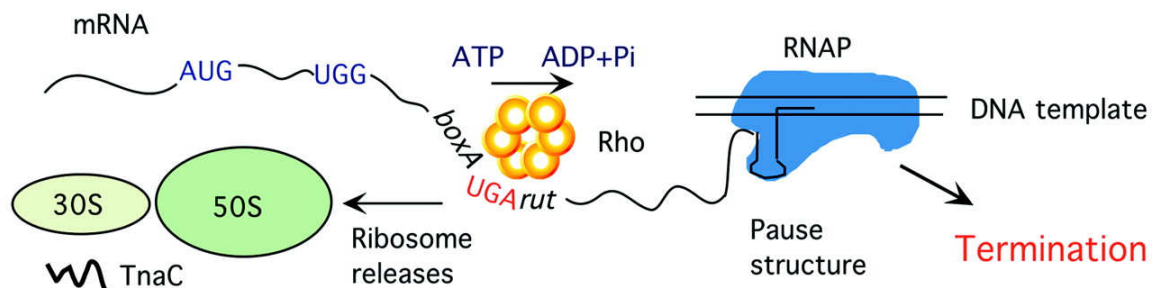
2) Antitermination in the presence of inducing levels of Trp

TnaC-tRNA — Trp — mRNA — AUG — UGG — UGA — Ribosome stalls at UGA codon — Rho — RNAP — DNA template — **Transcription**
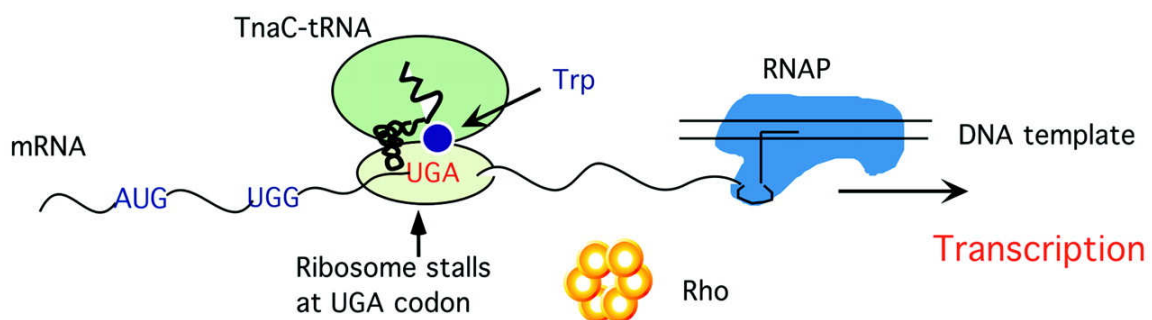
Figure 1.4: Model for *tna* operon regulation in *E. coli*. (1) In the absence of inducing levels of Trp, the translating ribosome reaches the TnaC stop codon, and RF2 promotes the hydrolysis of TnaC-tRNA[Pro]. The ribosome is released, so that the Rho factor has access to its *rut* binding site, contacts a paused polymerase, and causes transcription termination. (2) In the presence of inducing levels of Trp, the free Trp binds to the ribosome and prevents normal termination of TnaC-peptide synthesis. Therefore, the ribosome stalls at the UGA stop codon and blocks the access of Rho to its *rut* binding site. Transcription termination is thereby prevented, and RNA polymerase continues transcription into the *tnaA* and *tnaB* coding region (Gong and Yanofsky, 2002b).

Transcription of the *tna* operon of *E. coli* is regulated by two mechanisms: While the initiation of transcription is regulated by catabolite repression, its continuation into the two

structural genes depends on tryptophan-induced transcription antitermination, *i.e.* preventing Rho factor from terminating the transcription (Botsford and DeMoss, 1971; Gong and Yanofsky, 2001; Stewart et al., 1986). In the presence of inducing levels of Trp (Fig. 1.4), the free Trp binds to the translating ribosome and inhibits RF2-promoted cleavage of the nascent TnaC-peptidyl-tRNA, TnaC-tRNA^{Pro}, at its UGA stop codon (Gong and Yanofsky, 2002b). Thus, TnaC-tRNA^{Pro} remains within the ribosome, resulting in ribosome stalling on the leader transcript. The stalled TnaC-70S complex temporarily blocks Rho factor's access to its *rut* binding site and prevents Rho-catalyzed transcription termination in the leader region of the operon. Therefore, transcription continues into the *tnaA* and *tnaB* structural genes (Stewart and Yanofsky, 1985), ultimately leading to the removal of excessive Trp from the cytoplasm. In the case of non-inducing levels of Trp (Fig. 1.4), the ribosome completes the synthesis of the leader peptide TnaC, the TnaC-peptidyl-tRNA is cleaved, and the translating ribosome is released. The *rut* site is then accessible for the Rho factor, which binds and contacts the paused polymerase, resulting in termination of transcription (Yanofsky, 2007).

Several features of the amino acid sequence of the TnaC nascent peptide have been identified to be important for ribosome stalling. These include the crucial tryptophan residue, located at position 12 (Trp^{12}), an aspartic residue, located at position 16 (Asp^{16}), the last amino acid in the TnaC peptide, proline at position 24 (Pro^{24}), as well as the spacing between Trp^{12} and Pro^{24} (Cruz-Vera et al., 2005; Cruz-Vera et al., 2007). Notably, all of these residues are highly conserved among predicted TnaC amino acid sequences from various bacterial species (Cruz-Vera and Yanofsky, 2008). Since the Pro^{24} of TnaC-tRNA^{Pro} is located within the P-site of the stalled complex (Gong et al., 2001), Asp^{16} and Trp^{12} are retained within the ribosomal exit tunnel.

Moreover, specific nucleotides and amino acids that form the peptide exit tunnel in the 50S ribosomal subunit have also been identified to be required for Trp-induced transcription antitermination. These include the lysine residue at position 90 (Lys^{90}) of ribosomal protein L22, the 23S rRNA segment between nucleotides 749-752, as well as the 23S rRNA nucleotide U2609 (Cruz-Vera et al., 2005). Since mutations of these ribosomal residues reduced or eliminated Trp binding to the ribosome, it has been suggested that interaction between the TnaC nascent chain and ribosomal tunnel components contribute in creating a free Trp binding site, possibly at the PTC (Cruz-Vera et al., 2007). There, the bound Trp presumably inhibits RF2 action, preventing cleavage of the nascent TnaC-tRNA^{Pro}. In addition, bound Trp has also been shown to inhibit the activity of some antibiotics, such as puromycin, an analog of RF2 function, and sparsomycin, a peptidyl transferase inhibitor,

suggesting that Trp acts at the PTC (Cruz-Vera et al., 2006; Cruz-Vera et al., 2005; Gong et al., 2001).

Recently, specific nucleotides within the ribosomal PTC were identified which also appear to be essential for Trp-induced transcription antitermination. These include replacements of 23S rRNA nucleotides in the U2585 region, specifically changes from G2583 to A2583 and U2584 to C2584, which were observed to reduce the maximum induction of *tna* operon expression by Trp *in vivo* (Yang et al., 2009).

Under Trp induction conditions TnaC-tRNA^{Pro} has a half-life of approximately 8 min (Gong et al., 2007). Therefore, cells must be capable of rescuing ribosomes from TnaC-stalled ribosome complexes via some mechanism of TnaC-peptidyl-tRNA cleavage and ribosome recycling. Gong and coworkers found out that both RRF and RF3 bind to TnaC-stalled ribosomes and cause the release of uncleaved peptidyl-tRNA by a common phenomenon called peptidyl-tRNA drop-off (Gong et al., 2007; Menninger, 1976). The drop-off TnaC-tRNA^{Pro} is then cleaved by peptidyl-tRNA hydrolase (Pth), separating the peptide from its tRNA (Gong et al., 2007; Kossel, 1970). Finally, RRF and RF3 promote ribosome recycling, so that the ribosomal subunits become available for new rounds of protein synthesis.

1.3.2 Ribosome stalling on the SecM nascent peptide

Another example of nascent chain-dependent ribosome stalling in prokaryotes is the secretion monitor (SecM) protein in *E. coli* that regulates the translation of the downstream *secA* gene in response to the secretion status of the cell (Oliver et al., 1998).

The *secA* gene encodes the protein-translocating ATPase, that drives the movement of secretory polypeptides into and across the bacterial plasma membrane along the Sec pathway (see Section 1.4). The expression of SecA is modulated according to the cell's ability to export proteins. Under conditions of excess protein secretion capacity SecA translation is repressed, whereas under conditions of limited protein secretion its translation is up-regulated (Oliver et al., 1998; Oliver and Beckwith, 1982). It was shown that the translation of SecA is modulated by multiple mechanisms (Oliver et al., 1998). First, the basal *secA* expression is translationally coupled with the translation of the upstream *secM* gene in the same transcription unit (Schmidt et al., 1988) in which the translation initiation Shine-Dalgarno (SD) sequence for *secA* is normally occluded in a mRNA stem-loop structure (McNicholas et al., 1997). Second, SecA may also act as an autogenous repressor of its own translation during

normal protein secretion (Schmidt and Oliver, 1989). Finally, the export status of SecM affects translation of *secA* in a *cis*-specific manner (Oliver et al., 1998).

The mature 170 amino acid protein SecM is exported to the periplasm where it is rapidly degraded by periplasmic proteases (Prc) such as the tail-specific protease (Nakatogawa and Ito, 2001). Despite its translocation to the periplasm, SecM executes its biological role only as a nascent polypeptide with its C-terminal region still embedded in the ribosome. In fact, translation of SecM undergoes elongation arrest at the proline residue at position 166 (Pro[166]), five codons upstream of the *secM* termination point, leading to an accumulation of SecM-peptidyl-tRNA (Nakatogawa and Ito, 2001; Nakatogawa and Ito, 2002).
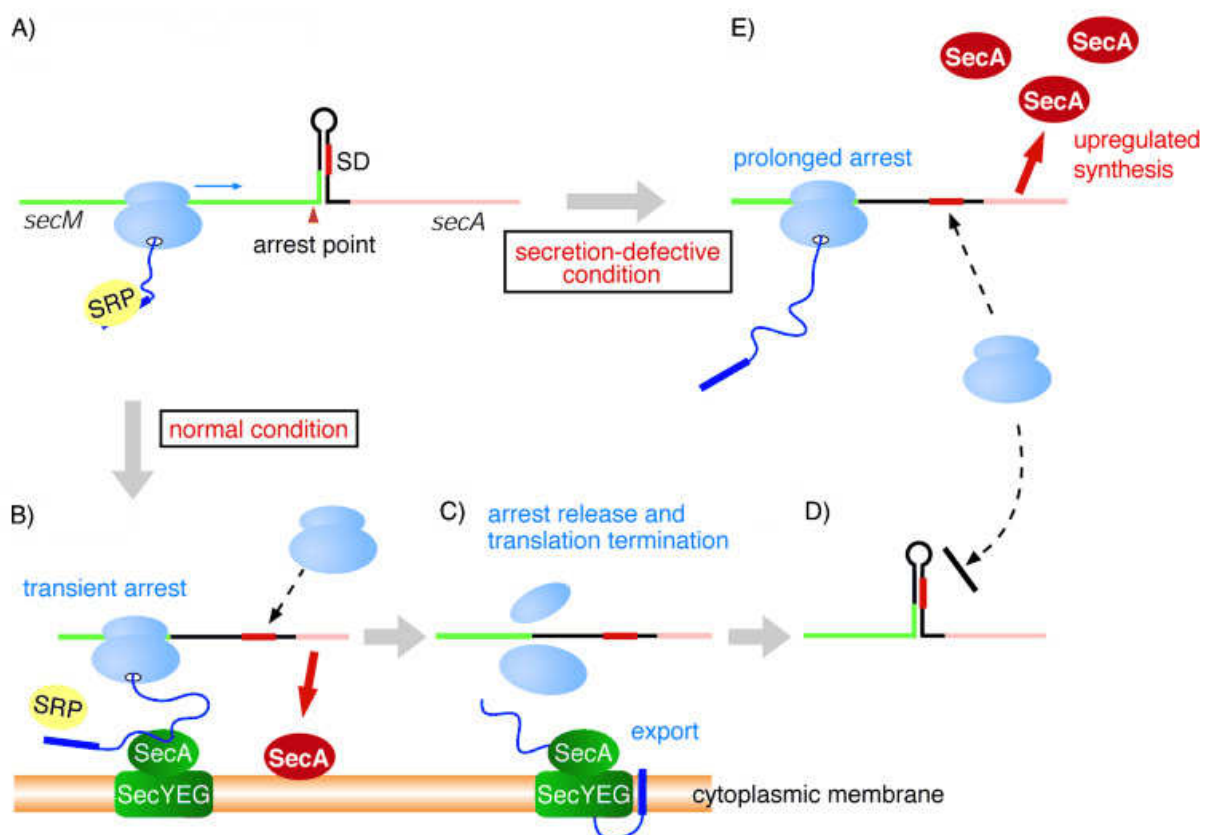
Figure 1.5: Model for SecM regulation of *secA* expression in response to the secretion status of the cell. (**A**) *secM* (green) and *secA* (pink) are cotranscribed into the *secM-secA* mRNA, in which the Shine-Dalgarno (SD) sequence for *secA* translation (red) is sequestered in a stem-loop structure. A stalled ribosome at the arrest point in *secM* will expose the SD sequence (shown in E). (**B**) Under normal conditions, SecM is cotranslationally targeted to the Sec machinery (dark green) by the signal recognition particle (SRP, yellow), which also brings the *secM-secA* mRNA into the vicinity of the Sec machinery. Thus, newly synthesized SecA (red) can readily adopt an active form. (**C**) Elongation arrest is cancelled by ongoing secretion, and translation terminates at the stop codon. (**D**) The stem-loop is reformed, which completes a normal cycle of SecA translation. (**E**) Under secretion-impaired conditions, SecM elongation arrest is prolonged, resulting in extended exposure of the SD sequence and therefore, leading to a higher *secA* translation initiation frequency (Nakatogawa and Ito, 2004).

Under secretion-proficient cellular conditions (Fig 1.5), the SecM elongation arrest is only transient, and SecM is released when the N-terminal region of the nascent chain interacts with the Sec protein export machinery. One possibility for the explanation of this arrest cancellation may be a "pulling" mechanism, in which the force generated by the Sec translocation machinery dissociates the SecM arrest sequence from the tunnel wall. Alternatively, the interaction of the ribosome-Sec machinery may induce a conformational change in the tunnel (Nakatogawa et al., 2004). Nevertheless, the transient ribosome stalling destabilizes the secondary structure in the *secM-secA* mRNA, thereby exposing the SD sequence and facilitating the synthesis of a basal level of SecA (Butkus et al., 2003; Nakatogawa and Ito, 2001). In contrast, under secretion-impaired conditions (Fig. 1.5), the elongation arrest is prolonged, which increases the exposure of the SecA SD sequence and consequently leads to an overproduction of the protein (Nakatogawa and Ito, 2001). Therefore, SecM elongation arrest is essential for the basal level expression of SecA as well as its up-regulation in response to a secretion defect (Murakami et al., 2004). In this way, SecM monitors protein translocation activity of the cell and accordingly modulates the translation frequency of *secA* (Oliver et al., 1998).

Detailed mutation studies showed that the 17 amino acid long SecM sequence ^{150}FXXXXWIXXXXGIRAGP^{166}, in which X can be any amino acid, is required and sufficient to cause translation arrest during elongation (Nakatogawa and Ito, 2002). The arrest motif is well conserved among SecM homologs that are known to exist at least in three other bacterial species (Sarker et al., 2000). It has been shown that the stalling sequence also works as an independent translation-arresting element even if present in an unrelated sequence (Nakatogawa and Ito, 2002). Toeprint analyses revealed that the critical Pro^{166} is not incorporated into the SecM nascent chain, but is positioned at the A-site when the ribosome stalls (Muto et al., 2006). Therefore, the nascent peptide is attached to tRNA^{Gly} located in the ribosomal P-site. The simultaneous presence of peptidyl-tRNA^{Gly} in the P-site and Pro-tRNA^{Pro} in the A-site of the stalled ribosome indicates that the stalling is caused by the inability of the PTC to catalyze formation of the Gly^{165}-Pro^{166} peptide bond (Muto et al., 2006). This inhibition of the PTC function is completely contrary to the ribosome stalling on the TnaC nascent peptide where the hydrolytic activity of the PTC is modulated.

Genetic studies indicate that the arrest sequence of SecM interacts with specific ribosomal components which are located close to the narrowest constriction of the exit tunnel. In fact, mutations of the nucleotides A2058 and A749-A753 of the 23S rRNA as well as mutations of two specific residues of the ribosomal protein L22, Gly^{91} and Ala^{93}, were shown to relieve the

stalling effect of the SecM nascent peptide (Nakatogawa and Ito, 2002). Furthermore, FRET results suggested that the SecM stalling sequence adopts a compact, rather than extended conformation in the exit tunnel (Woolhead et al., 2006). This is likely to be required for engaging sensory elements of the tunnel, since some sort of signal must be propagated to the PTC in order to modulate its function (Muto et al., 2006). Based on cryo-EM data, Mitra and coworkers have already proposed a model where the SecM signal is communicated to the PTC via a cascade of rRNA rearrangements (Mitra et al., 2006).

1.4 Prokaryotic membrane insertion pathways

Since approximately 25% to 30% of the bacterial proteins function in the cell envelope or outside of the cell, their partial or complete translocation across or into the cytoplasmic membrane is a decisive step in the biosynthesis of these proteins (Driessen and Nouwen, 2008). In bacteria, both secreted and membrane proteins are initially synthesized in the cytoplasm and are then targeted to the inner membrane for translocation. Secretory proteins have N-terminal, cleavable signal sequences and cross the membrane completely. Membrane proteins, on the other hand, usually do not contain such signal sequences, but instead, their first transmembrane (TM) segment functions as an internal signal for targeting and insertion. These so-called signal anchor sequences are usually more hydrophobic than cleavable signal sequences (Luirink et al., 2005). The hydrophobic segments of membrane proteins are integrated into the lipid bilayer whereas the hydrophilic regions are either translocated across the membrane or remain in the cytoplasm.

The insertion of most proteins into biological membranes is a process that is initiated by protein translocases. In *E. coli*, there are three known translocases (Xie and Dalbey, 2008). The Sec translocase is the general translocase that transports unfolded proteins across and integrates membrane proteins into the cytoplasmic membrane. A second translocase, the YidC insertase, inserts not only Sec-independent proteins but also assists in the insertion of membrane proteins in the Sec pathway. A third translocase is the twin-arginine translocation (Tat) machinery which is responsible for the export of proteins that are already folded and typically have bound cofactors (reviewed in (Lee et al., 2006)). Here, only the Sec and YidC systems that are used to insert proteins into the cytoplasmic membrane of *E. coli* are further described (Fig. 1.6).
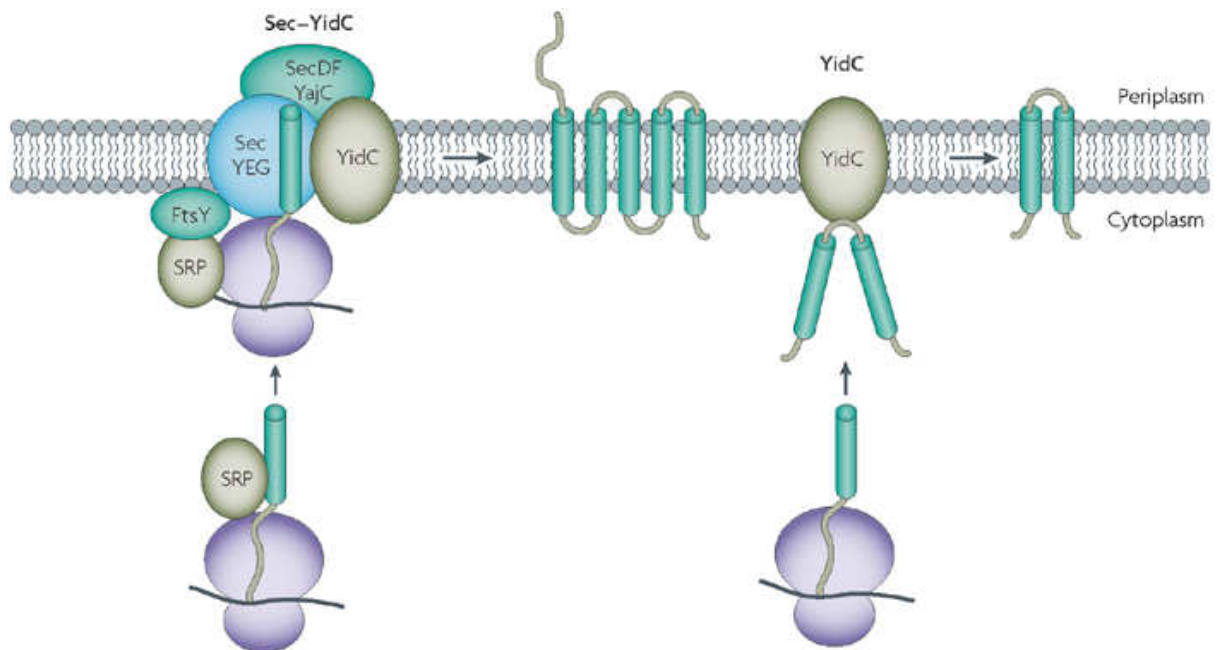
Figure 1.6: The Sec pathway and the YidC-only pathway for membrane insertion. In *E. coli*, the SecYEG-SecDFYajC complex is the general translocase that inserts newly synthesized polypeptides into the cytoplasmic membrane. Most Sec-dependent proteins are targeted to the membrane by the signal recognition particle (SRP) and the SRP receptor (FtsY). The insertase YidC can assist in the insertion of membrane proteins in the Sec pathway (left side) or function independently to promote membrane protein insertion (right side). Some Sec-independent proteins are also targeted by the SRP (Xie and Dalbey, 2008).

1.4.1 The Sec pathway for membrane insertion

In bacteria, the Sec pathway is the major route of protein export and membrane protein insertion. This pathway involves the Sec translocase which comprises the SecYEG core and the accessory components SecDFYajC, SecA and YidC (Xie and Dalbey, 2008) (Fig. 1.6, left side). SecYEG constitutes the highly conserved, membrane-embedded protein-conducting channel (PCC). The pore-forming subunit of the heterotrimeric complex is SecY, which consists of 10 TM segments (Van den Berg et al., 2004). SecE and SecG consist of three and two TM segments, respectively. It has been suggested that TM helices of substrates exit the translocon laterally into the lipid bilayer through a putative gate located between helices 2 and 7 in SecY (Van den Berg et al., 2004). SecDFYajC is a trimeric complex that enhances both the *in vivo* translocation of secretory proteins (Pogliano and Beckwith, 1994) and insertion of membrane proteins (Chen et al., 2005). YajC is not essential for protein export or membrane protein insertion (Xie and Dalbey, 2008). The molecular motor protein SecA uses ATP hydrolysis to promote translocation of polypeptide chains and is essential for posttranslational protein export. It is thought to be required for translocation of large hydrophilic domains of membrane proteins (Andersson and von Heijne, 1993; Neumann-Haefelin et al., 2000). The

YidC component seems to act as an integral membrane chaperone that is involved in the lateral transfer of TM segments from SecYEG into the lipid bilayer (Kuhn et al., 2003). Well-characterized examples of membrane proteins that use both the Sec translocase and YidC are the leader peptidase (Lep) (Houben et al., 2000) and the cell division protein FtsQ (Urbanus et al., 2001).

The majority of inner membrane proteins (IMPs) are targeted as ribosome-bound nascent chains (RNCs) to the Sec translocase by the evolutionarily conserved signal recognition particle (SRP) pathway which requires the SRP and the SRP receptor (Bernstein, 2000) (Fig. 1.6, left side). *E. coli* SRP consists of a complex of a 4.5S RNA and a 48 kDa GTPase P48 or Ffh (fifty-four homolog), which is homologous to the mammalian SRP54 (Poritz et al., 1990). SRP binds to hydrophobic signal anchor sequences of IMPs as they emerge from the ribosome. The ribosome-nascent-chain-SRP complex is then targeted to the SRP receptor, which, in most cases, is located at the membrane surface (Herskovits et al., 2001). The *E. coli* SRP receptor contains only one subunit, FtsY, which is a homolog of the mammalian SRα subunit (Luirink et al., 2005). FtsY and Ffh form a complex in which both proteins reciprocally stimulate each other's GTPase activities (Shan and Walter, 2005). Upon GTP hydrolysis, the SRP is released from FtsY and the nascent membrane protein is transferred to the Sec translocase where it gets integrated into the lipid bilayer (Xie and Dalbey, 2008).

1.4.2 The YidC-only pathway

There are proteins that insert into the membrane independently of the Sec translocase. These proteins do not insert spontaneously into the membrane, as suggested earlier (Geller and Wickner, 1985), but instead, they use a distinct pathway. In 2000, YidC was found to be a new membrane insertase (see Section 1.5) that can also function independently of the Sec translocase in bacteria (Samuelson et al., 2000; Scotti et al., 2000; Stuart and Neupert, 2000). The YidC-only pathway (Fig. 1.6, right side) mediates the insertion of a diverse group of Sec-independent substrates, including viral coat proteins and protein subunits of the respiratory chain. Although the currently identified range of substrates of the YidC-only pathway is relatively limited, YidC is required for the membrane insertion of the phage proteins M13 procoat (Samuelson et al., 2000) and Pf3 coat, the major envelope component of the Pf3 filamentous phage (Chen et al., 2002). Endogenous substrates for YidC are the ring-forming F_o subunit c of the *E. coli* F_1F_o ATP synthase (Yi et al., 2003), subunit II of the cytochrome *bo* oxidase (CyoA) (Celebi et al., 2006; van Bloois et al., 2006), and the double membrane-

spanning MscL protein that forms the pentameric mechanosensitive channel of large conductance (Facey et al., 2007). How proteins of the YidC-only pathway are targeted to the membrane is still subject of controversy, as conflicting results have been obtained (Kol et al., 2008). But it is generally accepted that the YidC-dependent M13 and Pf3 coat proteins do not require the SRP pathway (Chen et al., 2002; de Gier et al., 1998). On the other hand, it has been shown that for instance the precursor form of CyoA, pre-CyoA, requires the SRP pathway for targeting to the membrane (Celebi et al., 2006).

1.5 The YidC/Oxa1/Alb3 protein family

YidC is a member of the YidC/Oxa1/Alb3 protein family which exist in all three domains of life. They catalyze the insertion of proteins into inner membranes of bacteria and mitochondria, and into thylakoid membranes of chloroplasts (Kiefer and Kuhn, 2007; Luirink et al., 2001). All members of this family are comprised of a core region of five TM segments which are flanked by N- and C-terminal regions of variable length (Fig. 1.7) (Yen et al., 2001). This core region represents the catalytically active domain of the protein and functions as a protein insertase, *i.e.* an enzyme promoting the integration of hydrophobic regions into the membrane (Funes et al., 2009). In addition to its integrase activity, the core region also contributes to the folding and assembly of integral membrane proteins (Dalbey and Kuhn, 2004).
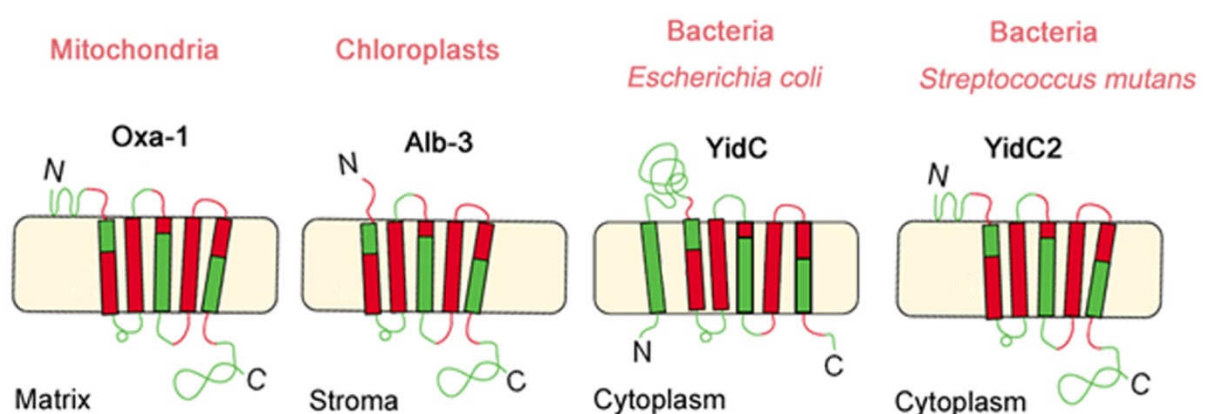
Figure 1.7: Schematic representation of the topology of members of the YidC/Oxa1/Alb3 protein family in bacteria, mitochondria and chloroplasts. Transmembrane (TM) domains are indicated as red and green boxes. YidC, Oxa1 and Alb3 have a conserved C-terminal region that comprises five predicted TM segments, with the exception of *E. coli* YidC which has six N-terminal TM segments. While *E. coli* YidC has a large periplasmic domain, both Oxa1 and Alb3 have long C-terminal extensions which in the case of Oxa1 functions as a ribosome-binding domain (adapted from (Kuhn et al., 2003)).

The founding member of this family is the mitochondrial protein Oxa1 (Oxidase assembly 1) which was initially identified by two independent genetic screens designed to identify proteins required for the assembly of the cytochrome oxidase complex (Bauer et al., 1994; Bonnefoy et al., 1994). It plays an essential role in the insertion of mitochondrial translation products into the mitochondrial inner membrane, such as cytochrome b of the bc_1 complex, or Atp6 of the F_1F_o ATP synthase, as well as for the integration of some nuclear encoded inner membrane proteins, such as Oxa1 itself (Preuss et al., 2005). Since mitochondria lack SRP, cotranslational insertion is achieved by an alternative mechanism: the Oxa1 protein can directly interact with the mitochondrial ribosome via its C-terminal positively charged extension (Jia et al., 2003; Szyrach et al., 2003). In addition to Oxa1, mitochondria contain a second member of the YidC/Oxa1/Alb3 protein family named Cox18 or Oxa2 which functions in a posttranslational manner (Funes et al., 2004).

Alb3 (albino3) is found in the thylakoid membranes of the chloroplast where it is has been shown to catalyze the insertion and assembly of light-harvesting complex proteins (LHCPs) (Bellafiore et al., 2002; Moore et al., 2000). These proteins are first posttranslationally imported from the cytoplasm to the stroma and then targeted to the thylakoid by the chloroplast SRP complex.

The YidC protein represents the prokaryotic member of the YidC/Oxa1/Alb3 protein family and is present in both Gram-negative and Gram-positive bacteria. The existence of members of this family in some but not all Archaea has also proposed by phylogenetic analysis. Although experimental verification has yet to appear, the putative archaeal YidC proteins are predicted to assume a topology similar to that of their bacterial homologues (Luirink et al., 2001; Zhang et al., 2009).

1.5.1 Structure and function of *Escherichia coli* YidC

Gram-negative bacteria, such as *E. coli*, contain only one member of the YidC/Oxa1/Alb3 protein family. *E. coli* YidC, the best-characterized prokaryotic YidC protein, is located in the bacterial inner membrane and comprises six predicted TM segments (Fig. 1.7). Compared to its homologues Oxa1 and Alb3, *E. coli* YidC has an additional TM segment close to its N-terminus and a large, nonessential periplasmic domain of 320 amino acid residues between the first and second TM segment (Ravaud et al., 2008). It functions both in conjunction with the Sec translocase as part of the cotranslational machinery, as well as on its own (Beck et al., 2001; Samuelson et al., 2000). To date, it has not been definitely established if the latter

function, *i.e.* the Sec-independent insertion route, is exclusively cotranslational (Kiefer and Kuhn, 2007).

YidC interacts with SecDFYajC, linking it to the Sec translocase *in vivo* (Nouwen and Driessen, 2002). In addition, it has been shown that the non-conserved periplasmic domain of *E. coli* YidC is required for the interaction with the SecF component of the SecDFYajC complex (Xie et al., 2006). The parts of YidC that are important for its function as a membrane insertase have been investigated using deletion and substitution mutants, revealing that TM segments 2, 3, and 6 are important for activity (Jiang et al., 2003). Although YidC is indispensable for viability in *E. coli*, the chloroplast protein Alb3 can substitute for YidC and promote membrane insertion of several Sec-independent proteins (Jiang et al., 2002). In addition, the mitochondrial Oxa1 protein can also functionally replace YidC in *E. coli* (Preuss et al., 2005), but it is unable to take over the Sec-associated function of YidC (van Bloois et al., 2005).

1.5.2 Structure and function of *Streptococcus mutans* YidC

The Gram-positive bacterium *Streptococcus mutans* is a major causative agent of human dental caries, which results from its ability to ferment a wide range of dietary carbohydrates, leading to the production of lactic acid and therefore to an erosion of the tooth enamel (Dong et al., 2008). Acid tolerance, which is necessary for cellular viability of *S. mutans*, is mainly achieved by an F_1F_o ATPase proton pump (Bender et al., 1986).

S. mutans contains two paralogs of the evolutionary conserved YidC/Oxa1/Alb3 protein family, known as YidC1 and YidC2 (Hasona et al., 2005). Both proteins are functional orthologs of *E. coli* YidC since they also promote membrane insertion of known YidC substrates in *E. coli*, such as the F_o components of the F_1F_o ATPase (Dong et al., 2008). Deletion of yidC2, but not yidC1, results in a stress-sensitive phenotype with decreased F_1F_o ATPase activity similar to the mutants lacking the SRP pathway in this organism (Hasona et al., 2005). On the other hand, double mutants lacking both YidC2 and SRP components are not viable, suggesting that YidC2 overlaps functionally with the SRP pathway to mediate cotranslational protein insertion.

S. mutans YidC2 is predicted to contain five TM segments and an extended hydrophilic C-terminal region which is similar to that of yeast *Saccharomyces cerevisiae* Oxa1 (Fig. 1.7). In the case of Oxa1, this positively charged C-terminal extension was shown to interact with mitochondrial ribosomes, thereby promoting cotranslational membrane protein insertion in

the absence of an SRP (Jia et al., 2003; Szyrach et al., 2003). Recently, Funes and coworkers could show that *S. mutans* YidC2 and mitochondrial Oxa1 partially complement each other, *i.e.* Oxa1 complements a lack of YidC2 in *S. mutans* and YidC2 also functions reciprocally in oxa1-deficient yeast mutants by mediating cotranslational insertion of mitochondrial translation products into the inner membrane (Funes et al., 2009).

1.6 Aims of the study

Ribosome stalling on the TnaC and SecM nascent peptide are two examples where interactions between the nascent chain and ribosomal tunnel components lead to inhibition of PTC activity. Although several features of the amino acid sequences as well as specific ribosomal nucleotides and residues of ribosomal proteins have been identified to be important for stalling (Nakatogawa and Ito, 2002; Yang et al., 2009), the exact stalling mechanisms remain unknown. In order to understand and compare the mechanisms by which TnaC and SecM act, the determination of cryo-EM structures of both, a TnaC-stalled and a SecM-stalled 70S ribosome was the aim of the first part of this study. To attain this goal, 3D reconstructions at high resolution as well as the visualization of the nascent chains in the ribosomal exit tunnels were important prerequisites.

The membrane protein insertase YidC is the prokaryotic member of the evolutionary conserved YidC/Oxa1/Alb3 protein family. It assists in cotranslational membrane protein insertion in the Sec pathway and also functions as an independent insertase (Xie and Dalbey, 2008). To date, not much is known about how YidC inserts Sec-independent membrane proteins into the cytoplasmic membrane, and how many copies of YidC are necessary for the insertion process. In order to address those questions, the determination of a cryo-EM structure of YidC bound to 70S ribosomes was the aim of the second part of this study.

II MATERIALS AND METHODS

2.1 Methods in molecular biology

2.1.1 Polymerase chain reaction

Polymerase chain reaction (PCR) was used to amplify DNA fragments for cloning or to create template DNA for *in vitro* transcription reactions. In general, 50 µl reactions, comprising 1 µM of forward and reverse primer (Table 2.1), 5-50 ng template DNA, 1 U proof-reading DNA-polymerase (Fermentas), 5 µl 10x reaction buffer with $MgSO_4$ (Fermentas), and 10 µM dNTPs (Fermentas) were set up on ice. Alternatively, DNA was amplified by PCR using the Phusion Flash High-Fidelity Master Mix (Finnzymes) according to the manufacturer's instructions. Here, 0.5 pM of forward and revers primer, and approximately 1 ng of template DNA was added to a 20 µl reaction. Each thermo cycling program used 30 cycles, where times and temperatures of denaturation, annealing and elongation were varied to achieve optimal amplification. PCR products were analyzed by agarose gel electrophoresis, and subsequently purified using the QIAquick® PCR purification kit (Qiagen) according to the manufacturer's protocol.

Table 2.1: Name and sequences of the used oligonucleotides.

Name	Sequence in 5' to 3' orientation
Primer for cloning of pET324-YidC2	
5'-YidC2	CATGCCATGGCTAAAAATTTACAAGCGTCTTTTATTTTCGGGC
3'-YidC2	CTAGTCTAGATTAGTGATGGTGATGGTGATGTTGCTTATGGTGACGCTGTTTCC
Primer for cloning of pBAT4-cbpSecM	
5'-cbp-SecM	TAATACGACTCACTATAGGGAATTGTGAGCGG
3'-cbp-SecM	GGAATTCAGAGGTAGTCATCACCATCACCATCACTTCAGCACGCCCGTCTGGATAAGCCAGGCGCAAGGCATCCGTGCTGGCCCT
3'-cbp-SecM-2	GCGCAAGGCATCCGTGCTGGCCCTCAACGCCTCACCTAAAAGCTTGAG
Primer for cloning of pBAT4-cbpTnaC-MscL[70/90/115]	
5'-TnaC-MscL	GGGGAATTCTACCCATACGATGTTCCAGATTACGCTGAAAACCTGTATTTTCAGGGAAGCATTATTAAAGAATTTCGC
3'-TnaC-MscL[70]	GCGCAGGGGGATATCCCTGCTTGTGTGACCTCAAAATGGTTCAATATTGACAACAAAATTGTCGATCACCGCCCTTGA AAGCTTGGG

3'-TnaC-MscL[90]	GATTTTCTGATTGTGGCCTTTTGTGTGACCTCAAAATGGTTCAATATTGACAA CAAAATTGTCGATCACCGCCCTTGAAAGCTTGGG
3'-TnaC-MscL[115]	GAACCAGCAGCCGCACCTGCACCATGTGTGACCTCAAAATGGTTCAATATTG ACAACAAAATTGTCGATCACCGCCCTTGAAAGCTTGGG
Primer for different MscL-constructs	
5'-MscL-His-HA	TAATACGACTCACTATAGGGAAAAGAAAATAAGGAGGTTCCTTCATGCATCA TCATCATCATTACCCATACGATGTTCCAGATTACGCTAGCATTATTAAAG AATTTCGC
3'-MscL[77]	GACACCGTAATGCATCACAACAGCAGGGATATCCCC
3'-MscL[114]	TGCAGGTGCGGCTGCTGGTTCTTCTTTTTTCCG
3'-MscL[125]	AATTTCTGTCAGTAATACTTCTTCTTTAGTTGGTGC
3'-MscL[136]	AGAGCGGTTATTCTGCTCTTTCAGCAAATCACG
5'-MscL-His-HA	TAATACGACTCACTATAGGGAAAAGAAAATAAGGAGGTTCCTTCATGCATCA TCATCATCATAGCATTATTAAAGAATTTCGC
5'-MscL-Strep	TAATACGACTCACTATAGGGAAAAGAAAATAAGGAGGTTCCTTCATGTGGA GCCACCCGCAGTTCGAAAAA AGCATTATTAAAGAATTTCGC
5'-MscL-His-Strep	TAATACGACTCACTATAGGGAAAAGAAAATAAGGAGGTTCCTTCATGCATCA TCATCATCATTGGAGCCACCCGCAGTTCGAAAAA AGCATTATTAAAGAATTTCGC
3'-MscL[125]-Lys	GCCGCACCTGCACCAACTAAAGAAAAAAAAGCGAAAAAAAAAGTT
3'-MscL[136]-Lys	GACAGAAATTCGTGATTTGCTGAAAAAAGCGAAAAAAAAAGTT
5'-MscL-His	TAATACGACTCACTATAGGGAAAAGAAAATAAGGAGGTTCCTTCATGCATCA TCATCATCATAGCATTATTAAAGAATTTCGC
3'-MscL[70]-SecM	GCGCAGGGGGATATCCCTGCTTTCAGCACGCCCGTCTGGATAAGCCAGGCGC AAGGCATCCGTGCTGGCCCT
3'-MscL[90]-SecM	GATTTTCTGATTGTGGCCTTTTTCAGCACGCCCGTCTGGATAAGCCAGGCGCA AGGCATCCGTGCTGGCCCT
3'-MscL[115]-SecM	GAACCAGCAGCCGCACCTGCACCATTCAGCACGCCCGTCTGGATAAGCCAGG CGCAAGGCATCCGTGCTGGCCCT

For amplification of the *S. mutans* YidC2 sequence, the pCR2.1-YidC2 plasmid (provided by Johannes M. Herrmann, University of Kaiserslautern, Germany) was used as a template in order to clone the pET324-YidC2 plasmid (pET324, (van der Does et al., 1996)) for YidC2 overexpression. The pBAT4-cbpTnaC plasmid (provided by Axel Innis, Yale University, New Haven, USA) served as a template for the cloning of both, the pBAT4-cbpSecM plasmid and the pBAT4-cbpTnaC-MscL[70/90/115] plasmids. In the case of the cloning of the pBAT4-cbpSecM plasmid two PCR reactions were carried out, the first with the 5'-cbp-SecM forward and the 3'-cbp-SecM revers primer using the pBAT4-cbpTnaC plasmid as a template, the

second with the 5'-cbp-SecM forward and the 3'-cbp-SecM-2 reverse primer using the first PCR product as a template. For the generation of various MscL-constructs which then were used for *in vitro* transcription reactions, the pET16b-MscL plasmid (provided by Andreas Kuhn, University of Hohenheim, Stuttgart, Germany (Facey et al., 2007)) served as a template for PCR.

2.1.2 Restriction digestion of DNA

A variety of restriction endonucleases were used to digest DNA in order to prepare defined fragments for cloning or to check cloned plasmids for presence of inserted DNA fragments. The reactions were set up as double restriction digests, using two restriction endonucleases at the same time. In general, an 80 µl restriction reaction was composed of 2-5 µg DNA, 3 U of restriction enzyme (Fermentas), an appropriate 10x reaction buffer, and nuclease-free water, and incubated over night at 37°C. The restriction reactions were subjected to agarose gel electrophoresis; the DNA fragments of interest were cut out from the gel and purified using the QIAquick® gel extraction kit (Qiagen) according to the manufacturer's protocol.

2.1.3 Ligation of DNA fragments

Ligation of digested DNA fragments was performed with T4 DNA ligase (Fermentas) according to the protocol provided with the enzyme. For a standard 20 µl ligation reaction, a fivefold molar excess of the digested DNA insert was mixed with the linearized vector, 2 µl 10x ligation buffer and 5 U of T4 DNA ligase, and incubated over night at 16°C.

2.1.4 Transformation of *Escherichia coli* cells

For transformation of chemically competent *E. coli* cells (Rosetta (DE3) or DH5α), 1 µl of plasmid DNA (pET324-YidC2-His) or 10 µl of a ligation reaction was incubated with 50 µl thawed cells for 10 min on ice. The cells were then heat-shocked for 1 min at 42°C in a water bath, and immediately cooled on ice for 2 min. Subsequently, 1 ml of pre-warmed LB medium was added, and the cells were recovered for one hour at 37°C on an Eppendorf Thermomixer. After short centrifugation, the cell pellet was resuspended in 100 µl LB medium and plated on antibiotic containing LB agar plates for overnight growth at 37°C.

2.1.5 Isolation of plasmid DNA and DNA Sequencing

Approximately 3 ml LB medium containing the appropriate antibiotics was inoculated with a single colony picked from the transformation plate and incubated over night at 37°C. Plasmid DNA for restriction analysis and sequencing was isolated from overnight cultures using the QIAprep® Spin Miniprep kit (Qiagen). DNA sequencing was performed by Eurofins MWG (Martinsried, Germany).

2.1.6 Agarose gel electrophoresis

Samples subjected to agarose gel electrophoresis were prepared by addition of SYBR® Green I (for DNA) and SYBR® Green II (for RNA) (Molecular Probes), respectively, to a final dilution of 1:10,000 and an appropriate amount of 10x loading dye (Ambion). The gels were made with 1% (w/v) agarose (electrophoresis grade, Invitrogen) in 1x TAE buffer (40 mM Tris, 20 mM acetic acid, 2 mM EDTA) and run for 20-40 min at a constant voltage of 100 V. DNA and RNA bands were visualized at a wavelength of 300 nm and documented using a UV light gel documentation system (INTAS UV system, INTAS).

2.2 Methods in protein biochemistry

2.2.1 Preparation of TnaC-stalled ribosome nascent chain complexes (RNCs)

The here described RNC purification method was established by our collaboration partner Axel Innis from the Steitz laboratory of the Yale University in New Haven and used for the purification of a TnaC-stalled 70S ribosome complex (carried out by Axel Innis), a SecM-stalled 70S ribosome complex, and for the purification of TnaC-stalled MscL-RNCs.

2.2.1.1 Stock solutions used for RNC purification

Amino acid stock solutions

Individual stock solutions (168 mM) for each of the 20 amino acids were prepared as follows:

- o Ala, Gly, His, Ile, Lys, Leu, Asn, Pro, Gln, Arg, Ser, Thr, and Val were dissolved in 60 mM Hepes/KOH pH 7.5.
- o Cys and Met were dissolved in the same buffer, with 8 and 4 mM DTT, respectively.
- o Glu and Tyr were dissolved in 60 mM HEPES and 0.7 M KOH.
- o Asp and Trp were dissolved in 60 mM HEPES and 0.7 M HCl.
- o Phe was dissolved in 60 mM HEPES/KOH pH 7.5.

To obtain a 4.13x amino acid stock solution 119 µl of each amino acid were mixed prior to usage.

<u>100x Master mix</u>

	Vendor	Conc
Adenosine 5'-Triphosphate, Disodium (ATP)	GE Healthcare	120 mM
Cytidine 5'-Triphosphate, Trisodium (CTP)	GE Healthcare	85 mM
Guanosine 5'-Triphosphate, Trisodium (GTP)	GE Healthcare	85 mM
Uridine 5'-Triphosphate, Trisodium (UTP)	Sigma/Fluka	85 mM
Folinic acid calcium salt pentahydrate	Sigma/Fluka	3.4 mg/ml
tRNA from *E.coli* MRE-600	Roche	17.06 mg/ml

<u>20x Salt solution</u>

	Vendor	Conc
L-Glutamic acid monopotassium salt monohydrate	Sigma/Fluka	2.6 M
L-Glutamic acid ammonium salt	Sigma/Fluka	200 mM
L-Glutamic acid hemimagnesium salt tetrahydrate	Sigma/Fluka	388 mM

<u>Other stock solutions</u>

	Vendor	Conc
Sodium pyruvate	Sigma/Fluka	1 M
β-Nicotinamine adenine dinucleotide (β-NAD)	Sigma-Aldrich	33 mM
Coenzyme A	Sigma	26 mM
Sodium oxalate	Sigma/Fluka	100 mM
Spermidine trihydrochloride	Sigma/Fluka	150 mM
1,4-Diaminobutane dihydrochloride (Putrescine)	Sigma/Fluka	100 mM

2.2.1.2 S30 extract preparation

The S30 extract used for a coupled *in vitro* transcription-translation reaction was prepared by our collaboration partner Axel Innis using a modified version of the protocol by Liu and coworkers (Liu et al., 2005): The genes encoding components of the tmRNA system were deleted from the chromosome of *E.coli* strain KC6 (Calhoun and Swartz, 2006) using the Red/ET recombination system (Gene Bridges). The resulting *ΔsmpBΔssrA* strain was grown at 37°C in a BioFlo-3000 fermenter containing 10L of 2xYTPG medium (16 g/L Bacto-Tryptone, 10 g/L yeast extract, 5 g/L NaCl, 22 mM NaH_2PO_4, 40 mM Na_2HPO_4, 100 mM glucose (Kang et al., 2000)) up to OD_{600} >10. The cell culture was chilled rapidly on ice and centrifuged at 8,000x g for 20 min at 4°C. The harvested cells were then resuspended into S30 buffer (10 mM Tris-acetate pH 8.2, 14 mM magnesium acetate, 60 mM potassium acetate, 2 mM DTT) and pelleted once more by centrifugation at 9,000xg for 30 min (4°C). Washed cells were weighed and resuspended to homogeneity in 1 ml of S30 buffer for each gram of cell paste. Cell lysis was achieved with a single pass through a microfluidizer set to a pressure of 17,500 psi and the resulting lysate was supplemented with DTT to yield a total concentration of 5 mM. The sample was then clarified by two rounds of centrifugation at 30,000x g (4°C) and transferred to an orbital shaker rotating at 280 rpm, where it was incubated at 37°C for 80 min. The extract was dialyzed against S30 buffer for 40 min at 4°C, using a membrane with a molecular weight cut-off of 12,000-14,000 (SpectraPor). Finally, the sample was clarified one more time by centrifugation at 4,000x g for 10 min at 4°C. The total protein concentration in the sample was determined by means of a Bradford colorimetric assay (BioRad) using a bovine serum albumin standardization curve. Aliquots of S30 extract were flash-frozen in liquid nitrogen and stored at -80°C.

2.2.1.3 RNC formation and purification

For the purification of TnaC-stalled RNCs 10 ml of Cell-Free Protein Synthesis (CFPS) reaction mixture were prepared according to the pipetting scheme depicted in Table 2.2 (Jewett and Swartz, 2004). All components of the *in vitro* transcription-translation (IVT) reaction were mixed, except the plasmid which was placed at the bottom of a 250 ml beaker. Subsequently, the IVT reaction mixture was added and incubated for 30 min at 30°C in a water bath.

Table 2.2: Pipetting scheme for 10 ml of Cell-Free Protein Synthesis reaction mixture.

Component	Stock	Final concentration	Volume to add
Salt solution	20x	1x	500 µl
Master mix	100x	1x	100 µl
Amino acid solution	4.13x	1x	2.4 ml
Sodium pyruvate	3 M	33 mM	110 µl
β–NAD	33 mM	0.33 mM	100 µl
Coenzyme A	26 mM	0.26 mM	100 µl
Sodium oxalate	100 mM	4 mM	400 µl
Spermidine	150 mM	1.5 mM	100 µl
Putrescine	100 mM	1 mM	100 µl
IPTG	1 M	0.5 mM	5 µl
Bis-Tris Acetate pH 7.0	1 M	60 mM	600 µl
EDTA-free one complete	100% pill/ml	0.1% pill/ml	10 µl
dH$_2$O (DEPC-treated)			ad 10 ml
E.coli MRE-600 tRNA	60 mg/ml	1.5 mg/ml	250 µl
S30 extract	38.5 mg/ml	9.9 mg/ml	2.57 ml
T7 Polymerase	37.5 mg/ml	0.1 mg/ml	500 µl
Plasmid	x µg/µl	15 µg/ml	x µl

The reaction mixture was loaded onto chilled linear 10-40% (w/v) sucrose gradients in 10 mM HEPES/NaOH pH 7.5, 10 mM Mg(OAc)$_2$, 50 mM KCl, 10 mM NH$_4$Cl. Gradients were then centrifuged in a Beckman SW32-Ti rotor at 110000x g for 4 hours at 4°C. To get 70S monosomes and polysomes approximately the bottom 2/3 of the gradient volume was collected, pooled from various gradients, and mixed with stock solutions to give final concentrations of 50 mM Tris-HCl pH 8.0, 2 mM L-tryptophan, 2 mM CaCl$_2$, 10 mM DTT and 10 mM Mg(OAc)$_2$. 2 ml of 50% slurry calmodulin sepharose matrix (GE-Healthcare) was washed with 10 ml loading buffer (50 mM Tris/HCl pH 8.0, 50 mM KCl, 10 mM NH$_4$Cl, 2 mM CaCl$_2$, 2 mM L-tryptophan, 10 mM Mg(OAc)$_2$, 10 mM DTT). The sepharose beads were added to the ribosome fraction of the gradient, and incubated over night at 4°C on a shaker. The binding was then transferred to a Poly-Prep Chromatography Column (BioRad), and the flow-through was collected and used for rebinding to the calmodulin column. The column was washed with 5 column volumes of loading buffer, and subsequently with 5 column volumes of wash buffer (50 mM Tris/HCl pH 8.0, 50 mM KCl, 10 mM NH$_4$Cl, 2 mM CaCl$_2$, 10 mM Mg(OAc)$_2$). Afterwards, the RNCs were eluted with 8 column volumes of elution buffer (50 mM Tris/HCl pH 8.0, 50 mM KCl, 10 mM NH$_4$Cl, 2 mM EGTA, 10 mM Mg(OAc)$_2$). The eluate was loaded onto chilled linear 10-40% (w/v) sucrose gradients and centrifuged in a SW32-Ti rotor at 110,000x g for 4 hours at 4°C. The monosome fraction

containing purified TnaC-stalled RNCs was collected at a fraction collector (Gilson) while recording the A_{254} profile at a gradient station (Biocomp). After adding 50 mM Tris/HCL pH 8.0 to the pooled fractions, the RNCs were pelleted in a Beckman TLA110 rotor at 50,000x g for 3 hours at 4°C. Finally, the purified RNCs were resuspended in 30 µl TnaC-RNC-buffer (20 mM HEPES pH 7.5, 50 mM KOAc, 10 mM Mg(OAc)$_2$, 2 mM DTT, 2 mM L-tryptophan), flash-frozen in liquid nitrogen, and stored at -80°C. The concentration of the TnaC-stalled RNCs was determined by SDS-PAGE analysis using 2 pmol of empty 70S ribosomes as reference. Note that for the purification of the SecM-stalled 70S ribosome complex the L-tryptophan was omitted from all buffers.

2.2.2 Preparation of SecM-stalled DP120-RNCs

The here described RNC purification method was mainly based on a protocol established by Michael Blau, a former member of the Beckmann lab (Halic et al., 2006), but with some buffer modifications according to Schaffitzel *et al.* (Schaffitzel and Ban, 2007).

2.2.2.1 In vitro transcription

mRNA coding for a His$_6$-tag, a HA-tag, the 120 N-terminal amino acids of the membrane protein dipeptidyl-aminopeptidase B (DP120) from *Saccharomyces cerevisiae*, and the last 21 C-terminal amino acids of the *E. coli* SecM stalling sequence was synthesized using the T7-MEGAscript^{TM} High Yield Transcription kit (Ambion). The corresponding DNA-construct was prepared by Shashi Bhushan.

Per 20 µl *in vitro* transcription reaction 0.5 µg template DNA was used, and the reaction was incubated overnight at 37°C in a water bath. The mRNA was precipitated by adding 25 µl nuclease-free water and 30 µl of LiCl precipitation solution (Ambion) to each reaction, and incubated for 5 hours at -20°C. After centrifugation for 15 min at 179,000x g, the mRNA was washed with 70% (v/v) ethanol, and the dried pellets were resuspended in nuclease-free water, flash-frozen in liquid nitrogen and stored at -80°C. The concentration of the mRNA was determined by measuring the absorption at 260 nm. For further analysis, agarose gel electrophoresis was used.

2.2.2.2 In vitro translation

The *E. coli* T7 S30 Extract for Circular DNA kit (Promega) was used for the *in vitro* translation (IVT) of the mRNA. Per 50 µl IVT-reaction 12 µg of mRNA was heated for 10 min at 65°C to break secondary structure, and immediately cooled on ice to prevent its reformation. The IVT-components, i.e. 5 µl amino acid mixture, 20 µl S30 Premix, and 15 µl T7 S30 Extract, were assembled on ice and added to the mRNA. The IVT-reaction was incubated for 30 min at 30°C in a water bath, and subsequently stopped by adding 500 µg/ml chloramphenicol.

2.2.2.3 RNC purification

For the purification of SecM-stalled DP120-RNCs, 4x 200 µl IVT-reactions were performed and spun through two 300 µl sucrose cushions (50 mM HEPES pH 7.2, 100 mM KOAc, 100 mM Mg(OAc)$_2$, 750 mM sucrose, 0.1% (w/v) Nikkol (Sigma-Aldrich), 500 µg/ml chloramphenicol, 5 mM β-Mercaptoethanol, 0.1% (w/v) EDTA-free complete protease inhibitor pill (Boehringer)) for 3 hours at 50,000x g in a Beckman TLA 120.2 rotor at 4°C. After centrifugation, the supernatant was quickly removed. Each pellet was resuspended in 800 µl 100 buffer (50 mM HEPES pH 7.2, 100 mM KOAc, 100 mM Mg(OAc)$_2$, 250 mM sucrose, 0.1% (w/v) Nikkol, 500 µg/ml chloramphenicol, 5 mM β-Mercaptoethanol, 0.1% (w/v) EDTA-free complete protease inhibitor pill, 0.2 U/ml RNAsin (Ambion)) and incubated for approximately one hour on ice. For affinity purification of the RNCs, 2x 750 µl TALON^{TM} Metal Affinity Resin (Clontech) were transferred into two Poly-Prep Chromatography Columns (BioRad) and equilibrated each with 5 ml 100/tRNA buffer (100 buffer + 10 µg/ml tRNA) to minimize unspecific binding. The resuspended ribosomes were added to the columns and incubated for 20 min at 4°C with gently agitation. Afterwards, the flow-through was collected, and the resins were washed each with 10 ml 100 buffer to remove unspecifically bound ribosomes. The bound RNCs were eluted each with 2.5 ml 100 mM imidazole pH 7.1 in 100 buffer, pooled and spun through a 200 µl sucrose cushion for 2 hours at 50,000x g in a TLA110 rotor at 4°C. The supernatant was immediately removed, and the resulting pellet was slowly resuspended in 50 µl grid buffer (40 mM HEPES pH 7.2, 50 mM KOAc, 100 mM Mg(OAc)$_2$, 125 mM sucrose, 0.05% (w/v) Nikkol, 250 µg/ml chloramphenicol, 2 mM DTT, 0.5% (w/v) EDTA-free complete protease inhibitor pill, 0.2 U/ml RNAsin) by incubation for 30 min on ice. The concentration of the ribosomes was

determined by measuring the absorption at 260 nm. Finally, the SecM-stalled DP120-RNCs were aliquoted, flash-frozen in liquid nitrogen, and stored at -80°C. Aliquots of each purification step were subjected to SDS-PAGE and subsequent western blot analysis.

2.2.3 Puromycin assay

The puromycin assay was carried out to analyze if the purified SecM-stalled DP120-RNCs are resistant to puromycin reaction as suggested by literature (Muto et al., 2006). 80S wheat germ RNCs (provided by Shashi Bhushan) which were stalled during translation of truncated DP120 mRNA were used as a control since here a positive puromycin reaction, *i.e.* the loss of the nascent chain, was expected.

Since the puromycin reaction is partially inhibited by the presence of chloramphenicol (Cannon, 1968), and the purified RNCs were finally resuspended in grid buffer containing chloramphenicol, the RNCs had to be pelleted again in order to remove this antibiotic. Therefore, the RNCs were centrifuged in a Beckman TLA100 rotor at 100000x g for 90 min at 4°C, and resuspended in grid buffer without chloramphenicol (40 mM HEPES pH 7.2, 50 mM KOAc, 10 mM Mg(OAc)$_2$, 125 mM sucrose, 0.05% (w/v) Nikkol, 2 mM DTT, 0.5% (w/v) EDTA-free complete protease inhibitor pill). For each reaction, 0.3 OD RNCs were mixed with puromycin buffer (2 mM puromycin, 40 mM HEPES pH 7.2, 50 mM KOAc, 10 mM Mg(OAc)$_2$, 125 mM sucrose, 0.05% (w/v) Nikkol, 2 mM DTT, 0.5% (w/v) EDTA-free complete protease inhibitor pill) and as a control with buffer without puromycin, respectively, and incubated for 15 min at 37°C. Subsequently, the reactions were spun through a 100 µl sucrose cushion (750 mM sucrose in grid buffer without chloramphenicol) for 90 min at 100,000x g in a TLA100 rotor at 4°C. Supernatant and pellet fractions were subjected to SDS-PAGE and subsequent western blot analysis.

2.2.4 Purification of *Streptococcus mutans* YidC2

2.2.4.1 Recombinant expression in Escherichia coli

S. mutans YidC2 was recombinantly expressed in the *E. coli* strain Rosetta (DE3) using the pET324-YidC2-His plasmid. Therefore, colonies from a fresh transformation plate were used to inoculate a pre-culture which was grown over night at 37°C in LB medium containing 100 µg/ml ampicillin, 34 µg/ml chloramphenicol, and 0.5% (w/v) glucose to prevent premature

expression of YidC2. 12 liter of LB medium containing the antibiotics ampicillin and chloramphenicol were inoculated with 240 ml of the overnight culture and grown at 37°C. At an OD_{600} of 0.8 expression of YidC2 was induced by the addition of 1 mM IPTG. After incubation of the expression culture for 2 hours at 30°C, cells were harvested in a SLC6000 rotor at 8000x g for 10 min. The cell pellet was resuspended in 60 ml of cold 50 mM Tris/HCL, pH 8.0, 20% (w/v) sucrose. At this step, it was possible to freeze the cells in liquid nitrogen and store them at -80°C.

2.2.4.2 Large scale isolation of membrane vesicles

The cell pellets from YidC2 overexpression were thawed on ice. DTT and PMSF were added to a final concentration of 2 mM and 0.1 mM, respectively. The cells were mechanically disrupted using a French press (Microfluidics) at 15000 psi with addition of 50 mM Tris/HCL pH 8.0. To remove cell debris the cell extract was centrifuged in a SS34 rotor at 4°C and 8000x g for 15 min. The supernatant containing inner and outer membrane vesicles was centrifuged in a Beckman Ti45 rotor at 125,000x g for 60 min at 4°C. 800 µl of 50 mM Tris/HCL pH 8.0, 2 mM DTT and 20% (v/v) glycerol were added to each pellet, and the pellet was resuspended using a douncer. The membrane vesicles were flash-frozen in 500 µl aliquots in liquid nitrogen and stored at -80°C.

2.2.4.3 Purification of YidC2 from membrane vesicles

S. mutans YidC2 was purified by metal affinity purification using the C-terminal His$_6$-tag for binding to Ni-NTA agarose beads with subsequent gel filtration. 10 µl aliquots of each purification step, as indicated in brackets, were taken for subsequent SDS-PAGE analysis. Membrane vesicles isolated out of 6 l *E. coli* culture were thawed on ice, and solubilized in 60 ml solubilization buffer (10 mM Tris/HCL, pH 8.0, 20% (v/v) glycerol, 2% (w/v) DDM) for one hour at 4°C with gently agitation (aliquot Sol, Solubilization). Nonsolubilized material was removed by ultracentrifugation in a Ti45 rotor at 125,000x g for 30 min at 4°C. For subsequent SDS-PAGE analysis the pellet was resuspended in 60 ml of 1% (w/v) SDS, 50 mM Tris/HCL, pH 8.0, and an aliquot was taken (P, pellet). 0.5 ml of Ni-NTA agarose beads (Qiagen) were washed with 10 ml water and equilibrated with 10 ml buffer A (10 mM Tris/HCL, pH 8.0, 20% (v/v) glycerol, 0.05% (w/v) DDM). 50 mM imidazole, 500 mM NaCl, and the equilibrated column material were added to the supernatant of the ultracentrifugation

containing the solubilized membrane protein YidC2 (aliquot S, supernatant), and incubated for at least one hour at 4°C on a shaker to allow binding of YidC2 to the Ni-NTA agarose beads. The binding was then transferred to a Poly-Prep Chromatography Column (BioRad), and the flow-through was collected. The flow-through was subsequently loaded onto the Ni-NTA column and again collected (aliquot FT, flow-through). The column material was washed twice, each with 5 ml washing buffer (10 mM Tris/HCL, pH 8.0, 20% (v/v) glycerol, 0.05% (w/v) DDM, 60 mM imidazole, 500 mM NaCl) (aliquots W1 and W2, wash). For the elution of YidC2, firstly 1 ml elution buffer (10 mM Tris/HCL, pH 8.0, 20% (v/v) glycerol, 0.05% (w/v) DDM, 500 mM imidazole, 500 mM NaCl) was added to the column and incubated for 15 min (aliquot E1, elution). Afterwards, YidC2 was directly eluted with the addition of 2 x 500 µl elution buffer (aliquots E2 and E3, elution).

After SDS-PAGE analysis of the samples taken during Ni-NTA purification, the elution fractions containing purified YidC2 were pooled and concentrated using a centrifuge filter device with a molecular weight cut-off of 10 kDa (Amicon Ultra-4, Millipore) at 1000x g for approximately 45 min. The concentrated eluate was loaded onto an equilibrated Superdex 200 10/300 GL gel filtration column (GE Healthcare) on an ÄKTA purifier liquid chromatography system, using the YidC2-buffer (20 mM HEPES, pH 7.2, 10 mM $Mg(OAc)_2$, 500 mM KOAc, 20% (v/v) glycerol, 0.05% (w/v) DDM). Subsequently, the peak fractions were analyzed by SDS-PAGE, pooled and concentrated to obtain a final YidC2 concentration of 1 mg/ml. The protein concentration was determined by measuring the absorption of UV light at $\lambda = 280$ nm in a photometer (BioPhotometer, Eppendorf). The purified *S. mutans* YidC2 was aliquoted, flash-frozen in liquid nitrogen, and stored at -80°C.

2.2.5 Reconstitution assays

Reconstitution assays were used to characterize the binding of *S. mutans* YidC2 and *E. coli* YidC, respectively, to 70S ribosomes, ribosomal subunits and MscL-RNCs under different salt conditions. After *in vitro* reconstitution of the binding components, centrifugation was used to separate the ribosome-bound fraction (pellet) from the non-bound fraction (supernatant).

For a typical 20 µl reconstitution reaction 2 pmol of ribosomes and 20 pmol of purified ligand were mixed in an appropriate compensation buffer to adjust the buffer conditions to 20 mM HEPES/KOAc, pH 7.2, 100-500 mM KOAc, 10 mM $Mg(OAc)_2$, 1 mM DTT, 0.5 mM PMSF, 5 mM Spermidin, 0.05 mM Spermin, 250 µg/ml chloramphenicol, 2 mM L-tryptophan, and

0.05% (w/v) DDM. After incubation for 15 min at RT and 10 min on ice, the binding approach was loaded onto a 600 µl sucrose cushion (750 mM sucrose, 20 mM HEPES/KOAc, pH 7.2, 100-500 mM KOAc, 10 mM Mg(OAc)$_2$, 1 mM DTT, 0.5 mM PMSF, 5 mM Spermidin, 0.05 mM Spermin, 250 µg/ml chloramphenicol, 2 mM L-tryptophan, 0.05% (w/v) DDM) in an ultra clear SW55 centrifugation tube (5x41 mm, Beckman) and centrifuged in a Beckman SW55 rotor at 50,000x g for 6 hours at 4°C. Subsequently, the centrifugation tubes were flash-frozen in liquid nitrogen and cut into two parts using a scalpel, 2/3 of the supernatant and 1/3 of the pellet fraction. The resulting fractions were TCA-precipitated and subjected to SDS-PAGE analysis.

2.2.6 Protein precipitation and SDS-PAGE

Protein precipitation was used for the concentration of proteins out of highly diluted reaction mixtures. After adjusting the sample volume with water to 1 ml, 100 µl of both, 72% (w/v) trichlor acetic acid (TCA) and 0.15% (w/v) natrium deoxycholate were added. The reactions were incubated for 20 min at 4°C and then centrifuged for 15 min at 179,000x g. The resulting pellet was washed with ice-cold (-20°C) acetone, air-dried and subsequently resuspended in 10 µl 1x sample buffer.

In order to separate proteins according to their molecular weights SDS-PAGE (Sodiumdodecylsulfate polyacrylamide gel electrophoresis) was performed using standard protocols (Laemmli, 1970). Samples were denatured at 65°C for 10 min and loaded on 15% polyacrylamide gels. Electrophoresis was performed at constant voltage of 150-200 V in standard running buffer (25 mM Tris, 192 mM Glycine, 0.1% (w/v) SDS) for approximately one hour. The size of the proteins was determined by comparison with a broad range protein marker (BioRad). Gels were stained with Coomassie staining solution (50% (v/v) methanol, 10% (v/v) acetic acid, 0.25% (w/v) Coomassie Brilliant blue R-250) and subsequently destained with destaining solution (40% (v/v) methanol, 10% (v/v) acetic acid). For detection of smaller amounts of proteins (< 100 ng/0.5 cm lane), e.g. after reconstitution assays, gels were stained with SYPRO orange (1:5000) (Invitrogen) in 7.5% (v/v) acetic acid in the dark for 45 min, subsequently washed with 7.5% (v/v) acetic acid for 45 sec and finally transferred to water. For visualization and documentation a fluorescence scanner (Typhoon 9400, Amersham Biosciences) was used.

2.2.7 Western blot analysis

Western blot analysis was used for the detection of HA-tagged nascent chains to analyze the RNC purification or for the puromycin assay. Proteins were transferred onto a PVDF membrane (Roth) with a semi-dry blotting procedure in transfer buffer (20% (v/v) methanol, 50 mM Tris, 40 mM Glycine, 0.037% (w/v) SDS) for 45 min at 1 mA/cm^2 (50 mA). Afterwards, the membrane was stained for 1 min in Amido black (Merck), digitized, destained with destaining solution (40% (v/v) methanol, 10% (v/v) acetic acid) and blocked with 5% (w/v) milk (Roth) in TBS buffer (50 mM Tris/HCl, pH 7.5, 150 mM NaCl) for 30 min to prevent unspecific antibody interaction. The primary antibody (HA-probe (F-7) mouse ab, Santa Cruz Biotechnology) was used in a 1:500 dilution in 2% BSA in TBS and incubated overnight at 4°C. Excess of first antibody was removed by washing the membrane three times with TBS-T buffer (50 mM Tris/HCl, pH 7.5, 150 mM NaCl, 0.1% (v/v) Tween 20). As secondary antibody, goat anti-mouse IgG-HRP (Santa Cruz Biotechnology) was used at a dilution of 1:5000 in 5% (w/v) milk in TBS. The membrane was incubated with the secondary antibody for at least 1h at RT and then washed three times with TBS-T buffer. For the chemiluminescence reaction, the membrane was incubated for 1 min with ECL (Chemiluminescent Detection kit, AppliChem), followed by exposure of the membrane to light-sensitive films (GE Healthcare) and subsequent developing using a Kodak Xomat M35 developing machine.

2.2.8 Preparation of YidC2-proteoliposomes

2.2.8.1 Preparation of preformed liposomes

For the reconstitution of the membrane protein YidC2 into liposomes, first of all, preformed liposomes were prepared. Therefore, 1 ml of *E. coli* phospholipids (Avanti Polar Lipids) in chloroform (20 mg/ml) was dried in a rotary evaporator at 30°C for approximately 30 min. The dried lipids were resuspended at room temperature in 1 ml of proteoliposome buffer (50 mM Hepes-KOH, pH 7.2, 100 mM KOAc, 10 mM Mg(OAc)$_2$, 1 mM DTT) yielding a final concentration of 20 mg/ml. In order to generate small unilamellar vesicles (SUVs) the lipid suspension was sonicated in six cycles (15 sec on/ 45 sec off) at an intensity of 4 µm on ice water. Aliquots of 0.5 ml of the SUV suspension were flash-frozen in liquid nitrogen and subsequently slowly thawed (~ 30 min) at RT in a polystyrene box. This freezing-thawing

step was carried out all in all three times in order to fuse the SUVs to large multi-lamellar vesicles (LMVs). After the third freezing step, the LMVs could be stored in liquid nitrogen. For the formation of large unilamellar vesicles (LUVs) the LMVs were extruded eleven times through a 400 nm polycarbonate filter using a mini-extruder (Avanti Polar Lipids). Subsequently, the LUVs were diluted (1:5) in proteoliposome buffer with 25% (v/v) glycerol to obtain a final concentration of 4 mg/ml of lipids and 20% of glycerol.

2.2.8.2 Reconstitution of YidC2 into detergent-destabilized liposomes

For the reconstitution of YidC2 into detergent-destabilized liposomes, the LUVs were iteratively solubilized with the detergent Triton X-100. Therefore, the LUVs were titrated with 2 µl aliquots of 10% (w/v) Triton X-100 stock solution per 5 ml LUV suspension of 4 mg/ml. After each addition the tube was gently inverted, and the destabilization of the liposomes was monitored by measuring the optical density of the lipid-detergent suspension at 540 nm. When the liposomes were fully saturated with the detergent (the optical density reaches its highest value), another five aliquots of 10% (w/v) Triton X-100 were added. In order to yield 1:100 (w/w) protein-to-lipid reconstitutions, 40 µg of the purified membrane protein (YidC2 or SecYEG) were added to 1 ml of detergent-destabilized liposomes and incubated for 15 min at RT with gentle agitation. For 1 ml of protein-liposome suspension 160 mg BioBeads SM-2 adsorbents (BioRad) were washed in a series of solutions: (1) twice in methanol, (2) twice in ethanol, (3) twice in demineralized water, and (4) twice in proteoliposome buffer. Afterwards, the BioBeads were resuspended in 1 ml of proteoliposome buffer. In order to remove the detergent, 40 mg of BioBeads (250 µl) were added to 1 ml of the protein-detergent-phospholipid suspension and incubated for 30 min at RT with gently agitation. Subsequently, another 40 mg of BioBeads were added to the suspension and incubated for 60 min at 4°C. After addition of another 40 mg of BioBeads the protein-detergent-phospholipid suspension was incubated over night at 4°C with gently agitation. Finally, again 40 mg of BioBeads were added to the suspension and incubated for 120 min at 4°C. The BioBeads were subsequently removed from the suspension by using a Poly-Prep Chromatography Column (BioRad) where the proteoliposomes ended up in the eluate. The BioBeads were washed with approximately 10 ml of proteoliposome buffer to lower the glycerol concentration to 2%. Afterwards, the proteoliposomes were collected by ultracentrifugation at 125,000x g in the Ti45 rotor at 4°C for 60 min, and subsequently resuspended in 200 µl of proteoliposome buffer.

2.2.8.3 Discontinuous flotation gradient centrifugation

In order to remove nonincorporated and/or aggregated membrane proteins, the reconstituted proteoliposomes were subjected to discontinuous flotation gradient centrifugation. Therefore, 200 µl of the reconstituted sample was first deposited in a 30% sucrose layer in proteoliposome buffer in an ultra clear SW55 centrifugation tube (5x41 mm, Beckman) and then carefully covered with successive layers of 20, 15, and 10% sucrose solution, each with a volume of 100 µl. After centrifugation at 190,000x g in a SW55 rotor for 2.5 h, the upper third of the supernatant containing the floated proteoliposomes (visible as whitish layer) was centrifuged again in a TLA100 rotor at 100,000x g for 30 min. The resulting pellet was finally resuspended in 200 µl proteoliposome buffer, flash-frozen in liquid nitrogen and stored at -80°C. In order to reveal the concentration of the proteoliposomes, different sample volumes ranging from 5 to 20 µl were subjected to SDS-PAGE analysis and subsequent Coomassie stain.

2.2.9 Flotation binding assays

Flotation binding assays were based on a protocol by Birgitta Beatrix (Moller et al., 1998) and used for characterization of the binding of 70S ribosomes and MscL-RNCs, respectively, to YidC2-proteoliposomes. After *in vitro* reconstitution of the binding components, discontinuous flotation gradient centrifugation was used to separate the proteoliposome-bound fraction (supernatant) from the non-bound fraction (pellet).

For a typical 20 µl reconstitution reaction 6 pmol of ribosomes and 5-10 µl (~ 20 pmol) of YidC2-proteoliposomes were mixed in a ribosome binding buffer (RBB) (40 mM HEPES/KOAc, pH 7.2, 50 mM KOAc, 10 mM Mg(OAc)$_2$, 1 mM DTT, 0.5 mM PMSF, 250 µg/ml chloramphenicol, 2 mM L-tryptophan) and incubated for 90 min at 30°C. 205 µl of 2.3 M sucrose in RBB were added to the binding approach and deposited at the bottom of an ultra clear SW55 centrifugation tube (5x41 mm, Beckman). Subsequently, the sucrose layer was carefully covered with 360 µl 1.9 M sucrose in RBB and 115 µl RBB. After centrifugation in a Beckman SW55 rotor at 50,000x g for 1 hour at 4°C, the centrifugation tubes were flash-frozen in liquid nitrogen and cut into two parts using a scalpel, 1/3 of the supernatant and 2/3 of the pellet fraction. The resulting fractions were TCA-precipitated and subjected to SDS-PAGE analysis.

2.2.10 Dynamic Light Scattering

Dynamic Light scattering (DLS) can be used for the determination of a size distribution profile of particles in solution by measuring the speed at which these molecules move under Brownian motion. In a DLS system, a laser passes through a measuring cell containing the sample, and the intensity of light which is scattered by the sample is measured. Thereby, the scattering intensity varies since the particles in solution are constantly moving. With the help of the autocorrelation function, the hydrodynamic radii of the particles can be determined. This technique was used to determine a size distribution profile of the liposomes and YidC2-proteoliposomes, respectively. Therefore, each sample was measured in a 70 µl sample volume-quartz cuvette on an 802 DLS spectrometer (Viskotek Corp., Houston, USA). Analysis of the test readings were carried out using the software OmniSIZE^{TM}3.0.

2.3 Electron microscopy

2.3.1 Negative-stain electron microscopy

Negative-stain electron microscopy (EM) was used to visually inspect the proteoliposome-preparations, and to pre-analyze the samples prior to grid preparation for cryo-EM. After washing the carbon coated holey grids (Quantifoil) with chloramphenicol, the grids were glow discharged in a plasma cleaner chamber (Harrick, UK) at 0.22 torr for 45 sec. Within 20 min after glow discharging, 3.5 µl of the sample was applied to the glow discharged side of the cleaned grid while holding it with tweezers, and then incubated for 45 sec. Afterwards, the grid was washed with five drops of water and subsequently stained with three drops of 2% uranyl acetate (Ted Pella, Inc., USA) and incubated for 15 sec. In order to remove excess sample, the grid was dried with pre-cut blotting paper triangles by carefully sliding it along the tweezers while holding the paper perpendicular to the grid. Afterwards, the grid was placed onto blotting paper and dried for 5 min. Analysis of the negative-stain grids were carried out on a Spirit microscope (FEI Tecnai G12 Spirit 120 kV cryo-microscope) or on a Morgagni microscope (100 kV FEI Morgagni electron microscope).

2.3.2 Cryo-electron microscopy

2.3.2.1 Sample preparation

Reconstituted, empty *E. coli* 70S ribosomes (provided by Viter Marquez), TnaC-stalled 70S ribosomes, SecM-stalled 70S ribosomes, and SecM-stalled DP120-RNCs were thawed on ice and applied to the grids in a concentration of 4 OD/ml. For the reconstituted samples, 2 pmol of ribosomes and 20 pmol of purified ligand were mixed in a 20 µl volume using an appropriate compensation buffer to adjust the buffer conditions mentioned in Section 2.2.5. The reconstitution reactions were incubated for 15 min at RT and 10 min on ice, and subsequently applied to the grids.

2.3.2.2 Grid preparation

The carbon coated holey grids (Quantifoil) were washed with chloramphenicol and subsequently glow discharged using a plasma cleaner chamber (Harrick, UK) at 0.22 torr for 30 sec in order to make the carbon surface hydrophilic. 3.5 µl of the sample were applied to the glow discharged side of the grid and subsequently vitrified in liquid ethane using the half automated Vitrobot^{TM} system (FEI, Eindhoven, Netherlands) under controlled conditions (4 °C, 100% humidity, 45 sec incubation time, 10 sec blotting) (Wagenknecht et al., 1988). The grids were then transferred to a grid box for long-term storage in liquid nitrogen.

2.3.2.3 Data collection

Low resolution datasets were automatically collected on a Tecnai G2 Spirit field emission gun electron microscope (Spirit microscope, Munich) at 120 kV. For the high resolution datasets, micrographs were recorded on a Tecnai Polara F30 field emission gun microscope (Max-Planck Institute of Molecular Genetics, Berlin) operated at 300 kV using a magnification of 39,000. After transferring the frozen grids under liquid nitrogen conditions into the specimen holder of the microscope, suitable meshes were chosen by hand for data collection which was carried out under low-dose conditions (~ 20 electrons per Å^2) with an exposure time of 1 sec and in a defocus range between 1.0 µm and 4.5 µm. The micrographs were developed and subsequently digitized on a Heidelberg drum scanner resulting in a pixel size of 1.23 Å (5334 dpi) on the object scale, and finally saved as high resolution TIFF-files.

2.4 Image processing and three-dimensional reconstruction

All datasets were processed with the SPIDER software package (Frank et al., 1996). Firstly, the document micsuse.rib containing the list of all micrographs which were used for processing was created with the SPIDER command "doc create". Furthermore, an existing params.rib document was edited according to the used parameters, such as the pixel size or the used decimation factor which sums values of two neighbouring pixels and is the preferred way to reduce the size of the images.

2.4.1 Power spectra and defocus determination

The contrast transfer functions (CTFs) as well as the defocus values of all scanned micrographs were determined with the program CTFFIND (Mindell and Grigorieff, 2003) using the script p_ctffind.rib (ctffind.sh, p_readmrc.py). The script p_ctffind.rib firstly converts the tiff file format into the mrc file format which then can be used by the SPIDER software. The subscripts ctffind.sh and p_readmrc.py determine the defocus values of the micrograph and convert the p_ctffind.rib output file into the spider document file format, respectively. The defocus values for the micrographs were saved in the output document defocus.rib. The script p_ctffind.rib calculates the power spectra for each micrograph which then were visually inspected in WEB (part of the SPIDER software package). Micrographs with bad quality power spectra, *i.e.* power spectra displaying drift or astigmatism were deleted from the micsuse.rib document, and only images with information in the frequency range below 10 Å were used for further processing of the high resolution datasets.

2.4.2 Particle selection

In order to determine the orientation of individual particles (see next section) data processing was performed on each particle as a separate image. Therefore, up to 4000 single particles of each micrograph were isolated in the next step. Firstly, the script sig_decimate.rib was used to generate two times decimated micrographs with a pixel size of 2.46 Å since this increased the signal-to-noise ratio (SNR) and reduced the calculation time and power. Particles were automatically picked from the micrographs by a local correlation algorithm (Roseman, 2003) through a comparison with projections of a reference 3D volume using the sig_pick.rib script. Afterwards, the micrographs were loaded in SIGNATURE (Chen and Grigorieff, 2007), the

automatically picked particles manually evaluated, and the coordinates of the single particles saved. The script p_window.rib was used to cut the single particles out of the micrographs according to the saved particle coordinates. After filtering and decimation of the particles using the p_flt.rib script, all particles were visually inspected in WEB. Subsequently, bad particles were removed from the dataset whereas the good particles were renumbered using the p_copygood.rib script.

The defocus group document defgrp.rib, where the micrographs were sorted according to their defocus values, was generated using the script p_makedefgrpfile.rib. Afterwards, micrographs with similar defocus values were manually assigned to the same defocus group.

2.4.3 Initial particle alignment

Since the obtained electron microscopy images correspond to 2D projections of random oriented ribosomal particles, the determination of the exact relative orientation of each particle was the next step in image processing. Alignment was performed using the "projection matching" method (Penczek et al., 1994) where computationally generated projections of an existing structure were compared with the actual electron microscopy images. During the initial particle alignment using the p_alidef.rib script, particles were aligned to projections of an existing *E. coli* 70S ribosome. For each micrograph the reference volume was multiplied with the corresponding CTF function which depends on the defocus value of the micrograph. This resulted into distorted reference projections akin to the experimental obtained electron microscopy images. For the initial alignment particles were decimated by a factor of 3, and an angular accuracy of 15 degrees was used which generated 83 projections. Shifts in x and y directions were allowed to a maximum range to ensure correct positioning of the particles. The resulting apmq files contained the best fitting projection as well as the shift and rotation parameters for each particle which were necessary to match the projection.

2.4.4 Three-dimensional reconstruction

The obtained shift and rotation parameters of the initial particle alignment were applied in order to generate a new set of particles for the 3D reconstruction using the scripts p_spinnem.rib, p_rotate, and p_angles.rib. Finally, the bp3f_n.rib script was used for the back-projection of the particles. For each defocus group one volume was back-projected

containing all particles, and two additional volumes were created with two independent halves of all particles. All odd and even volumes were CTF corrected according to their defocus group and added up to create two volumes each containing half of the particles. These two volumes were compared, and the Fourier shell correlation (FSC) was calculated which was used for the resolution determination at a cut-off value of 0.5. The volumes which were generated with all particles in each defocus group were also CTF corrected and added up to a final volume. This resulting volume was masked and filtered to a proper resolution and used as a new reference in the following refinement procedure.

2.4.5 Refinement

Refinement is an iterative process of alignment and back-projection whereby the masked and filtered output volume of the previous round was used as a new reference volume for the next round of refinement. The aim of several refinement rounds was the improvement of the resolution of the dataset. Before starting this process, transformation files had to be created using the script p_maketrans.rib. These transformation files contained shifts and rotation parameters which have to be applied to the particles in order to match the reference projection. Since refinement was partially done with three times and two times decimated particles, respectively, the original undecimated particles were rotated and shifted after each refinement round using the transformation files in order to avoid a loss of information.

In the first round, particles were aligned to the volume created after the first back-projection whereby all possible references were offered to each particle, i.e. refinement without angular restriction was performed. In the next rounds filter parameter and alignment algorithms were varied so that the particles were compared only with reference projections inside defined angular restrictions. To allow a better alignment of the particles angular restriction and angular accuracy were slowly reduced in the following rounds resulting in an increased number of compared reference projections. Back-projections were generally carried out with the "bp32f" command which calculates 3D reconstructions faster in Fourier space, i.e. an alternative mathematical representation of an image that describes the image not as a density but with phases and amplitudes. During the last refinement rounds every micrograph displayed one defocus group, undecimated particles were used, and the back-projections were carried out with the "bprp" command which is using a slower real space back-projection algorithm resulting in higher resolution reconstructions.

2.4.6 Three-dimensional reconstruction and sorting of the datasets

For the high resolution dataset of the TnaC-stalled 70S ribosome 220 micrographs were recorded which after visual inspection of the power spectra resulted in 128 micrographs used for image processing. After automatic particle selection and subsequent visual inspection, approximately 346,000 single particles were aligned to projections of an existing empty *E. coli* 70S ribosome. Using an empty 70S ribosome as reference, the dataset was classified into two sub-datasets comprising 83,000 particles of empty 70S ribosomes and 263,000 particles of programmed ribosomes with density for peptidyl-tRNA. After sorting of the dataset, the 263,000 programmed ribosomes were used for further refinement rounds.

Approximately 400 micrographs were recorded for the high resolution dataset of the SecM-stalled 70S ribosome. After visual inspection of the power spectra, 254 micrographs were used for image processing. Automatic particle selection followed by visual inspection of the particles yielded 740,000 single particles which also were aligned to projections of an existing empty *E. coli* 70S ribosome. The dataset was sorted for the presence of peptidyl-tRNA using an empty 70S ribosome as reference, resulting in 383,000 particles of programmed ribosomes and 357,000 particles of empty 70S ribosomes. The remaining 383,000 particles of programmed ribosomes were used for further refinement.

2.5 Structural interpretation and modeling

After the reconstruction of the 3D structure in sufficient resolution structural analysis was carried out in order to answer specific biological questions. First of all, cryo-EM densities for the large and small ribosomal subunit, the P-site tRNA, the mRNA and the nascent chain were isolated using binary masks.

Structural interpretation and modeling of the TnaC-70S complex was done in collaboration with Daniel Wilson, Axel Innis (Yale University, USA), Elizabeth Villa (Max Planck Institute of Biochemistry, Germany), and Leonardo G. Trabuco (University of Illinois, USA). Initial models for the 30S and 50S subunits were based on models of the *E. coli* 70S ribosome by X-ray crystallography (Berk and Cate, 2007; Berk et al., 2006) and cryo-EM (Villa et al., 2009), which were then refined by molecular dynamics flexible fitting (MDFF) (Trabuco et al., 2008). The tRNA[Pro] and P-site mRNA codon were generated using PARADISE (http://paradise-ibmc.u-strasbg.fr/xwiki/bin/view/Main/) (Jossinet and Westhof, 2005) based

on the similarity with tRNA[fMet] and P-site codon from the X-ray structure of the *Thermus thermophilus* programmed 70S ribosome (Selmer et al., 2006) and then adjusted manually with Coot (Emsley and Cowtan, 2004). The CCA-Pro[24] position of the TnaC nascent chain was modeled based on an alignment with the *Haloarcula marismortui* 50S subunit in complex with CCA-pcb (Schmeing et al., 2005a; Schmeing et al., 2005b), where the Pro24 was obtained by simple mutation of Phe in the CCA-pcb ligand. The Cα model for the TnaC chain was built manually into the cryo-EM density using Coot. This was used for restrained conformational sampling by the program Rapper (de Bakker et al., 2006), side chains were modeled with SCWRL 3.0 (Canutescu et al., 2003), followed by MDFF with a fixed position for Pro24. An assembly of ten different backbone conformers for the TnaC peptide was generated with root-mean-square fluctuation (RMSF) of less than 2 Å for all Cα atoms. Furthermore, MDFF simulations of the nascent chain and the exit tunnel were carried out starting from various unbiased conformations. Visualization of cryo-EM maps and models was performed using VMD (Humphrey et al., 1996) and Chimera (Pettersen et al., 2004), and alignment of pdbs was performed using PyMol (http://www.pymol.org). All figures were prepared using the programs Chimera and PyMol.

III RESULTS

3.1 Structural insight into the TnaC stalling mechanism

The TnaC system in *E. coli* is one of the best biochemically characterized examples of nascent chain-dependent ribosome stalling. However, structural information regarding nascent chain behavior of the TnaC leader peptide in the ribosomal exit tunnel is necessary for a better understanding of the underlying mechanism. Therefore, cryo-EM and single particle analysis was used to reconstruct an *E. coli* 70S ribosome which was stalled during translation of the TnaC leader gene in the presence of inducing levels of free Trp.

3.1.1 Purification of a TnaC-stalled 70S ribosome complex

In order to get a high resolution cryo-EM structure of a TnaC-stalled 70S ribosome complex, the preparation of a homogenous sample was a prerequisite. Cloning of the stalling construct, ribosome nascent chain complex (RNC) formation and purification was carried out by our collaboration partner Axel Innis from the Steitz laboratory of the Yale University in New Haven, USA.

The stalling construct (Fig. 3.1A), containing the sequence of a calmodulin-binding peptide (cbp) affinity-tag, a hexahistidine-tag (His$_6$-tag) and the 24-residue leader peptide TnaC, was cloned into the pBAT4 vector (Peranen et al., 1996), yielding the pBAT4-cbpTnaC plasmid. A coupled *in vitro* transcription-translation reaction using a cell-free protein synthesis reaction mixture (Jewett and Swartz, 2004) and the pBAT4-cbpTnaC plasmid as a template was loaded onto a sucrose gradient and centrifuged in order to get the monosomal fraction (Fig. 3.1B). These ribosomes were then affinity-purified using the cbp affinity-tag (see Section 2.2.1). Non-programmed ribosomes ended up in the flow-through (FT) fraction whereas unspecific bound ribosomes could be eliminated in the washing steps (Fig. 3.1C). The TnaC-stalled RNCs were finally eluted from the calmodulin sepharose column using EGTA. All purification steps were carried out in the presence of 2 mM Trp. In the case of a control reaction where no template was added to the coupled *in vitro* transcription-translation reaction, as expected, no ribosomes could be eluted from the column (Fig. 3.1C).

Out of 5 ml cell-free protein synthesis reaction mixture approximately 40 pmol of concentrated TnaC-stalled RNCs could be purified. Subsequent negative-stain electron

microscopy (negative-stain EM) revealed that the quality of the prepared sample was suitable for cryo-EM and single particle analysis (data not shown).
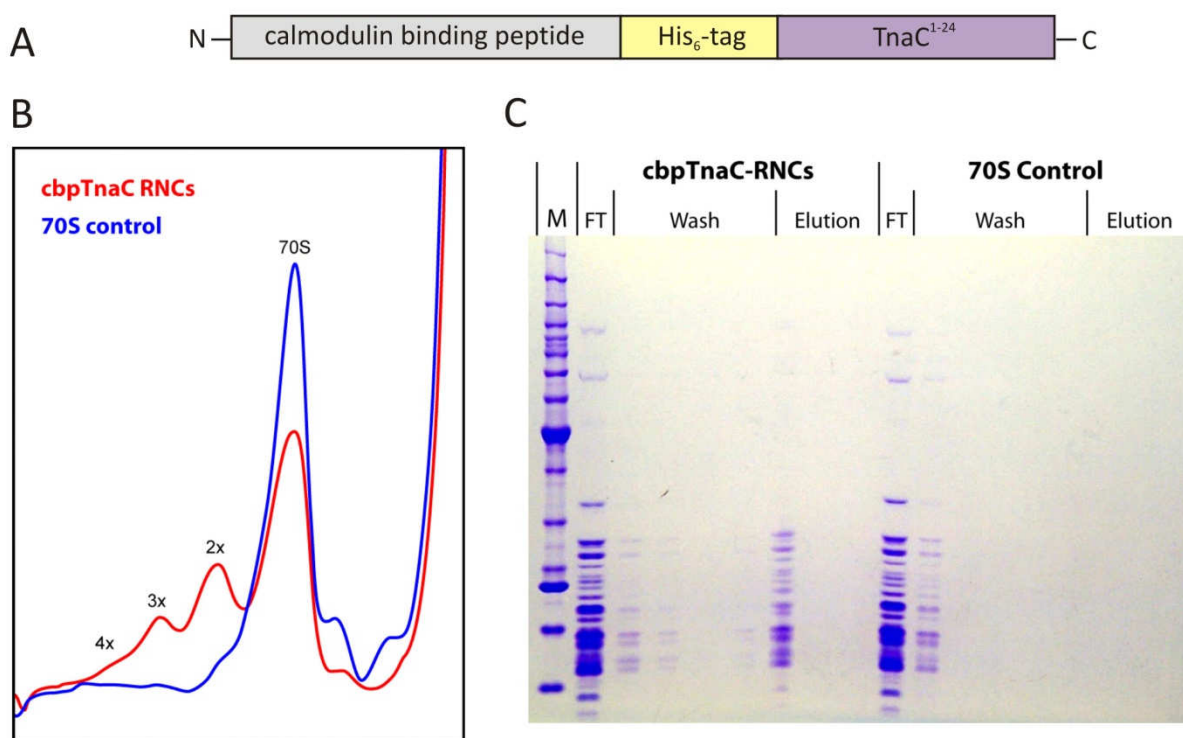

Figure 3.1: Purification of TnaC-stalled RNCs. (**A**) Schematic representation of the TnaC-stalling construct. (**B**) Chromatogram showing the A_{260} profile of the 10-40% sucrose gradient loaded with a cell-free protein synthesis reaction mixture programmed with pBAT4-cbpTnaC (red trace) and a control reaction with no added template (blue trace). (**C**) SDS-PAGE analysis of the flow-through (FT), wash and eluate fractions from the affinity purification of the monosomal fraction from B on a calmodulin sepharose column. 'M' stands for molecular weight marker and the two more intense bands in this lane correspond to 50 kDa and 20 kDa, respectively (figure B and C provided by Axel Innis).

3.1.2 Cryo-EM structure of the stalled TnaC-70S ribosome complex

After cryo-EM and 3D reconstruction an empty *E. coli* 70S control ribosome as well as a stalled TnaC-70S ribosome complex could be visualized successfully. The final 3D reconstruction of the empty 70S control ribosome contained approximately 93,500 particles and has a resolution of 6.6 Å, based on the FSC with a cutoff value of 0.5 (Fig. 3.2A). In order to obtain a homogeneous population of the TnaC-70S complex the dataset, containing approximately 346,000 single particles, was sorted according to the presence of peptidyl-tRNA. Only 24% of the particles showed no P-site tRNA, indicating that the purification of the TnaC-stalled ribosomes was highly efficient. The remaining 263,000 particles were used

for the final 3D reconstruction of the TnaC-70S complex, yielding a resolution of 5.8 Å according to the FSC 0.5 cut-off criterion (Fig. 3.2B).
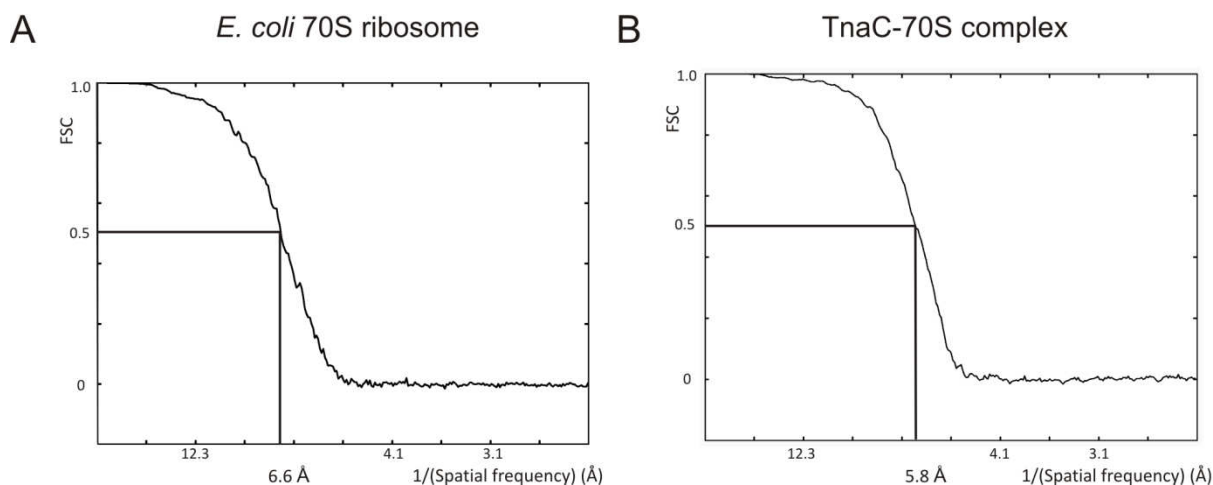
Figure 3.2: Resolution curves. FSC curves for the cryo-EM reconstruction of the (**A**) empty *E. coli* 70S ribosome, and (**B**) the TnaC-70S complex, showing that the resolution is 6.6 Å and 5.8 Å according to a cut-off of the FSC at 0.5, respectively. According to the more lenient 3σ criterion the resolution is 5.3 Å and 4.7 Å, respectively.

In order to verify the resolution suggested by the FSC 0.5 cut-off criterion, the TnaC-70S cryo-EM reconstruction was compared with the model for the X-ray structure of the *E. coli* 70S ribosome (Schuwirth et al., 2005) filtered to 7, 6 and 5 Å resolution (Fig. 3.3). Starting at 5 Å resolution it is possible to see phosphate bumps of RNA nucleotides (Fig. 3.3H) which are not resolved at lower resolutions. A comparison of the structural details in the area around Helix 19 (H19) in domain I of the 23S rRNA revealed that the density map of the TnaC-70S complex (Fig. 3.3E) mostly resembles the model for the X-ray structure of the *E. coli* 70S ribosome filtered to 6 Å resolution (Fig. 3.3G). Therefore, the TnaC-70S cryo-EM reconstruction has indeed a resolution of approximately 6 Å which is in agreement with the resolution suggested by the FSC 0.5 cut-off criterion.
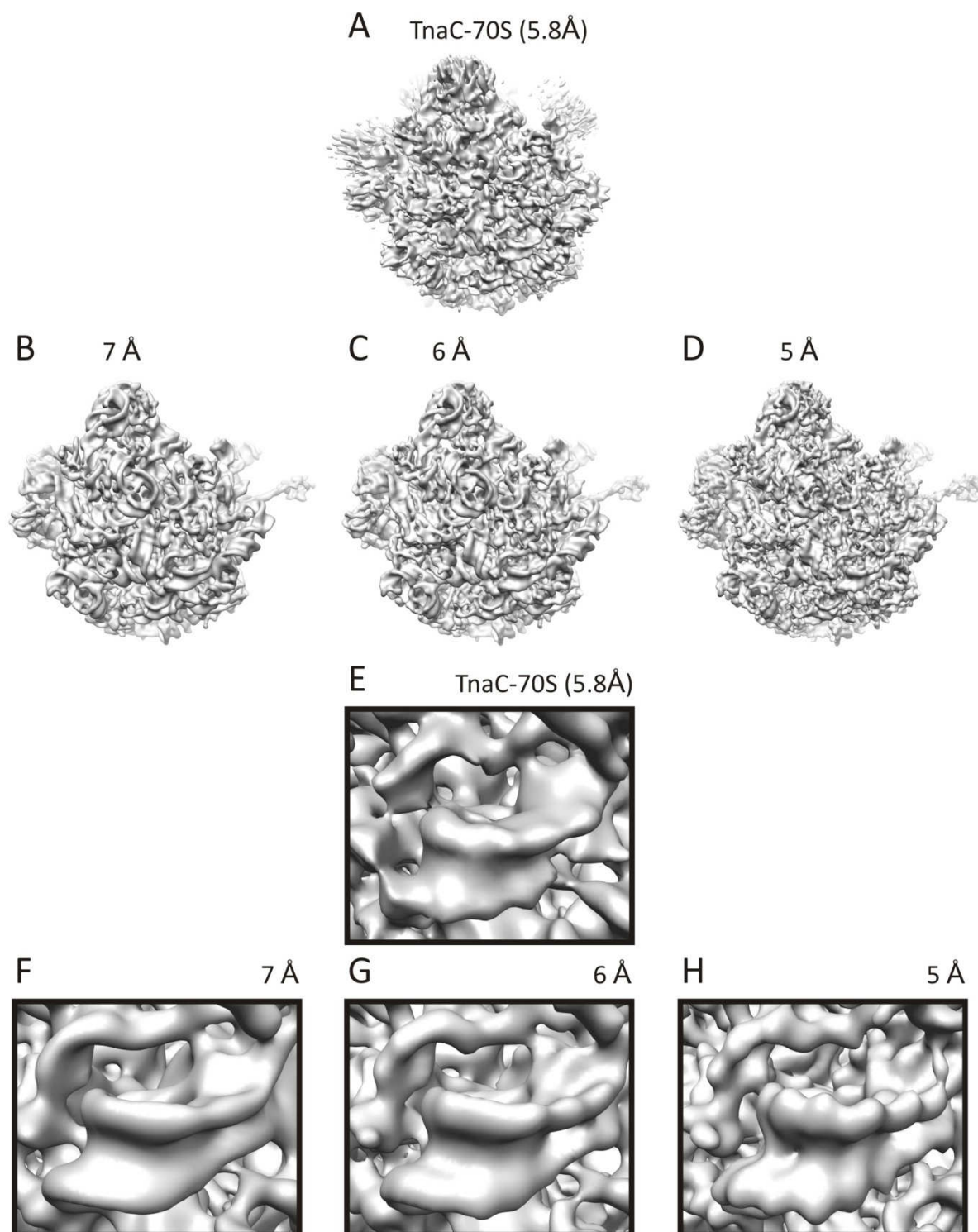
Figure 3.3: Comparison of the density map of the TnaC-70S complex with filtered models of the *E. coli* 70S ribosome. (**A**) View onto the back of the 50S subunit of the cryo-EM map of the TnaC-70S complex at 5.8 Å resolution. (**B**)- (**D**) Models for the *E. coli* 70S ribosomes (PDB2AW4; (Schuwirth et al., 2005)) filtered to (B) 7 Å, (C) 6 Å and (D) 5 Å resolution, and viewed as in (A). (**E**) Close up of density for the area around Helix 19 (H19) in domain I of the 23S rRNA in the cryo-EM map of the TnaC-70S complex. (**F**)- (**H**) Comparable view to (E) for the filtered maps from (B)- (D).

Both cryo-EM reconstructions have the typical appearance of an *E. coli* 70S ribosome, showing densities that can be attributed to the small and large ribosomal subunit, respectively

(Fig. 3.4A, C). In contrast to the empty 70S control ribosome (Fig. 3.4A), the TnaC-70S complex (Fig. 3.4C) reveals additional density for the mRNA (see Section 3.1.7) as well as a single peptidyl-tRNA within the intersubunit space.
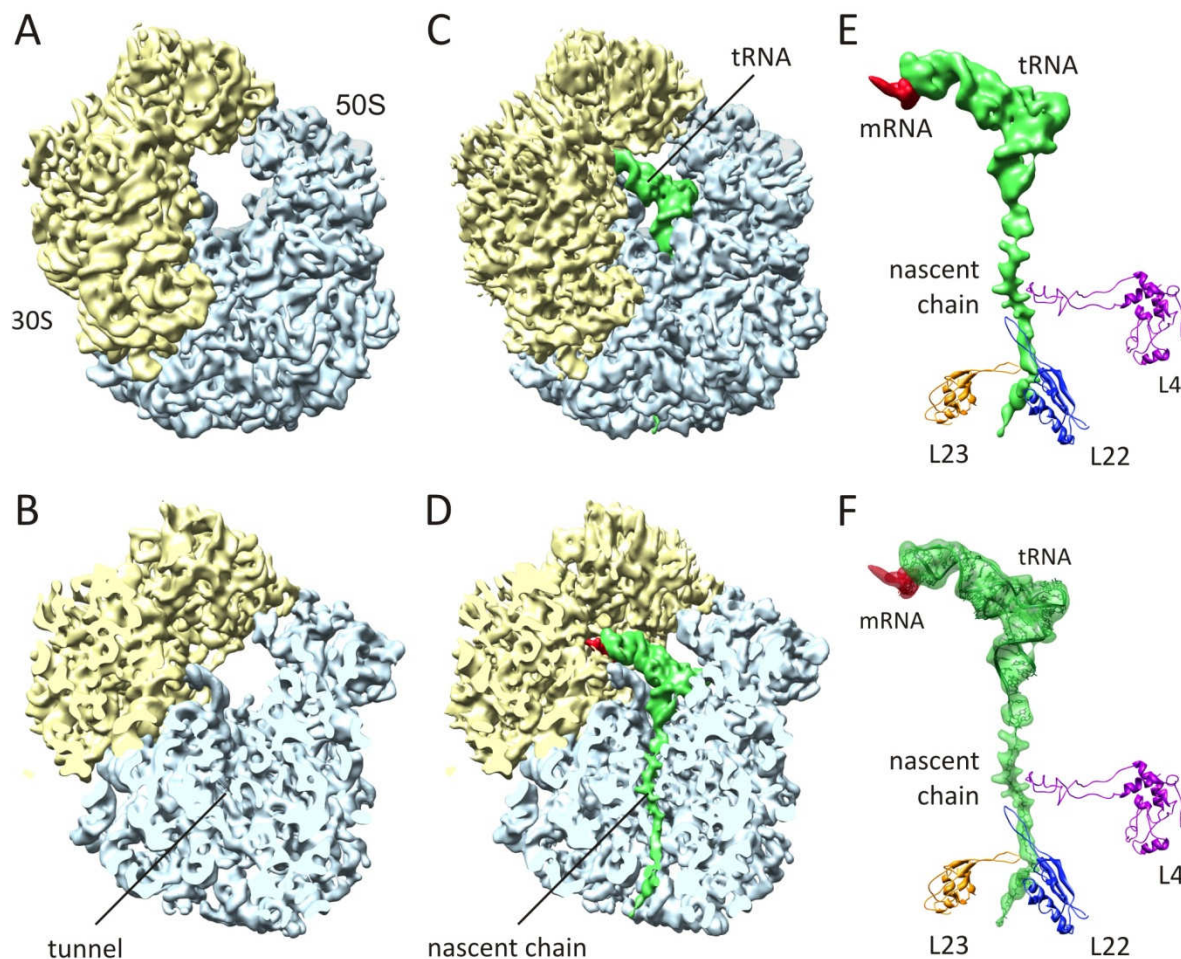
Figure 3.4: Cryo-EM reconstructions of the empty 70S control ribosome and the TnaC-70S complex. (**A**) Cryo-EM reconstruction of the control E. coli 70S ribosome at 6.6 Å resolution, with small and large subunit coloured yellow and blue, respectively. (**B**) Section through the empty ribosome in (A) to show the empty tunnel on the large subunit. (**C**) The 5.8 Å resolution cryo-EM density of the TnaC-70S complex, with additional density for P-site tRNA shown in green. (**D**) Section through the TnaC-70S ribosome in (C) to show the presence of a nascent chain (green) within the exit tunnel. (**E**) Isolated density for the P-site tRNA, associated nascent chain (green), and mRNA (red) from (C). The relative positions of ribosomal proteins L4 (purple), L22 (blue) and L23 (orange) are indicated. (**F**) Fitting of molecular models for the Pro-tRNA^{Pro} and TnaC nascent chain into the cryo-EM density from (E).

Remarkable, however, is the presence of additional density within the ribosomal exit tunnel in the TnaC-70S complex that can be attributed to the TnaC nascent polypeptide chain (Fig. 3.4D). As expected, the tunnel of the 70S control ribosome (Fig. 3.4B) is indeed empty.

The observed nascent chain density within the exit tunnel is dependent on the displayed contour level which generally defines boundaries of a molecule for visualization. Strong features are also visible at high contour levels whereas weak features, like noise, disappear. In the case of the TnaC-stalled ribosome, even at high contour levels, robust density for the C-terminal half of the nascent chain is visible (Fig. 3.5A, B), which becomes continuous throughout the entirety of the tunnel at lower contour levels (Fig. 3.5E, F). Therefore, the TnaC nascent chain is a strong feature of the cryo-EM reconstruction of the TnaC stalled ribosome. This density was used to fit a molecular model of all 24 amino acids of the TnaC leader peptide using the molecular dynamics flexible fitting (MDFF) method (Trabuco et al., 2008) (Fig. 3.4F).
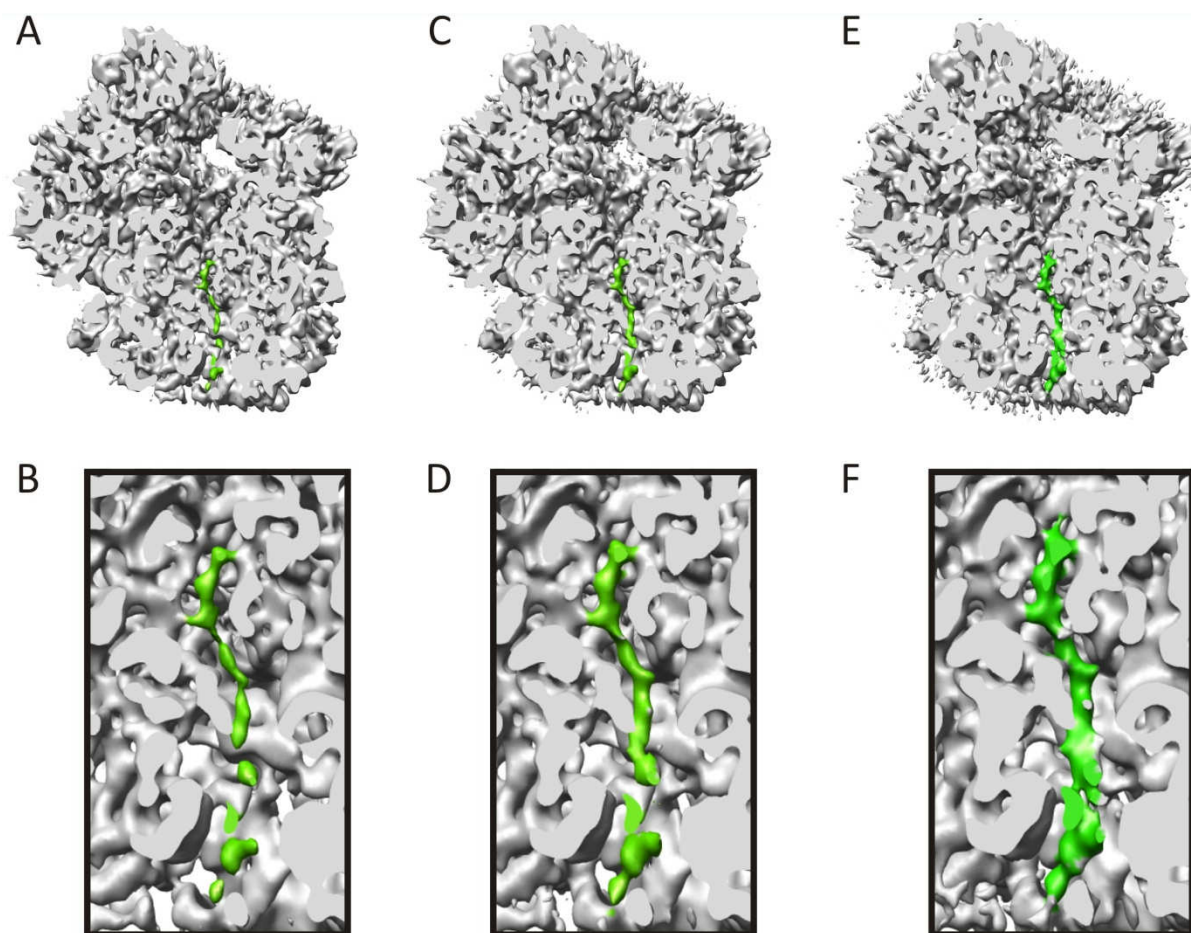
Figure 3.5: Visualization of the TnaC nascent chain within the exit tunnel of the cryo-EM map of the TnaC-70S complex at three different contour levels. (**A**, **C**, **E**) Section through the 5.8 Å TnaC-70S complex, showing the nascent chain (colour-zoned green) within the ribosomal exit tunnel at decreasing contour levels. (**B**, **D**, **F**) Enlargement of the exit tunnel region from (A, C, E).

3.1.3 The TnaC nascent chain adopts an extended conformation
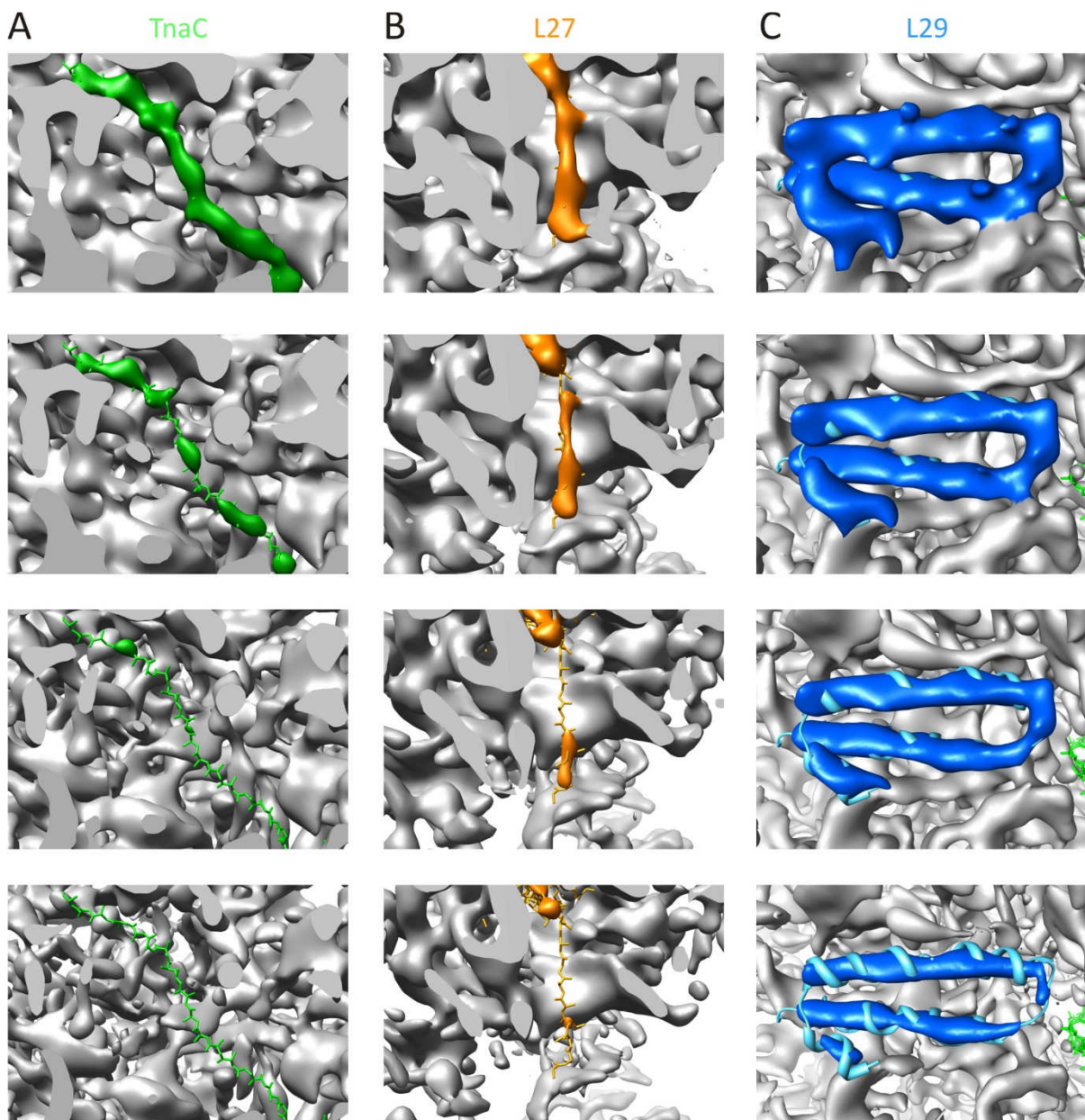
Figure 3.6: Comparison of the cryo-EM density of TnaC and ribosomal proteins L27 and L29.
(**A**) A series of four panels at different contour levels showing the same section through the 5.8 Å
TnaC-70S complex to reveal the nascent chain (colour-zoned green) within the exit tunnel. The model
for the TnaC nascent chain (green) is included for reference. (**B**) Density for the extended N-terminal
region of ribosomal protein L27 (colour-zoned orange) shown at identical contour levels as for TnaC
in (A). The fitted model for L27 (orange) is shown as reference. (**C**) Density for the highly α-helical
ribosomal protein L29 (colour-zoned blue) shown at identical contour levels as for TnaC in (A) and
L27 in (B). The fitted model for L29 (cyan) is included for reference.

In order to determine whether the TnaC nascent chain adopts an extended or an α-helical
conformation within the ribosomal exit tunnel, the cryo-EM density of the TnaC nascent
chain was compared with both the extended N-terminal region of ribosomal protein L27 and

the α-helical protein L29 at four different contour levels (Fig. 3.6). The higher the displayed contour level the less density for the extended N-terminal region of ribosomal protein L27 is visible (Fig. 3.6B). In the case of the α-helical ribosomal protein L29 clearly more density is visible at the same displayed contour level (Fig. 3.6C bottom) when compared to the extended region of L27. The observed cryo-EM density for the TnaC nascent chain (Fig. 3.6A) displays properties similar to the extended N-terminal region of ribosomal protein L27 but different from the α-helical ribosomal protein L29. Therefore, the TnaC nascent chain adopts an extended conformation within the ribosomal exit tunnel.

3.1.4 Nascent chain-ribosome interactions within the exit tunnel

Since not only several features of the amino acid sequence of the TnaC nascent peptide have been identified to be crucial for ribosome stalling but also specific nucleotides and amino acids that form the ribosomal exit tunnel (see Section 1.3.1), it has been suggested that the TnaC nascent chain interacts with ribosomal tunnel components (Cruz-Vera et al., 2007). Inspection of the ribosomal exit tunnel of the TnaC-70S complex actually revealed that the density for the TnaC nascent chain fuses with the tunnel wall at a multitude of sites. These contact sites are distributed along the entire length of the tunnel and vary depending upon the contour level (Table 3.1 and Fig. 3.7). Due to the fact that the resolution of the TnaC-70S cryo-EM reconstruction is limited to 5.8 Å, all subsequent analyses were restricted to the backbone trace of the TnaC leader peptide.

Table 3.1: Contacts between TnaC nascent chain and components of the ribosomal exit tunnel.

TnaC Nascent chain residue[*1]	Ribosomal contact partner[*2]	Ribosomal component	Threshold value (σ)[*3]
+3-(-1)	A508	23S rRNA	2.4
Asn2	A492/G493	23S rRNA	2.5
Asn2	A1321	23S rRNA	continuous
Leu4	His9	L22	2.8
His5	Gly71	L23	1.3
Cys7	Arg84	L22	1.0
Thr9	Arg95	L22	2.5
Lys11	Arg67	L4	1.6
Trp12[*4]	**Arg92[*4]**	L22	2.2
Phe13	**A751[*4]**	23S rRNA	2.5
Asn14	Gly64-Thr65	L4	1.3
Asp16[*4]	U747	23S rRNA	1.9
Asp16[*4]	**A2058-A2059[*4]**	23S rRNA	2.0
Lys18[*4]	**U2609/A752[*4]**	23S rRNA	3.8

Ile19	**A2058-A2059**[*4]	23S rRNA	3.0
Asp21	U2586/U1782	23S rRNA	3.4
His22	A2062	23S rRNA	3.9
Arg23	G2061	23S rRNA	4.0
Arg23-Pro24	G2505-U2506	23S rRNA	2.2
Pro24[*4]	U2585	23S rRNA	2.1

[*1]Positions are approximate, so the closest residue(s) to the contact site are given, based on MDFF fitting of TnaC nascent chain to cryo-EM density

[*2]Positions are approximate, but the closest components to the contact are given based on MDFF fitting of *E. coli* 70S crystal structure to TnaC-70S cryo-EM density.

[*3]The sigma threshold value provides a relative measure of the strength of the connection, such that the higher the sigma value the stronger the density connection between nascent chain and tunnel wall.

[*4]Residues of the nascent chain or components of the ribosome that have been implicated in TnaC mediated stalling are highlighted in grey.

At the PTC, additional density is observed connecting Pro[24] of TnaC and U2585 of the 23S rRNA (Fig. 3.7A), whereas the neighbouring U2586, together with U1782, appear to form a connection in the region where Asp[21] is likely to be located (Fig. 3.7A). Mutations of 23S rRNA nucleotides in the U2585 region have been shown to reduce the maximum induction of *tna* operon expression *in vivo*, but without reducing the affinity for Trp (Yang et al., 2009). It is also known that the carboxyl-terminal residue of TnaC, Pro[24], is highly conserved and essential for ribosome stalling, since Pro24Ala mutations abolish the Trp-dependent inhibition of TnaC-tRNA cleavage at the PTC (Cruz-Vera and Yanofsky, 2008). Very strong density links G2061 and A2062 to the region near residues Arg[23] and Asp[21], respectively, of the TnaC nascent chain (Fig 3.7B). Although A2062 has not been analyzed for its effects on TnaC stalling, mutations at this position have been shown to relieve the translational arrest mediated by the ErmC leader peptide (Vazquez-Laslop et al., 2008).

Deeper in the tunnel, two connections can be observed linking A2058 and A2059 with the TnaC nascent chain close to the presumed location of residues Asp[16] and Lys[18] (Fig. 3.7C). This may explain the protection of these nucleotides from sparsomycin-enhanced chemical modification caused by the methylation agent dimethyl sulfate (DMS) in the presence of Trp (Cruz-Vera et al., 2006). Asp[16] is highly conserved within the TnaC leader peptide and was shown to be also important for TnaC stalling, since Asp16Ala mutations abolish the Trp-dependent inactivation of the PTC (Cruz-Vera and Yanofsky, 2008). Ribosomes with A2058G mutations are slightly more responsive to Trp-induced stalling in the rrn Δ6 strain, which contains one out of seven wild-type *rrn* (*ribosomal RNA*) operons on its chromosom and was used to rule out general effects of mutant rRNAs on protein synthesis (Cruz-Vera et al., 2005). In contrast, the same mutation strongly reduces secM-mediated translational stalling (Nakatogawa and Ito, 2002). Strong density that extends out from the TnaC nascent

chain at the presumed location of Lys[18] fuses with the ribosomal tunnel where U2609 and A752 are located (Fig. 3.7C). The adjacent nucleotide A751, however, appears to contact the TnaC peptide in the vicinity of Phe[13] (Fig. 3.7C). Consistently, inserting an adenylate at position 751 or introducing the change U2609C in the 23S rRNA have been reported to eliminate Trp-mediated induction (Cruz-Vera et al., 2005).
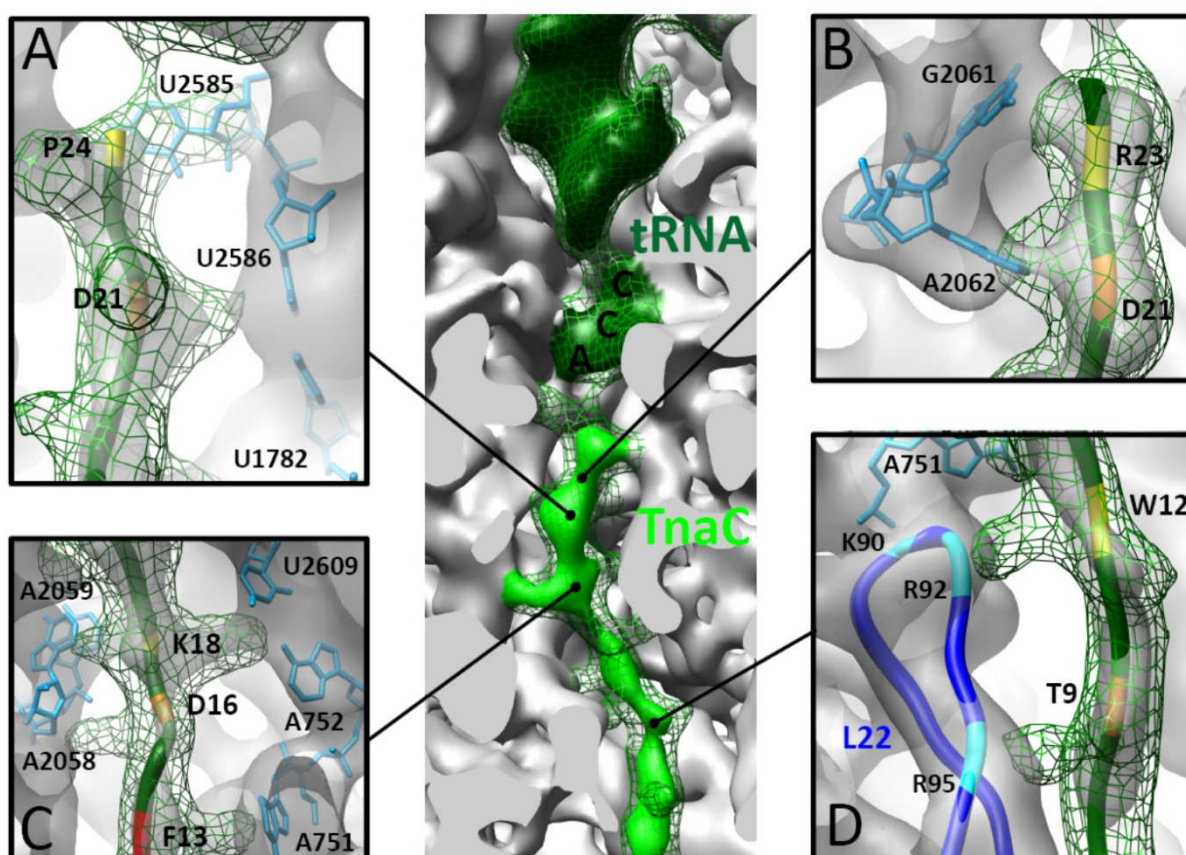
Figure 3.7: Interaction between the TnaC nascent peptide chain and the ribosomal tunnel. The central panel shows a section through the large ribosomal subunit revealing contact points between the TnaC nascent chain (light green) and the ribosomal tunnel (grey). Density attributed to the P-site tRNA is coloured dark green and the position of the CCA-end is indicated. Density for the P-site tRNA and TnaC nascent chain at a lower contour level is shown as a green mesh. (**A**)- (**D**) Different views of selected connections between the TnaC nascent chain (green ribbon) and nucleotides of the 23S rRNA (blue sticks) or ribosomal protein L22 (blue ribbon). The cryo-EM density map of the TnaC-70S complex is shown as a transparent grey surface, whereas the isolated TnaC nascent chain at a lower contour level is shown as a green mesh. Residues of the TnaC nascent chain closest to the tunnel wall connection are highlighted yellow, orange or red.

The TnaC nascent chain makes two major contacts with the β-hairpin of ribosomal protein L22 (Fig. 3.7D): One connects Arg[95] of L22 with the nascent chain near the putative location of Thr[9], whereas the other is found at the tip of the loop, where Lys[90] and Arg[92] are located, and fuses with TnaC in the vicinity of the highly conserved Trp[12] residue. This latter contact should be important for TnaC-stalling since mutations of Trp[12] in TnaC as well as Lys[90] in

L22 have been shown to eliminate Trp-mediated induction (Cruz-Vera et al., 2005). Another hint for its importance comes from the observation that the spacing between Trp[12] and Pro[24] is also critical for efficient stalling (Cruz-Vera and Yanofsky, 2008; Cruz-Vera et al., 2005; Gong and Yanofsky, 2002a). Crosslinks between the neighbouring Lys[11] with 23S rRNA nucleotides in the vicinity of A751, which also makes contact with the tip of L22, provide an additional evidence for the close proximity of Trp[12] to the tip of the β-hairpin of L22 (Cruz-Vera et al., 2005).

3.1.5 Distinct conformations of nascent chains within the ribosomal exit tunnel

As already mentioned (see Section 1.2.3), the surface of the ribosomal exit tunnel is predominantly hydrophilic and contains no significantly large hydrophobic parts in order to interact with hydrophobic sequences within translating nascent chains. While this general non-stick characteristic of the exit tunnel may be the case for the majority of nascent chains, recent biochemical studies indicate that peptides containing multiple positively-charged residues can cause transient pausing during translation elongation (Lu and Deutsch, 2008). Although the N-terminal region of the used TnaC stalling construct (Fig. 3.1A) is not native to the real TnaC sequence, the nascent chain makes extensive interactions with the ribosome along the entire length of the exit tunnel (Fig. 3.8A). The visualization of density for approximately 10 additional N-terminal amino acids indicates that even residues unrelated to the stalling process can adopt a distinct conformation by establishing specific interactions with components of the exit tunnel. In order to verify this hypothesis, the path of the TnaC nascent chain within the ribosomal exit tunnel was compared with a recently solved cryo-EM structure of a yeast 80S RNC complex at 6.1 Å resolution, which was stalled during translation of a truncated dipeptidyl-aminopeptidase B (DP120) mRNA (Fig. 3.8B) (Becker et al., 2009). Although the DP120 sequence has no stalling capacity, density for this nascent chain is visible, indicating a preferred conformation within the exit tunnel. Moreover, the path that the DP120 nascent chain follows within the ribosomal exit tunnel clearly differs from the path of the TnaC nascent chain (Fig. 3.8C, D). Accordingly, different nascent chains, which have little or no sequence conservation, can interact with the exit tunnel in a distinct manner and adopt individual conformations.
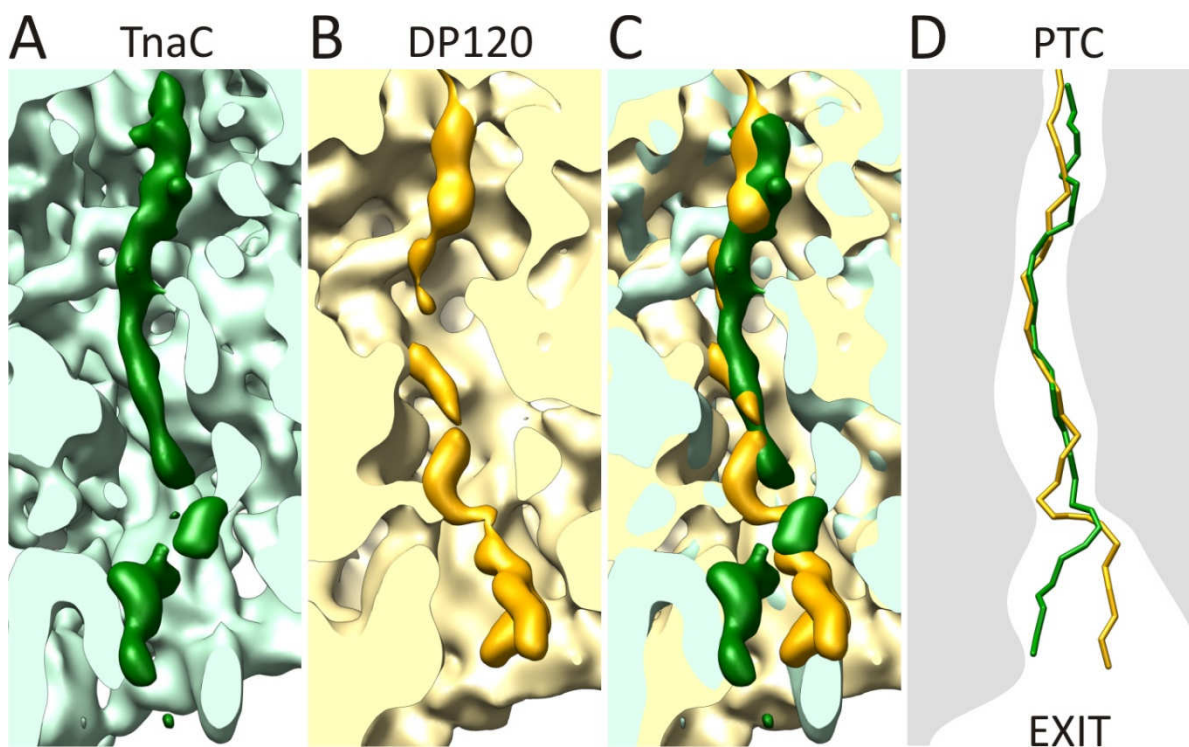
Figure 3.8: Comparison between the paths of TnaC and DP120 nascent chains through the ribosomal tunnel. (**A**) Section through the large subunit (light green) showing the path of the TnaC nascent chain (dark green) through the ribosomal tunnel. (**B**) Section through the large subunit (yellow) showing the path of the DP120 nascent chain ((Becker et al., 2009); orange) through the ribosomal tunnel. (**C**) Superposition of (A) and (B). (**D**) Schematic highlighting the similarities and differences between the TnaC and DP120 nascent chain in terms of contacts and passage through the tunnel.

3.1.6 Inactivation of the peptidyl transferase center

The PTC of the ribosome catalyzes both peptide bond formation and peptidyl-tRNA hydrolysis. In the case of the TnaC-stalled ribosome hydrolysis of the nascent TnaC-tRNA^{Pro} is prevented (Gong and Yanofsky, 2002a). In order to understand the inhibition of the hydrolytic activity it was important to examine the conformation of the PTC in the cryo-EM reconstruction of the TnaC-70S complex (Fig. 3.9).

Precise positioning of the CCA-ends of A- and P-site tRNAs at the PTC is necessary to ensure efficient peptide bond formation (Fig. 3.9A). Specific conformational changes of highly conserved nucleotides of the 23S rRNA within the PTC are associated with binding of different ligands to the PTC. For example, it has been observed that the two most flexible nucleotides in the PTC, A2602 and U2585, adopt dramatically different conformations in ribosome structures of various functional states (Fig. 3.9B) (Schmeing et al., 2005a). Since these two nucleotides are important for the peptide release function of the PTC (Polacek et al.,

2003; Youngman et al., 2004), their conformation in the TnaC-70S complex was examined (Fig. 3.9 C) and compared with the situation in a control RNC-70S complex stalled by truncation of the mRNA (Halic et al., 2006) (Fig. 3.9D). In both cases, density accounting for the P-site tRNA and surrounding 23S rRNA nucleotides can be observed, with the exception for the universally conserved A2602. This nucleotide appears to be disordered in the control RNC-70S complex (Fig. 3.9D) whereas clear density for A2602 is visible in the TnaC-70S complex indicating that A2602 adopts a distinct conformation (Fig. 3.9C). This conformation resembles the position that A2602 also adopts when the translation inhibitor sparsomycin is bound at the PTC (Schmeing et al., 2005b). In addition to A2602, continuous density between the nascent chain and the location of U2585, suggests that this flexible base (see Fig. 3.9B) shifts to interact with Pro[24] of the TnaC nascent chain (Fig. 3.9C).
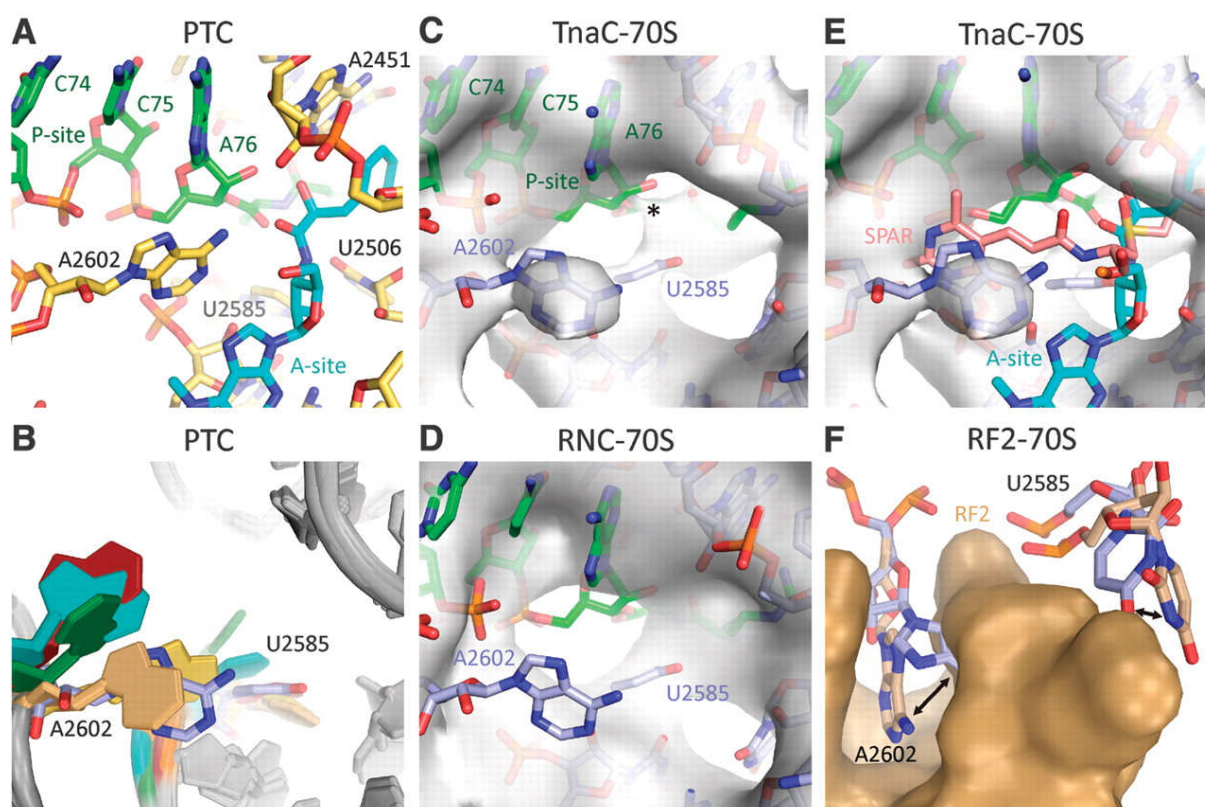
Figure 3.9: Silencing of the peptidyl transferase center (PTC). (**A**) Conformation of 23S rRNA nucleotides at the PTC when tRNA CCA-end mimics are bound to A- (cyan) and P-sites (green) (PDB1VQN, (Schmeing et al., 2005a). (**B**) Comparison of positions of A2602 from various ribosome crystal structures (red, PDB1VQK, (Schmeing et al., 2005b); teal, PDB1S72, (Klein et al., 2004); yellow, PDB2I2T, (Berk et al., 2006); gold, PDB3D5A/B, (Laurberg et al., 2008); blue, PDB1VQ9, (Schmeing et al., 2005b); green, PDB1VQN, (Schmeing et al., 2005a)). (**C**) View into the PTC of the TnaC-70S complex, with the fitted model of the CCA-Pro of the P-site tRNA (green) and nucleotides of the 23S rRNA (blue) from PDB1VQ9 (Schmeing et al., 2005b) shown as sticks. The density map is shown as a transparent grey surface, with an asterisk indicating the density connecting the tRNA with the nascent chain. (**D**) View into the PTC of 70S-RNC complex (Halic et al., 2006), with fitted models as in (A). Note the lack of density (grey) for nucleotide A2602. (**E**) As in (A), but with the antibiotic sparsomycin (SPAR, red; PDB1VQ9; (Schmeing et al., 2005b)) and the terminal A76 and aminoacyl

59

moiety of an A-site tRNA (A-site, cyan; PDB1VQN; (Schmeing et al., 2005a)) included. (**F**) Comparison of A2602 and U2585 positions (arrowed) between TnaC-70S complex (blue) and RF2-70S complex (gold;(Weixlbaumer et al., 2008), with RF2 shown as surface representation (gold).

Inactivation of the PTC in the TnaC-stalled ribosome requires free Trp, whose binding site has been proposed to overlap with that of the antibiotic sparsomycin (Cruz-Vera and Yanofsky, 2008; Cruz-Vera et al., 2006; Cruz-Vera et al., 2007). Furthermore, binding of Trp-tRNA at the ribosomal A-site can also induce TnaC stalling in the absence of free Trp, leading to the suggestion that the free Trp molecule binds where the aminoacyl-moiety of an A-site tRNA is located at the PTC (Gong and Yanofsky, 2002a), which also overlaps with the sparsomycin binding site. Nevertheless, no additional density that could be attributed to the free Trp molecule is observed within the sparsomycin-binding site, or in the A-site of the PTC (Fig. 3.9E).

The observed conformations of A2602 and U2585 in the TnaC-70S complex are not compatible with simultaneous cohabitation of termination release factor 2 (Weixlbaumer et al., 2008) (Fig. 3.9F). Therefore, the RF-promoted hydrolysis and release of the nascent chain from the P-site tRNA cannot occur, i.e. the PTC is in an inactive conformation.

3.1.7 The decoding site on the 30S subunit of the TnaC-70S complex

The decoding center of the 30S ribosomal subunit mediates the correct base pairing between anticodons of aa-tRNAs and codons in the mRNA. Thereby, discrimination against non-cognate tRNA, which generally has two or three mismatches, near-cognate tRNA, which usually involves a single mismatch, and cognate tRNA is very important for the accuracy of protein synthesis. The decoding site is a region around the ribosomal A-site that includes helix 44, the 530 loop, and helix 34 of 16S rRNA (Ogle et al., 2001). An internal loop of helix 44 contains two universally conserved bases, A1492 and A1493, which were shown to be essential for A-site tRNA binding (Yoshizawa et al., 1999). It has been suggested that during decoding, these bases would flip out from their stacked position inside the internal loop into the minor groove of the codon-anticodon helix, in a way that would allow discrimination of cognate from near-cognate tRNA (Carter et al., 2000).

Inspection of the decoding site of the TnaC-70S cryo-EM reconstruction revealed additional density that can be attributed to the mRNA of the transcribed TnaC leader sequence. The density for the mRNA spans the A-, P- and E-sites of the ribosome (Fig. 3.10). Furthermore, the region around the two universally conserved bases, A1492 and A1493, could be assigned

unambiguously, and compared to a control RNC-70S complex stalled by truncation of the mRNA (Halic et al., 2006) (Fig. 3.11).
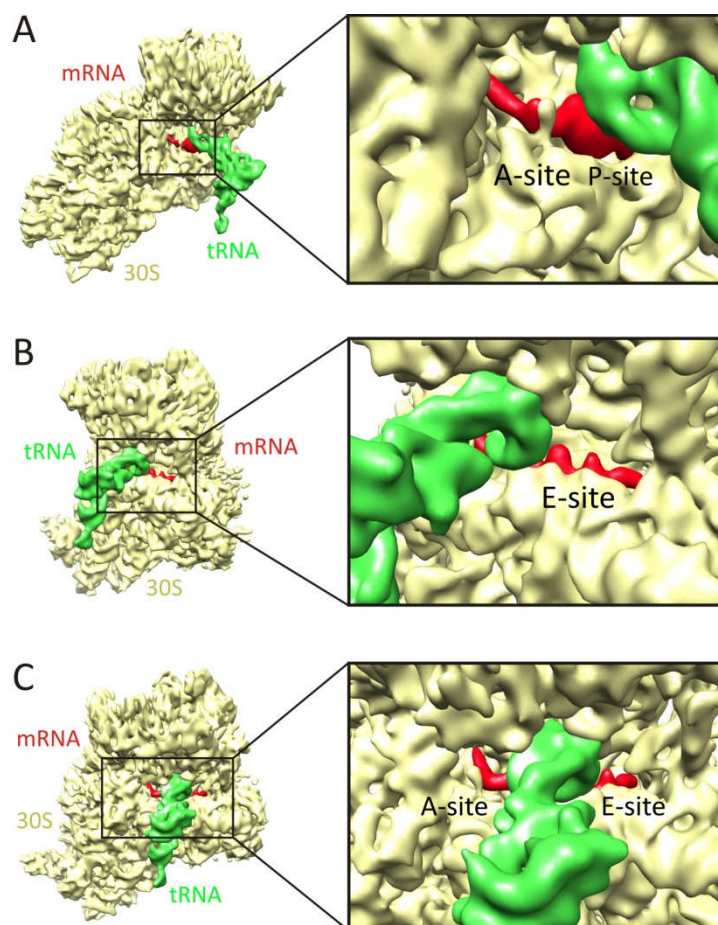
Figure 3.10: Visualization of density for the mRNA in the cryo-EM map of the TnaC-70S complex. (**A**) View into the A-site of the 30S subunit (yellow) of the cryo-EM map of the TnaC-70S complex, with density for the mRNA and P-site tRNA coloured red and green, respectively. (**B**) View into the E-site of the 30S subunit (yellow) of the cryo-EM map of the TnaC-70S complex, with density for the mRNA and P-site tRNA coloured red and green, respectively. (**C**) Simultaneous view into A- and E-sites of the 30S subunit (yellow) of the cryo-EM map of the TnaC-70S complex, with density for the mRNA and P-site tRNA coloured red and green, respectively.

In the case of the control RNC-70S complex, both A1492 and A1493 are located within the density of helix 44 (Fig. 3.11A). Here, density is visible for the P-site codon of the mRNA but not for the A-site codon (Fig. 3.11B). This observation is consistent with the fact that the RNC-70S complex was stalled using truncated mRNA lacking a stop codon (Halic et al., 2006). In the cryo-EM reconstruction of the TnaC-stalled ribosome, a hole in the density for helix 44 is visible (Fig. 3.11C) indicating that the density attributed to the universally conserved nucleotide A1493 has flipped-out of the internal loop of helix 44 in order to interact with the A-site codon of the mRNA. In contrast to the control RNC-70S complex, density is present for both A- and P-site codons of the mRNA (Fig. 3.11D), which is consistent with the fact that the TnaC-70S complex was stalled using the TnaC leader sequence with a stop codon in the A-site.
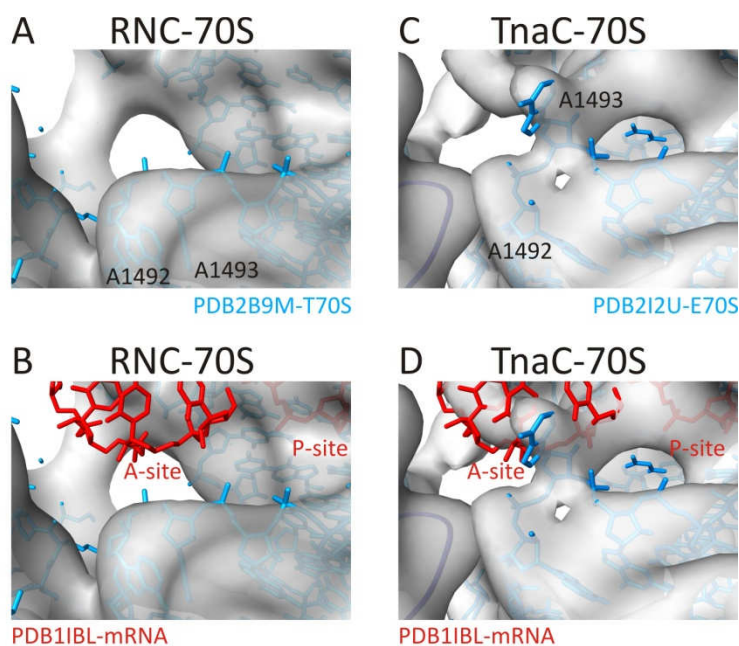
Figure 3.11: Comparison of the conformation of A1493 in the A-site of RNC-70S and TnaC-70S complexes. (**A**) View into the A-site of the RNC-70S complex (Halic et al., 2006), with cryo-EM map (grey) and fitted models for the 30S subunit (blue, PDB2B9M; (Petry et al., 2005)). (**B**) Same as (A), but with location of mRNA (red) in A- and P-site (PDB1IBL; (Ogle et al., 2001)). (**C**) View into the A-site of the TnaC-70S complex, with cryo-EM map (grey) and fitted model for the 30S subunit (blue, PDB2I2U; (Berk et al., 2006)). (**D**) Same as (C), but with location of mRNA (red) in A- and P-site (PDB1IBL; (Ogle et al., 2001)).

3.2 Structural analysis of the SecM stalling mechanism

After the successful elucidation of the cryo-EM structure of a TnaC-stalled 70S ribosome complex, structural analysis of the SecM stalling mechanism in *E. coli* was the next goal in this study in order to compare the two biochemically well-characterized examples of nascent chain-dependent ribosome stalling in prokaryotes. Although a cryo-EM structure of a SecM-stalled *E. coli* ribosome is already existent, where the authors claim that they could visualize the nascent chain within the ribosomal exit tunnel (Mitra et al., 2006; Mitra et al., 2005), the resolution of ~ 15 Å is not sufficient to analyze the SecM stalling mechanism in detail. Therefore, cryo-EM and single particle analysis was used to reconstruct an *E. coli* 70S ribosome which was stalled during translation of the SecM stalling sequence.

3.2.1 Purification of a SecM-stalled 70S ribosome complex

In order to ensure a correct comparison between the cryo-EM structures of a TnaC-stalled and a SecM-stalled 70S ribosome, the latter was prepared in the same way as the sample of the TnaC-stalled 70S ribosome, except for the presence of 2 mM Trp in all purification steps. Therefore, the stalling construct (Fig. 3.12A), containing the sequence of a cbp affinity-tag, a His$_6$-tag and the last 21 C-terminal amino acids of the SecM stalling sequence, was also cloned into the pBAT4 vector, yielding the pBAT4-cbpSecM plasmid (see Section 2.1).
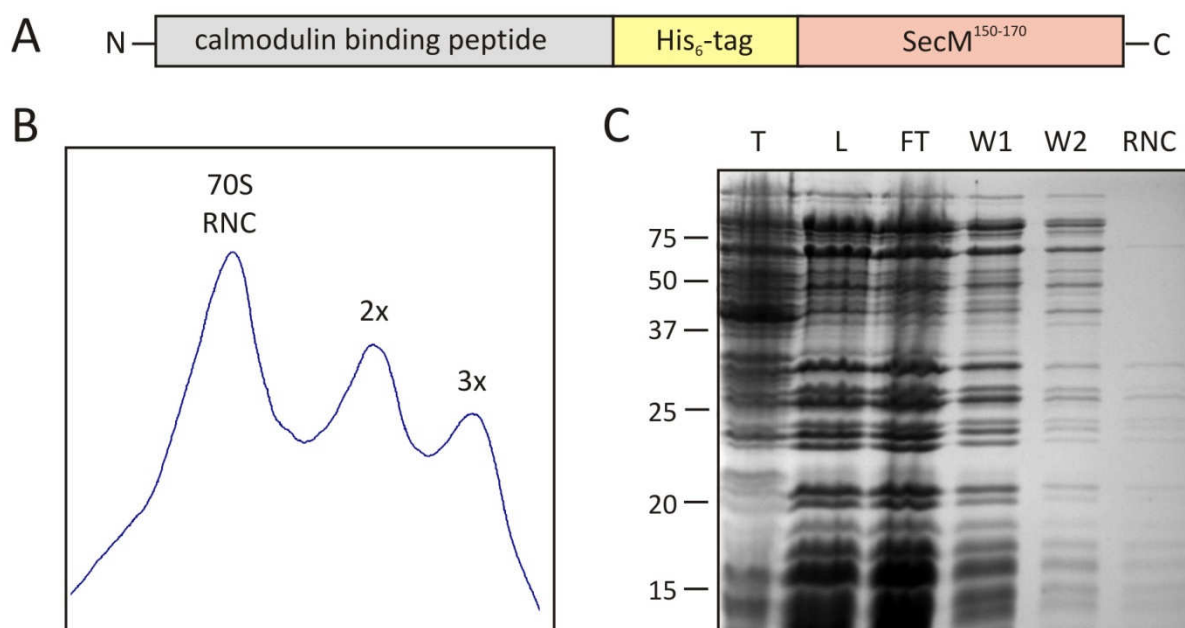
Figure 3.12: Purification of SecM-stalled RNCs. (A) Schematic representation of the SecM-stalling construct, which contained amongst others the 17 important residues of the SecM stalling sequence as well as five additional C-terminal amino acids (^{167}QRLT^{170}), and a stop codon at the end. **(B)** Chromatogram showing the A_{260} profile of the 10-40% sucrose gradient loaded with a cell-free protein synthesis reaction mixture programmed with pBAT4-cbpSecM. **(C)** Coomassie-stained SDS-PAGE analysis of different fractions taken during SecM-RNC purification. T, *in vitro* translation reaction (1/200); L, load onto the calmodulin sepharose column (1/200); FT, flow-through (1/200); W1, W2, washing steps (1/10); RNC; elution fraction using EDTA (1/10). Note the characteristic pattern of ribosomal proteins in the final fraction.

The pBAT4-cbpSecM plasmid then served as a template in a coupled *in vitro* transcription-translation reaction using the *E. coli* S30 translation extract which was prepared by our collaboration partner Axel Innis. In order to get the monosomal fraction (Fig. 3.12B), the reaction mixture was loaded onto a sucrose gradient and centrifuged (see Section 2.2.1). The ribosomes were then affinity-purified using a calmodulin sepharose matrix. Unspecifically bound ribosomes and contaminants could be eliminated in the washing steps, and the purified SecM-stalled RNCs were finally eluted from the column using EGTA (Fig. 3.12C). The purity of the obtained ribosomes can be recognized by the characteristic pattern of ribosomal proteins in the eluted fraction (Fig. 3.12C, RNC).

Out of 10 ml cell-free protein synthesis reaction mixture only 6 pmol of concentrated SecM-stalled RNCs could be obtained, which is much less than the yield of the purified TnaC-RNCs. In spite of the low yield, subsequent negative-stain EM revealed that the quality of the prepared SecM-stalled 70S ribosomes was comparable to those of the TnaC-stalled 70S ribosomes, and therefore suitable for cryo-EM and single particle analysis (data not shown).

3.2.2 Cryo-EM structure of the stalled SecM-70S ribosome complex

Cryo-EM and 3D reconstruction of the SecM-stalled 70S ribosome complex revealed the typical appearance of a stalled 70S ribosome akin to the cryo-EM reconstruction of the TnaC-stalled 70S ribosome. Since the occupancy of a tRNA in the ribosomal P-site was comparatively low, the whole dataset containing ~ 740,000 single particles was sorted according to the presence of peptidyl-tRNA. Only 52% of the dataset, i.e. approximately 383,000 particles, showed a P-site tRNA in the intersubunit space of the ribosome which is much lower than the occupancy of peptidyl-tRNA observed in the TnaC-70S complex (see Section 3.1.2). In contrast, the occupancy with an A-site tRNA was so low that even sorting did not lead to an improvement. Therefore, the particles with a P-site tRNA were then used for the final 3D reconstruction of the SecM-stalled 70S ribosome complex, yielding a resolution of 6.2 Å, according to the FSC 0.5 cut-off criterion (Fig. 3.13).
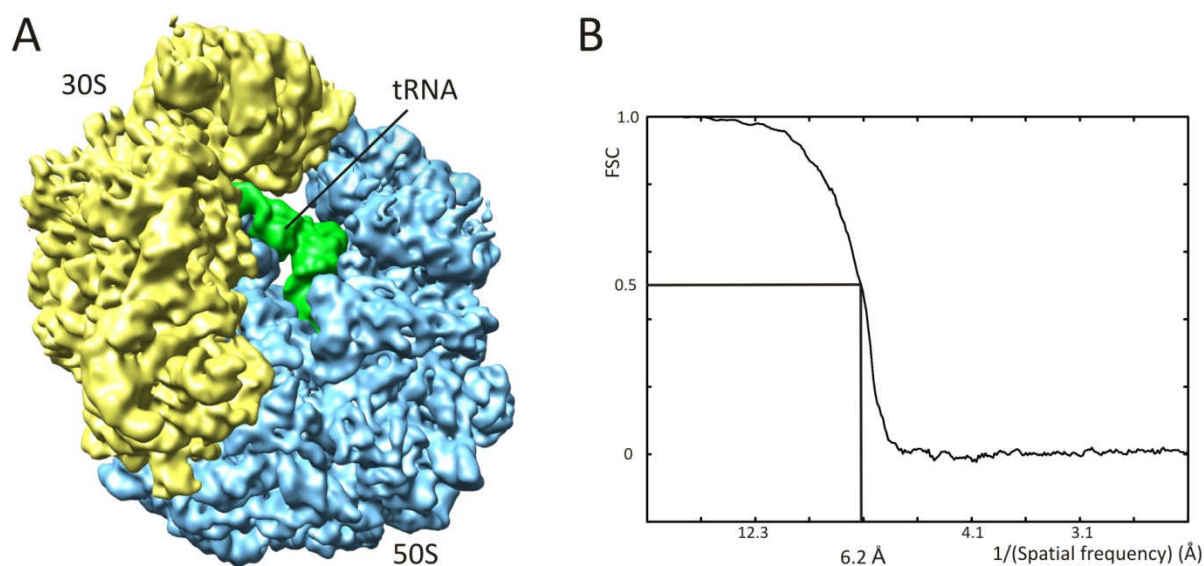
Figure 3.13: Cryo-EM reconstruction and resolution curve of the SecM-70S complex. (**A**) Cryo-EM reconstruction of the SecM-stalled 70S ribosome at 6.2 Å resolution, with small and large subunit coloured yellow and blue, respectively. Additional density for the P-site tRNA is shown in green. (**B**) FSC curve for the final cryo-EM reconstruction, showing that the resolution is 6.2 Å, based on the FSC with a cut-off value of 0.5.

3.2.3 The decoding site of the SecM-70S cryo-EM reconstruction

Since the decoding site of the TnaC-70S cryo-EM reconstruction revealed additionally density that could be attributed to the mRNA of the transcribed TnaC leader sequence (Section 3.1.7),

it was important to examine the situation in the SecM-stalled 70S ribosome, as well. Here, additional density that can be attributed to the mRNA of the transcribed SecM stalling sequence can also be observed (Fig. 3.14). But, in contrast to the mRNA of the TnaC-70S complex which spans the A-, P- and E-sites of the ribosome, density for the mRNA in the SecM-70S complex is only visible near the P- and E-sites of the 30S ribosomal subunit (Fig. 3.14A, B).
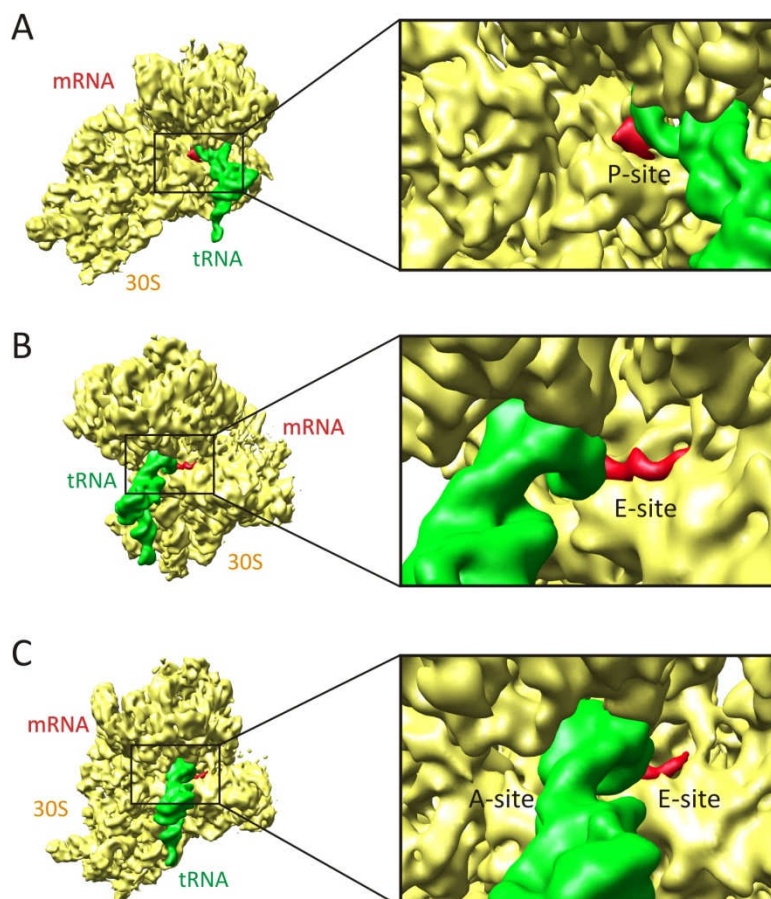
Figure 3.14: Visualization of density for the mRNA in the cryo-EM map of the SecM-70S complex. (**A**) View into the A- and P-site of the 30S subunit (yellow) of the cryo-EM map of the SecM-70S complex, with density for the mRNA and P-site tRNA coloured red and green, respectively. (**B**) View into the E-site of the 30S subunit (yellow) of the cryo-EM map of the SecM-70S complex, with density for the mRNA and P-site tRNA coloured red and green, respectively. (**C**) Simultaneous view into A- and E-sites of the 30S subunit (yellow) of the cryo-EM map of the SecM-70S complex, with density for the mRNA and P-site tRNA coloured red and green, respectively.

Furthermore, closer inspection of the decoding region where the two universally conserved bases of helix 44, A1492 and A1493, are located revealed another difference to the TnaC-stalled 70S complex. In the cryo-EM reconstruction of the SecM-stalled ribosome density for A1493 that would indicate that this nucleotide has flipped out of helix 44 in order to interact with the A-site codon of the mRNA is not observable (Fig. 3.15A). This is consistent with the fact that there is no density present for the A-site codon of the mRNA (Fig. 3.15B). On the other hand, the decoding region shows similarities to the control RNC-70S complex which was stalled using a truncated mRNA lacking a stop codon at the end (Halic et al., 2006) (Fig. 3.11A, B). Here, in both reconstructions density is visible for the P-site codon of the mRNA

but not for the A-site codon. This observation is contrary to the fact that the stalling construct used for the preparation of the SecM-stalled 70S complex has a stop codon at the end.
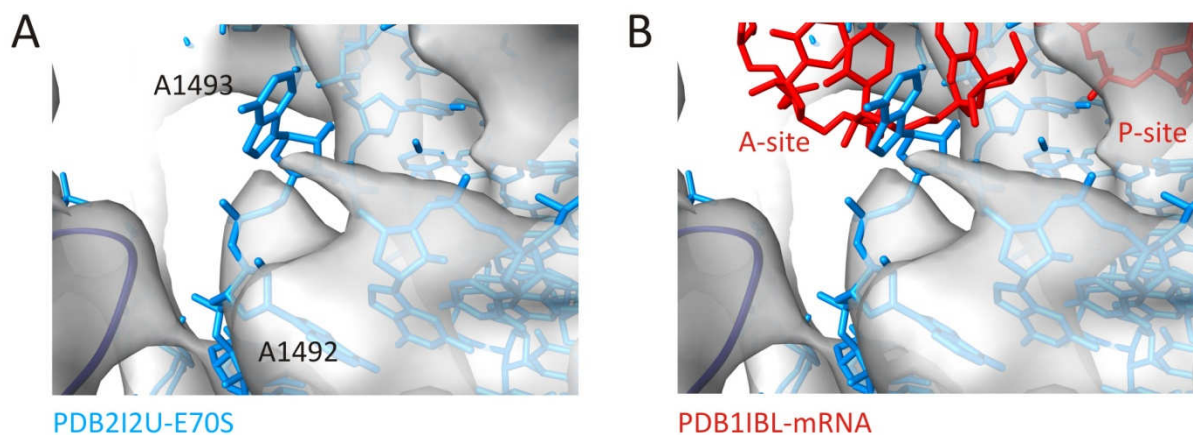
Figure 3.15: Conformation of A1493 in the A-site of the SecM-70S complex. (**A**) View into the A-site of the SecM-70S cryo-EM reconstruction showing the cryo-EM map in grey and a model for the 30S subunit in blue (PDB2I2U; (Berk et al., 2006)), where A1493 has flipped-out of the internal loop of helix 44. Note the lack of density for this nucleotide. (**B**) Same as (A), but with location of mRNA (red) in A- and P-site (PDB1IBL; (Ogle et al., 2001)), showing that density is visible for the P-site but not for the A-site codon.

3.2.4 The ribosomal exit tunnel of the SecM-70S cryo-EM reconstruction

In order to compare the TnaC-stalling with the SecM-stalling mechanism, visualization of the SecM nascent chain is an indispensable prerequisite. Inspection of the ribosomal exit tunnel of the SecM-70S cryo-EM reconstruction revealed that almost no extra density that can be attributed to the SecM nascent chain is visible at higher contour levels (Fig. 3.16A-D). In fact, continuous extra density within the tunnel region can only be observed at a very low contour level, where already so much noise appears that one cannot be sure whether this density can be unambiguously assigned to the SecM nascent chain (Fig. 3.16E, F). Therefore, interpretation of the SecM-stalling mechanism on the bases of this cryo-EM reconstruction is not possible.
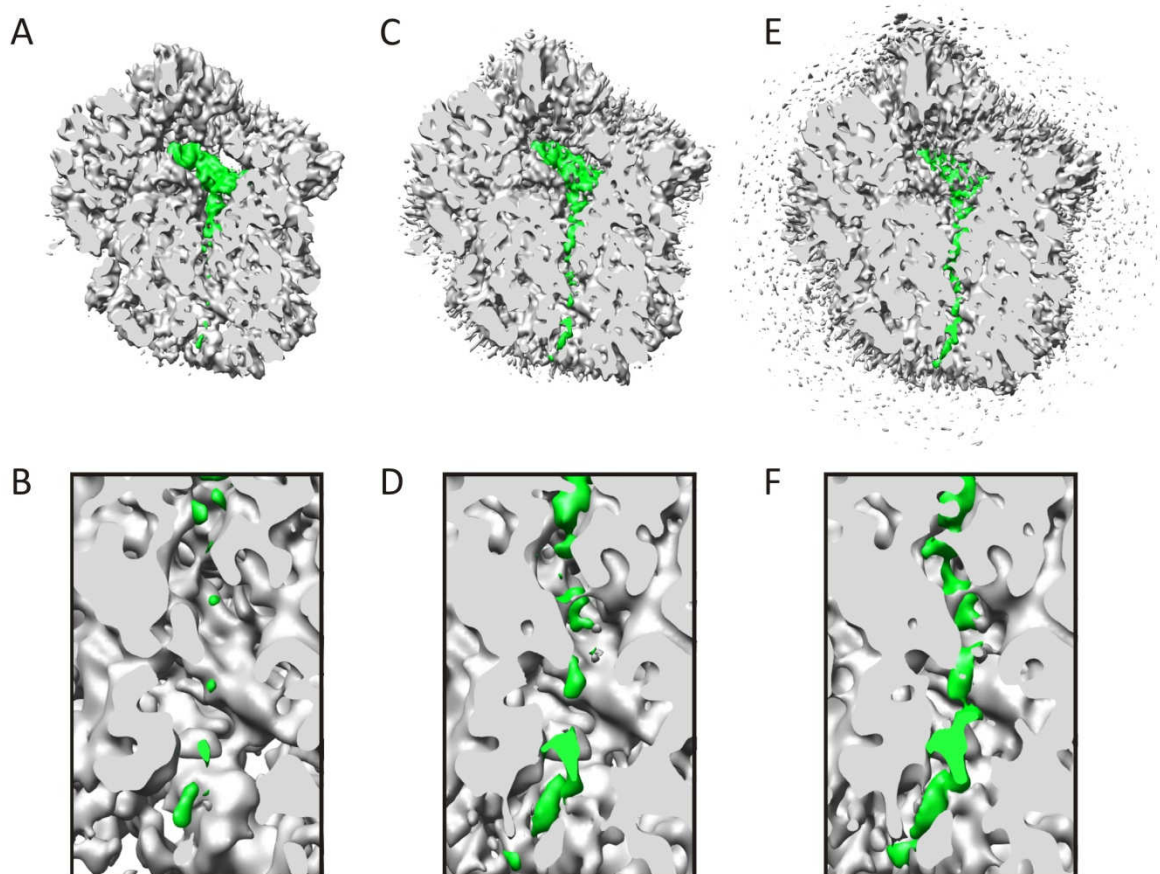
Figure 3.16: Visualization of the SecM nascent chain within the exit tunnel of the cryo-EM map of the SecM-70S complex at three different contour levels. (**A**, **C**, **E**) Section through the 6.2 Å SecM-70S complex, showing the nascent chain (colour-zoned green) within the ribosomal exit tunnel at decreasing contour levels. (**B**, **D**, **F**) Enlargement of the exit tunnel region from (A, C, E). Note that the nascent chain is only visible at a very low contour level, where already noise appears.

Especially conspicuously, however, is a strong density within the ribosomal exit tunnel, which is visible even at a relatively high contour level (Fig. 3.17). This extra density forms a connection - like a bridge - between the conserved β-hairpin loop of ribosomal protein L22 and the extended loop of protein L4, which both are located at the narrowest part of the exit tunnel. This observation is really interesting since there is an analogy to a working model for the SecM arrest sequence action proposed by Berisio and coworkers. Their structural studies showed that a macrolide antibiotic, troleandomycin (TAO) binds to the RNA wall of the ribosomal exit tunnel, displacing the β-hairpin region of L22 from the wall and causing it to flip across the tunnel (Berisio et al., 2003). Due to the identified arrest-suppressing mutations of two specific residues located in the β-hairpin region of L22 (Nakatogawa and Ito, 2002), they proposed that the SecM stalling sequence may act like TAO to halt its own passage through the constriction of the tunnel, which is now occluded by the L22 tip (Berisio et al., 2003).
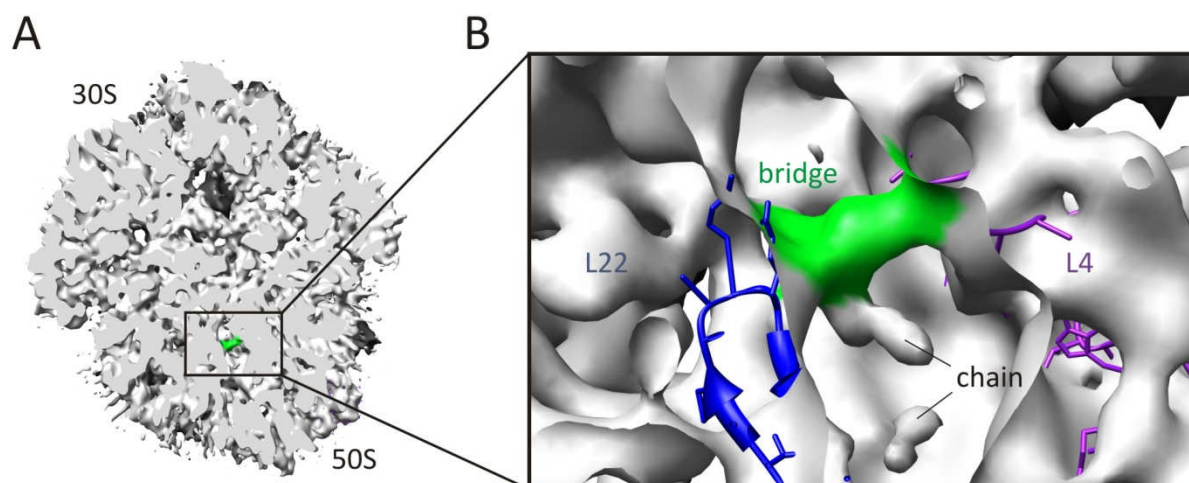
Figure 3.17: Visualization of a bridge connecting ribosomal proteins L22 and L4 in the cryo-EM map of the SecM-stalled ribosome. (**A**) Section through the 6.2 Å SecM-70S complex (grey), showing a strong density (green) within the ribosomal exit tunnel. The displayed contour level equates to the contour level shown in Fig. 3.16C. (**B**) Enlargement of the tunnel region from (A) to show the bridge (green) connecting the β-hairpin loop of ribosomal protein L22 (blue) with the extended loop of protein L4 (purple).

3.2.5 Purification of a SecM-stalled DP120-ribosome nascent chain complex

Visualization of the SecM nascent chain within the ribosomal exit tunnel as well as observation of an A-site tRNA is an important prerequisite for the structural analysis of the SecM-stalling mechanism. Since neither the nascent chain nor an A-site tRNA was visible in the first SecM-70S cryo-EM reconstruction another SecM-stalled 70S complex was purified. This time, the purification method was mainly based on a protocol established by Michael Blau, a former member of the Beckmann lab (Halic et al., 2006), but with some modifications according to Schaffitzel *et al*. (Schaffitzel and Ban, 2007). As already mentioned, there is a low resolution cryo-EM structure of a SecM-stalled 70S ribosome (Mitra et al., 2005). In this reconstruction the authors claimed that they could visualize the nascent chain within the tunnel region and in addition, they could also observe densities for the A-, P- and E-site tRNAs. The main difference in their preparation of SecM-stalled RNCs was the usage of non-physiological high concentrations of magnesium ions (100 mM $Mg(OAc)_2$) (Schaffitzel and Ban, 2007). Therefore, the new SecM-stalled 70S complex was also purified in the presence of 100 mM $Mg(OAc)_2$, which is tenfold higher than the concentration used for the first preparation of SecM-stalled RNCs.
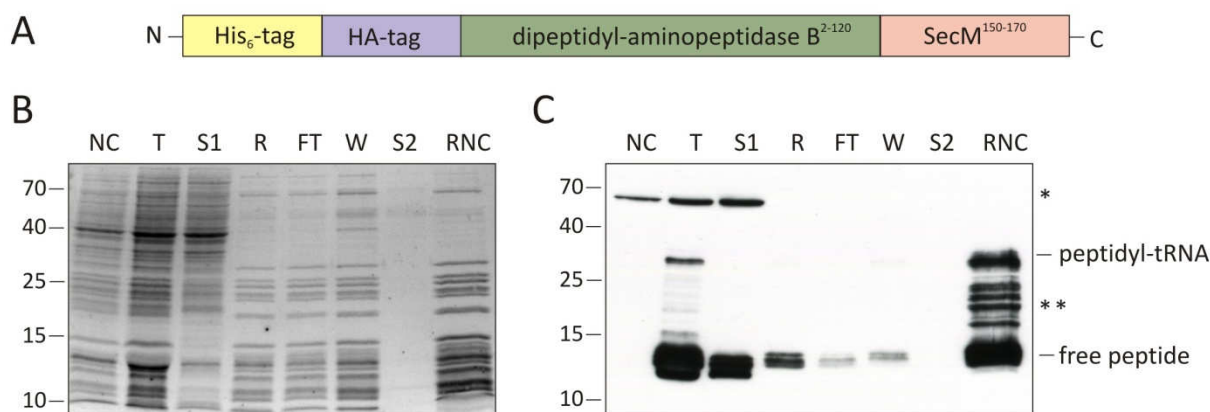
Figure 3.18: Purification of SecM-stalled D120-RNCs. (**A**) Schematic representation of the nascent chain construct used for the preparation of SecM-stalled DP120-RNCs. (**B**, **C**) A mRNA coding for the construct shown in (A) was translated in an *E. coli in vitro* translation system and RNCs pu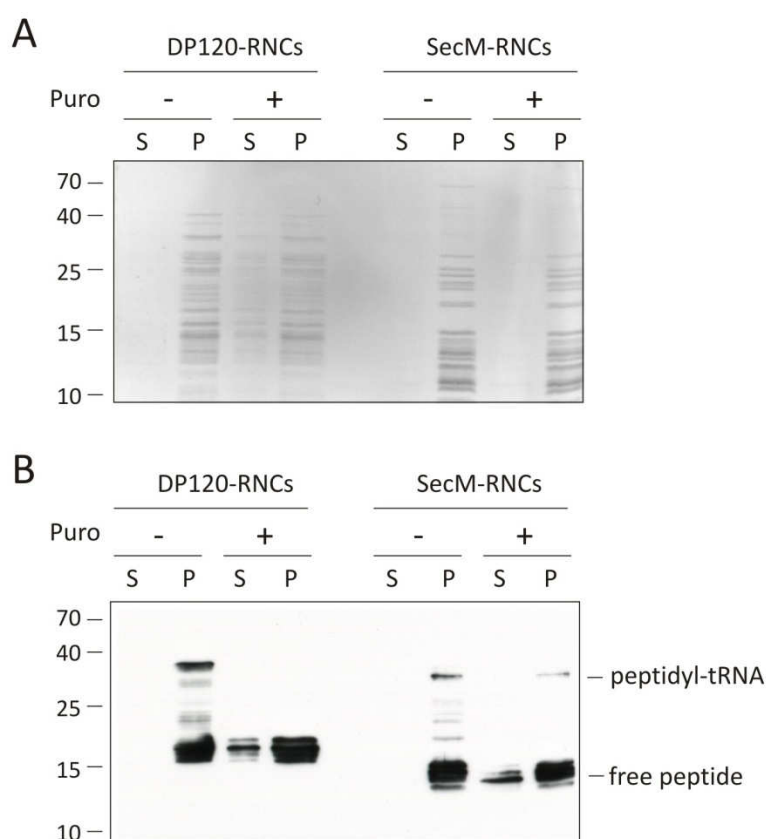rified as described in Section 2.2.2. Aliquots of fractions were subjected to SDS-PAGE, blotted onto PVDF-membrane, stained with amido black (B) and probed using a monoclonal anti-HA antibody (C). NC, negative control, i.e. translation without mRNA; T, translation (1/100); S1, supernatant (1/100) after the first centrifugation; R, ribosomal pellet (1/100); FT, flow-through (1/100) after incubation with the column material; W, wash (1/10); S2, supernatant (1/10) after centrifugation of the eluted fraction; RNC, ribosomal pellet (1/10) after elution using imidazole. One asterisk marks an unspecific signal due to a cross reaction of the translation extract with the antibody, the two asterisks mark degradation products.

A linear DNA template, containing the sequence of a His$_6$-tag for the purification, an hemagglutinin (HA)-tag for detection, the first 120 amino acids of the membrane protein dipeptidyl-aminopeptidase B (DP120) from yeast and the last 21 C-terminal amino acids of the SecM stalling sequence (Fig. 3.18A), was prepared by Shashi Bhushan and used for an *in vitro* transcription reaction. The mRNA served then as a template for the translation reaction using an *E. coli in vitro* system (Promega). The ribosomes were affinity-purified by metal affinity chromatography (see Section 2.2.2). Aliquots of different fractions were subjected to Western blot analysis, where the stalled ribosomes are detectable by two specific signals: the DP120-SecM peptide still bound to tRNA at around 30 kDa and the free DP120-SecM peptide at around 13 kDa (Fig. 3.18C). Non-programmed ribosomes ended up in the flow-through (FT) fraction whereas unspecific bound ribosomes and contaminants could be eliminated in the washing step. SecM-stalled DP120-RNCs were finally eluted from the column using imidazole. When comparing the specific signal before purification (R) and after purification (RNC) (Fig. 3.18C) it is apparent that a several-fold stronger RNC-specific signal indicates at least a 4-fold enrichment. Assuming that after the *in vitro* translation reaction approximately 15 to 20% of the ribosomes are programmed (Beckmann et al., 2001), at least 70 to 80% of the eluted ribosomes can be expected to carry a nascent chain. Out of 1 ml *in*

vitro translation reaction 68 pmol of concentrated SecM-stalled DP120-RNCs could be purified and used for further analysis.

3.2.6 Biochemical and structural analysis of the SecM-stalled DP120-RNCs

In order to determine whether there is A-site tRNA occupancy in the purified SecM-stalled DP120-RNCs a puromycin assay was carried out. The antibiotic puromycin normally binds to the ribosomal A-site and causes premature chain termination during translation by releasing the nascent peptide as peptidyl puromycin (Cannon, 1968). In the case of the SecM stalling it has been shown that the arrested SecM$^{1-165}$-tRNA^{Gly} that resides at the ribosomal P-site is completely resistant to puromycin if the A-site is occupied by Pro^{166}-tRNA^{Pro} (Muto et al., 2006).

Figure 3.19: Puromycin assay to check for A-site tRNA occupancy. Control DP120-RNCs and SecM-stalled RNCs were incubated with and without puromycin (2 mM; Puro) at 37°C for 15 min and subsequently centrifuged. Supernatant (S) and pellet fractions (P) were subjected to SDS-PAGE, blotted onto PVDF-membrane, stained with amido black (**A**) and probed using a monoclonal anti-HA antibody (**B**). The control DP120-RNCs which were stalled using truncated mRNA are completely puromycin sensitive whereas the SecM-stalled DP120-RNCs are partially resistant.

In the puromycin assay, the SecM-stalled *E. coli* DP120-RNCs were compared with control 80S wheat germ RNCs (provided by Shashi Bhushan) which were stalled during translation of truncated DP120 mRNA (Fig. 3.19). As expected, puromycin treatment of the control DP120-RNCs caused the release of the nascent chain from the ribosomal P-site since no signal for the peptidyl-tRNA can be detected in the pellet fraction after Western blot analysis (Fig. 3.19B).

Instead, a signal for the free peptide can be observed in the supernatant fraction which is not visible without puromycin treatment. In the case of the SecM-stalled DP120-RNCs a signal for the peptidyl-tRNA can still be observed in the pellet fraction after puromycin treatment (Fig. 3.19B). Since, however, also a signal for the free peptide is visible in the supernatant fraction some nascent chains must have been released as peptidyl puromycin. Therefore, the A-site of the SecM-stalled DP120-RNCs should be at least partially occupied by a tRNA.
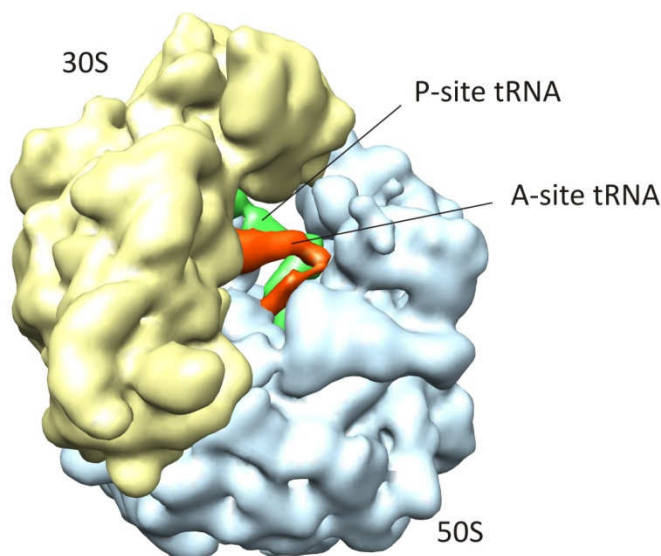
Figure 3.20: Preliminary cryo-EM reconstruction of the SecM-stalled DP120-RNCs at 11 Å resolution. The small ribosomal subunit is shown in yellow and the large ribosomal subunit in blue. Densities that could be attributed to the P-site tRNA and to the A-site tRNA are coloured in green and orange, respectively. Note that the structure is not sorted yet.

In order to verify the result of the puromycin assay, a preliminary 3D structure of the SecM-stalled DP120-RNCs was determined using cryo-EM and single particle analysis. This first 3D reconstruction with a resolution of around 11 Å shows not only a P-site tRNA but also an A-site tRNA which are not completely resolved yet (Fig. 3.20). Therefore, the dataset needs to be further refined and sorted according to the presence of A- and P-site tRNA. The hence resulting structure of the SecM-stalled complex should then be analyzed for the presence of the SecM nascent chain within the ribosomal exit tunnel.

3.3 Towards a high resolution structure of a ribosome-YidC complex

The aim of the second part of this study was the determination of a cryo-EM structure of the membrane protein insertase YidC2 bound to 70S ribosomes. In order to attain this goal, firstly *S. mutans* YidC2 was purified and then *in vitro* reconstituted with *E. coli* 70S ribosomes. After SDS-PAGE analysis of several reconstitution assays, cryo-EM and single particle reconstruction was used to investigate whether YidC2 can be visualized on the 70S ribosome.

3.3.1 Purification of *Streptococcus mutans* YidC2

For the purification of the membrane protein YidC2 from the Gram-positive bacterium *Streptococcus mutans* a protocol had to be established. In order to obtain sufficient amounts and purity, *S. mutans* YidC2 was heterologously overexpressed in *E. coli* cells and purified by metal affinity chromatography using the C-terminal His_6-tag and subsequent gel filtration chromatography (Fig. 3.21).
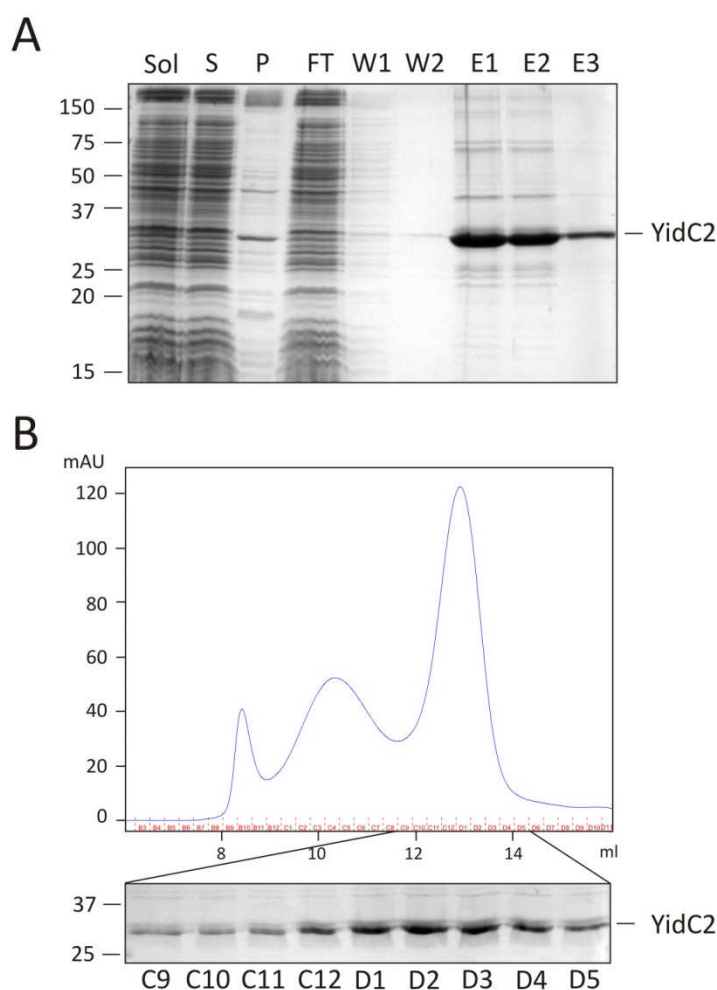
Figure 3.21: Purification of *S. mutans* YidC2 from isolated membrane vesicles. (**A**) Coomassie-stained SDS-PAGE analysis of different samples taken during Ni-NTA affinity chromatography: Sol, solubilization (1/6000) of membrane vesicles isolated from 6 l *E. coli* culture; S, supernatant (1/6000) which was then incubated with Ni-NTA agarose beads; P, pellet (1/6000) containing insoluble material; FT, flow-through (1/6000) of the column; W1, W2, washing steps (1/500); E1 (1/100), E2 (1/50), E3 (1/50), elution fractions which were concentrated and subsequently loaded onto a gel filtration column. (**B**) Elution profile of the gel filtration showing the fraction numbers (red) and absorption at $\lambda = 280$ nm (blue), and SDS-PAGE analysis of the peak fractions C9-D5 (1/20).

The sequence of *S. mutans* YidC2 (provided as pCR2.1-YidC2 plasmid by Johannes M. Herrmann) as well as a C-terminal His$_6$-tag were cloned into the overexpression vector pET324 (van der Does et al., 1996), yielding the pET324-YidC2-His plasmid. For the heterologous overexpression of YidC2, the pET324-YidC2-His plasmid was transformed into *E. coli* Rosetta (DE3). For the purification (see Section 2.2.4), firstly, membrane vesicles (MVs) containing both, inner and outer membranes were isolated from cells overexpressing YidC2, and then solubilized with the detergent dodecylmaltoside (DDM). After removing nonsolubilized material by centrifugation, the supernatant containing solubilized YidC2 was subjected to metal affinity chromatography using nickel-nitrilotriacetic acid (Ni-NTA) agarose beads (Fig. 3.21A). Unspecifically bound proteins could be eliminated in the washing steps under high salt conditions (500 mM KOAc). Bound YidC2 protein was finally eluted from the column using 500 mM imidazole. The eluted fractions were pooled, concentrated and subsequently loaded onto a gel filtration column (Superdex 200) in order to remove aggregated proteins (Fig. 3.21B). This last purification step led to an improved quality of the purified membrane protein since YidC2 tended to aggregate in reconstitution experiments performed without prior gel filtration chromatography. The peak fractions of the gel filtration were analyzed by SDS-PAGE (Fig. 3.21B) and subsequently concentrated. From 12 liter *E. coli* culture approximately 0.5 mg *S. mutans* YidC2 of sufficient purity could be obtained.

3.3.2 Reconstitution and cryo-EM of the 70S ribosome-YidC2 complex

S. mutans YidC2 contains an extended C-terminal region akin to the C-terminal ribosome binding domain of the mitochondrial YidC homologue Oxa1 (Jia et al., 2003; Szyrach et al., 2003). Therefore, it was assumed that the extended C-terminal region of YidC2 might also support binding to empty ribosomes. In order to test this hypothesis, a reconstitution assay was performed where empty 70S ribosomes (provided by Daniel Wilson) were incubated with excess amounts of purified YidC2 under different salt conditions. Through subsequent centrifugation the ribosome-bound fraction (pellet) was separated from the non-bound fraction (supernatant), and then subjected to SDS-PAGE analysis (see Section 2.2.5). YidC2 can only be detected in the pellet fraction if it is bound to ribosomes.

According to the reconstitution assay, YidC2 binds to empty 70S ribosomes in a salt-dependent manner (Fig. 3.22A). Strongest binding could be observed under low salt conditions (50-200 mM KOAc) whereas almost no binding is obtained at higher salt concentrations (400 and 500 mM KOAc).
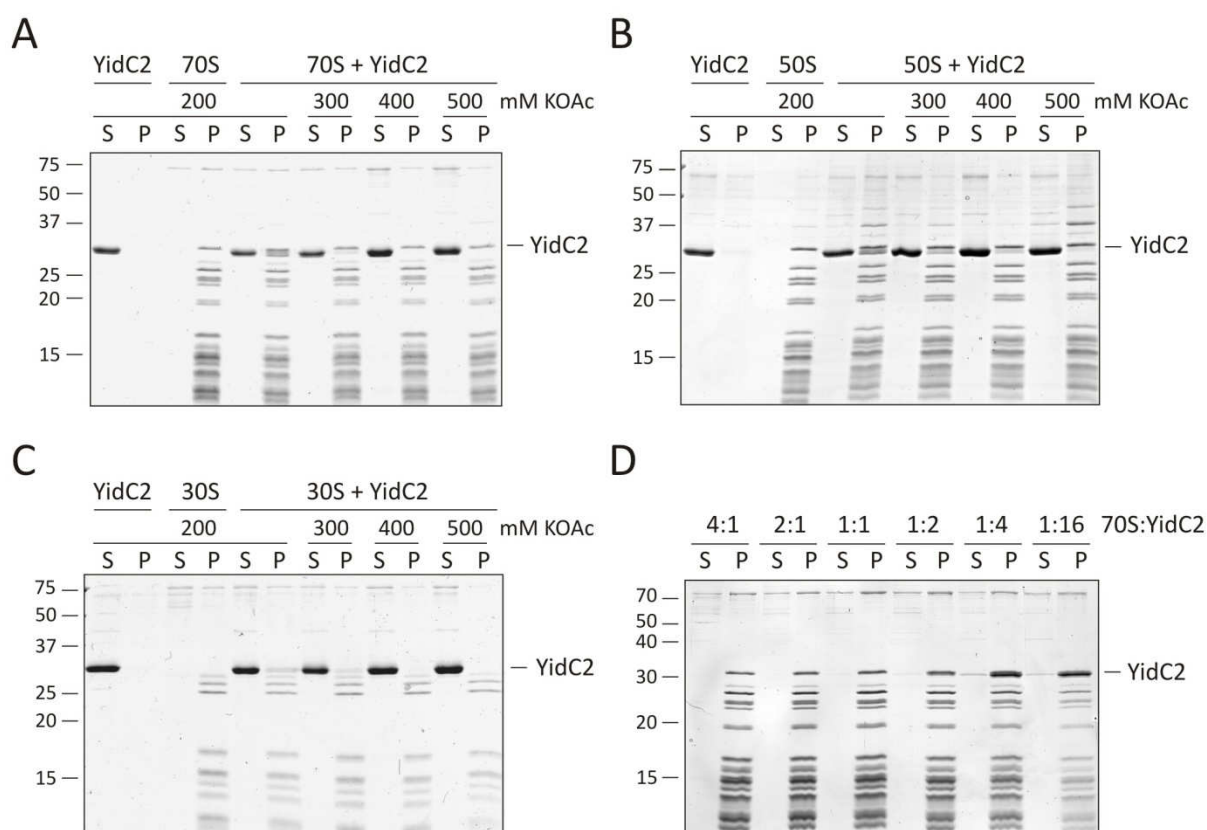
Figure 3.22: Reconstitution assays of *S. mutans* YidC2 to 70S ribosomes and ribosomal subunits under different salt conditions. 70S ribosomes and ribosomal subunits, respectively, were *in vitro* reconstituted with excess amounts of purified YidC2 and subjected to centrifugation through a sucrose cushion. The resulting supernatant (S) and pellet (P) fractions were then analyzed by SDS-PAGE and subsequent Coomassie-staining. (**A**) Binding of YidC2 to empty 70S ribosomes under different salt conditions (200-500 mM KOAc). (**B**) Binding of YidC2 to 50S subunits. (**C**) Binding of YidC2 to 30S subunits. YidC2 binds to 70S ribosomes as well as to the ribosomal subunits in a salt-dependent manner. (**D**) Binding of YidC2 to 70S ribosomes in different molar ratios at 100 mM KOAc.

In order to investigate whether the observed binding to 70S ribosomes is specific, YidC2 was also bound to 50S and 30S ribosomal subunits (provided by Daniel Wilson), respectively. Analysis of the reconstitution assays revealed that YidC2 binds, as expected, in the same way to 50S subunits (Fig. 3.22B) as it does to 70S ribosomes. However, YidC2 also binds to 30S subunits (Fig. 3.22C). Therefore, the binding to empty 70S ribosomes is most likely non-specific. This result could be confirmed by another reconstitution assay (Fig. 3.22D). Here, it was shown that the binding of YidC2 to 70S ribosomes could not be saturated, *i.e.* the more YidC2 was added to the ribosomes the more it was bound.

Although the reconstitution assays revealed that the binding of *S. mutans* YidC2 to 70S ribosomes is unspecific, cryo-EM and single particle analysis was used to investigate whether YidC2 can be visualized on the ribosome. A total of three different cryo-EM structures of 70S-YidC2 complexes using the final salt concentrations 50 mM (Fig. 3.23A), 100 mM and

200 mM KOAc, respectively, were solved (data not shown). In none of these reconstructions additional density was detected that could be attributed to YidC2. Even filtering of the in Fig. 3.23A exemplarily shown 6.6 Å resolution map of the 70S-YidC2 complex to a lower resolution (Fig. 3.23B) where flexible-bound ligands are maybe visible did not lead to success. Thus, it can be concluded that under these conditions, it was not possible to visualize YidC2 bound to an empty 70S ribosome.
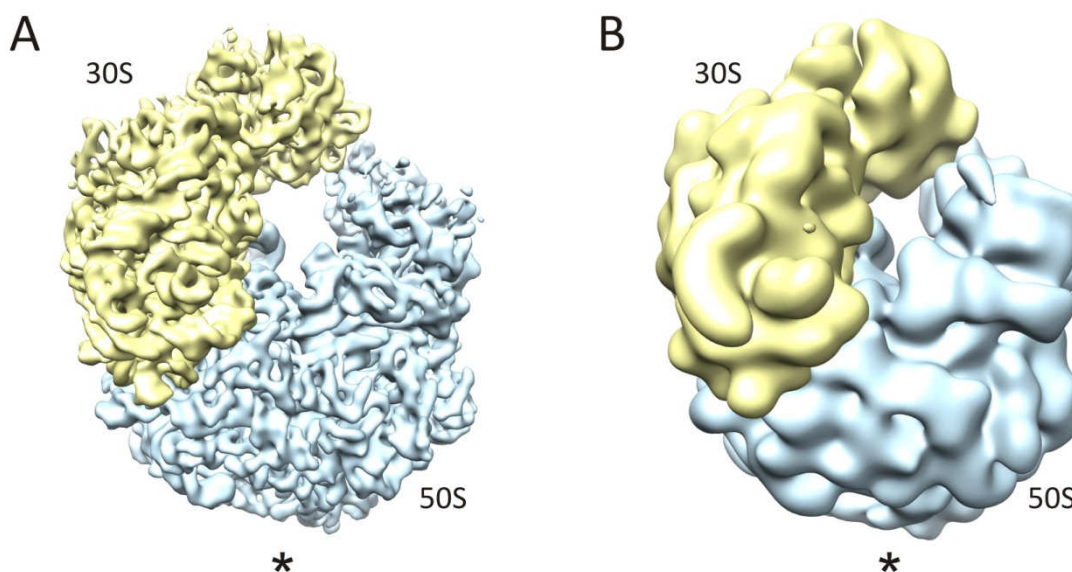
Figure 3.23: Cryo-EM reconstruction of the 70S-YidC2 complex. (**A**) Cryo-EM structure of YidC2 bound to empty 70S ribosomes under low salt conditions (50 mM KOAc) at 6.6 Å resolution. The small ribosomal subunit is shown in yellow, the large subunit in blue. The asterisk marks the expected position of YidC2 near the tunnel exit of the large ribosomal subunit (Kohler et al., 2009). (**B**) Same as in (A), but filtered to 20 Å resolution. Density that could be attributed to YidC2 could not be detected.

3.3.3 Generation of YidC-substrate specific ribosome-nascent chain complexes

In order to achieve an increased binding affinity of YidC, 70S ribosomes were programmed with an mRNA coding for a YidC specific substrate, the mechanosensitive channel of large conductance (MscL) (Facey et al., 2007). By usage of MscL, it is expected that the binding of YidC can be enhanced by providing additional specificity of the MscL nascent chain. This could lower the conformational heterogeneity of YidC which would lead to a better visibility in cryo-EM.
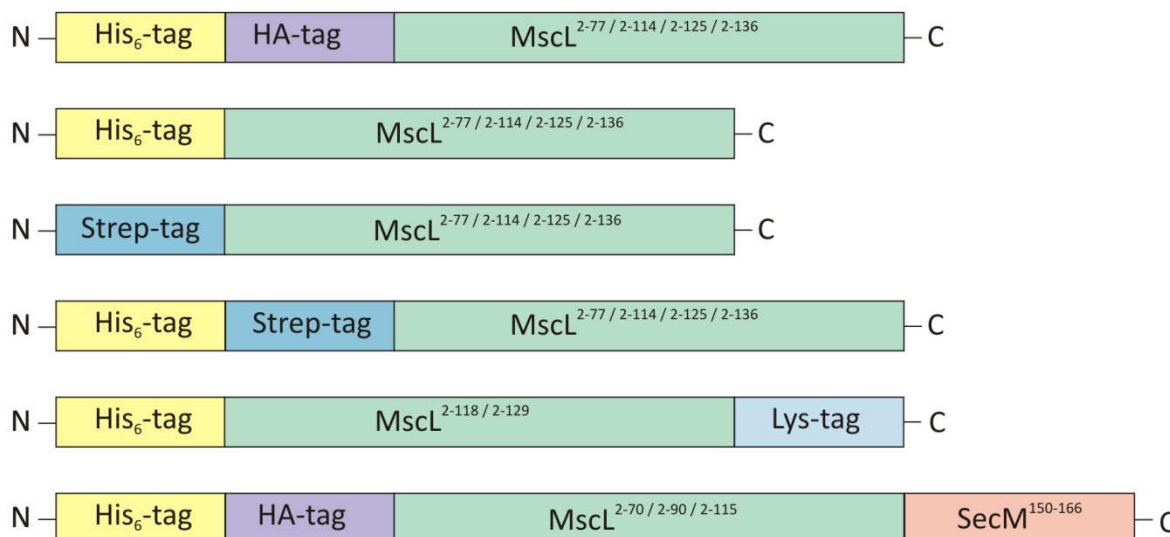
Figure 3.24: Schematic representation of the different MscL-nascent chain constructs used for *in vitro* test translations. Neither of them could be detected by western blot analysis.

Since the interaction of YidC with the MscL nascent chain might be dependent on the length of the nascent chain, different chain lengths were used (Fig. 3.24). First of all, mRNA encoding for a His_6-tag which is required for the purification of RNCs, a HA-tag required for western blot analysis, and the first 77, 114, 125, and 136 (i.e. full length MscL) amino acids, respectively, of the MscL peptide was generated by *in vitro* transcription reaction. Here, truncated mRNA without a stop codon was used to stall the translation reaction at the last codon, which would lead to artificially stalled RNCs with peptidyl-tRNA at the P-site. In order to test the translation efficiency of the stalling constructs, *in vitro* translation reactions were carried out and subjected to western blot analysis. Since no translation signals could be detected on the western blot (data not shown) and also several attempts, such as using different blotting membranes (PVDF, nitrocellulose), different blotting times, and different blotting systems (semi-dry, tank-blot) did not lead to success, further constructs were generated. These constructs (Fig. 3.24) varied in the used tags or showed a different combination of tags, or even had a different stalling mechanism, such as SecM. Nevertheless, *in vitro* translation reactions using these constructs could also not be detected by western blot analysis. However, radioactively performed *in vitro* translation reactions (carried out by Heidi Sieber) (Fig. 3.25) revealed that in principle the translation of MscL-mRNA works. However, it is most likely not efficient enough for RNC-preparation based on the purification method established by Michael Blau (Halic et al., 2006).
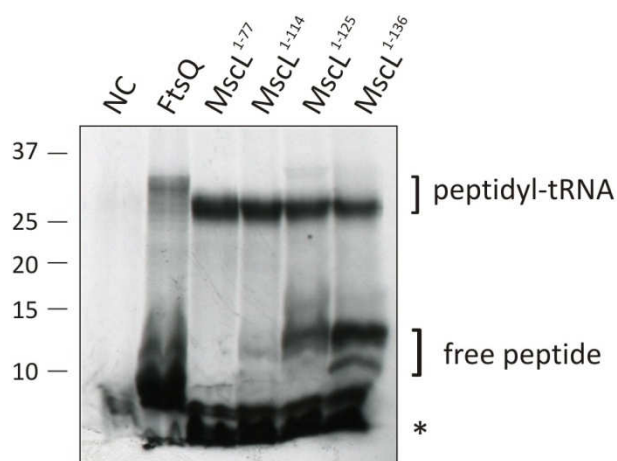
Figure 3.25: Radioactive detection of *in vitro* translation reactions of the different MscL-mRNAs. MscL-mRNAs varying in the length of the MscL nascent chain were used as templates for *in vitro* translation reactions using [35S]-Methionine for detection. NC, negative control of the test translation without the use of an mRNA; FtsQ, served as a positive control. The * marks surplus [35S]-Methionine. The radioactive assay was carried out by Heidi Sieber.

Since the cryo-EM structure of a TnaC-stalled 70S ribosome complex could be successfully elucidated (see Section 3.1), the RNC purification method established by our collaboration partner Axel Innis was used for the generation of TnaC-stalled MscL-RNCs (Fig. 3.26).
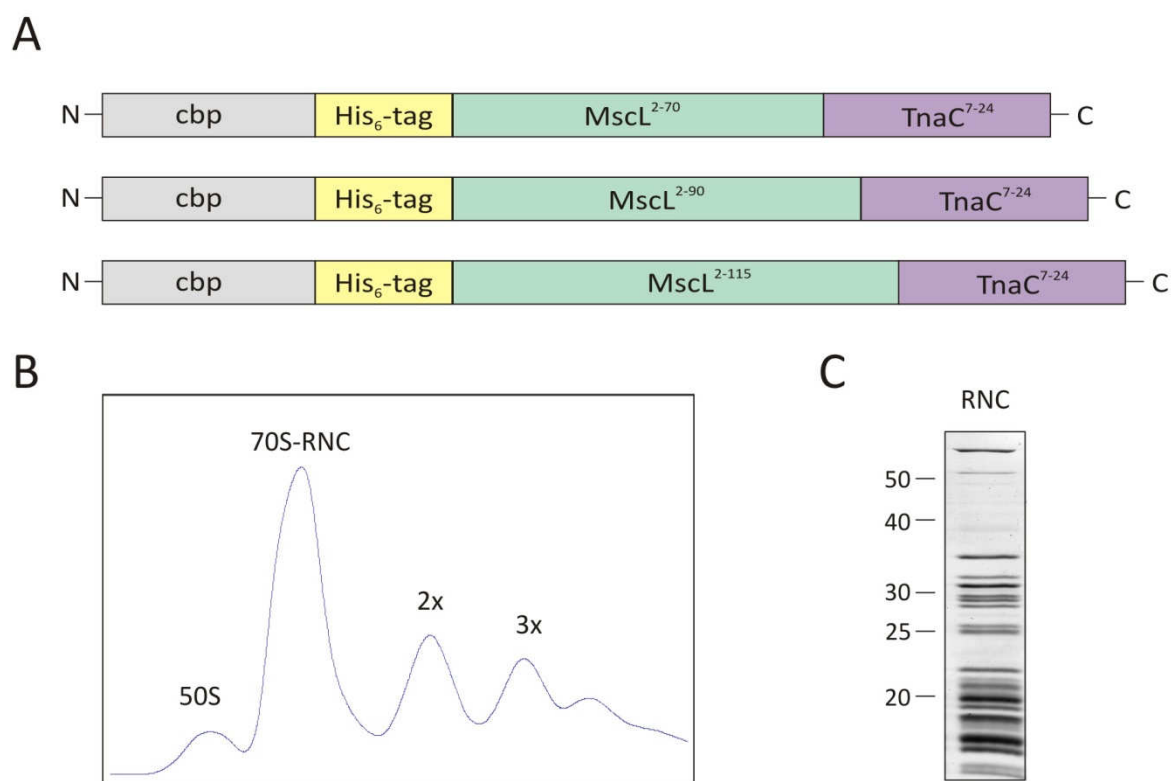
Figure 3.26: Purification of TnaC-stalled MscL-RNCs. (**A**) Schematic representation of the three different TnaC-stalled MscL nascent chain constructs, containing a calmodulin binding peptide (cbp) and a hexahistidine-tag (His$_6$-tag). (**B**) Chromatogram of the MscL^{115}-RNC purification, showing the A$_{260}$ profile of the 10-40% sucrose gradient loaded with a cell-free protein synthesis reaction mixture programmed with the plasmid pBAT4-MscL^{115}. (**C**) Coomassie-stained SDS-gel of the TnaC-stalled MscL^{115}-RNCs.

For that purpose, three different stalling constructs (Fig. 3.26A), containing the sequence of a cbp affinity-tag, a His$_6$-tag, the first 70, 90, and 115 amino acids, respectively, of MscL and the last 17 amino acids of the TnaC leader peptide, were cloned into the pBAT4 vector, which then served as a template for a coupled *in vitro* transcription-translation reaction. The TnaC-stalled MscL-RNCs were purified as already described in Section 3.1, yielding ~ 40 pmol of concentrated MscL-RNCs (Fig. 3.26C) when using a 10 ml cell-free protein synthesis reaction mixture. The three different TnaC-stalled MscL-RNCs which vary in the length of the MscL nascent chain were used for both, reconstitution assays and cryo-EM analysis.

3.3.4 Reconstitution and cryo-EM of a MscL-RNC-YidC complex

A reconstitution assay was performed in which the binding of *S. mutans* YidC2 to empty 70S ribosomes was compared with the binding to the different MscL-RNCs varying in the length of the nascent chains. Therefore, empty 70S ribosomes and the different MscL-RNCs, respectively, were incubated with excess amounts of purified YidC2 under low salt conditions (100 mM KOAc). After subsequent centrifugation the supernatant and pellet fractions were subjected to SDS-PAGE analysis (Fig. 3.27). According to the reconstitution assay, *S. mutans* YidC2 binds to the different MscL-RNCs in the same manner as it binds to empty 70S ribosomes.
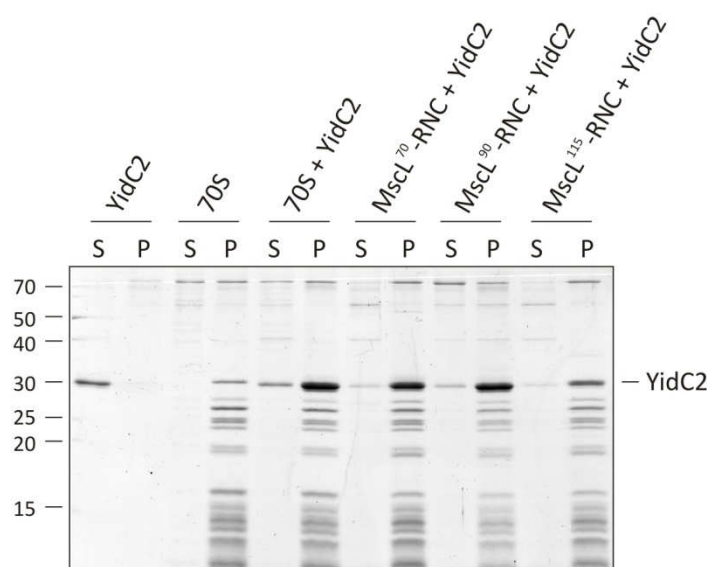
Figure 3.27: Reconstitution assay for comparison of the binding of *S. mutans* YidC2 to 70S ribosomes and different MscL-RNCs, respectively. 70S ribosomes and different MscL-RNCs, respectively, were *in vitro* reconstituted with excess amounts of purified *S. mutans* YidC2 and subjected to centrifugation through a sucrose cushion. The resulting supernatant (S) and pellet (P) fractions were analyzed by SDS-PAGE and subsequent Coomassie-staining. Note that no clear difference in the binding could be detected.

The same result could be achieved in another reconstitution assay where *E. coli* YidC, which was purified by our collaboration partner Stephanie Ravaud from the Sinning laboratory at the University of Heidelberg, was bound to empty 70S ribosomes and to the different MscL-

RNCs, respectively (Fig. 3.28). Since no difference in the specificity of the binding of *S. mutans* YidC2 and *E. coli* YidC, respectively, to empty 70S ribosomes and to the different MscL-RNCs could be detected using a biochemical assay, cryo-EM could shed light on it.
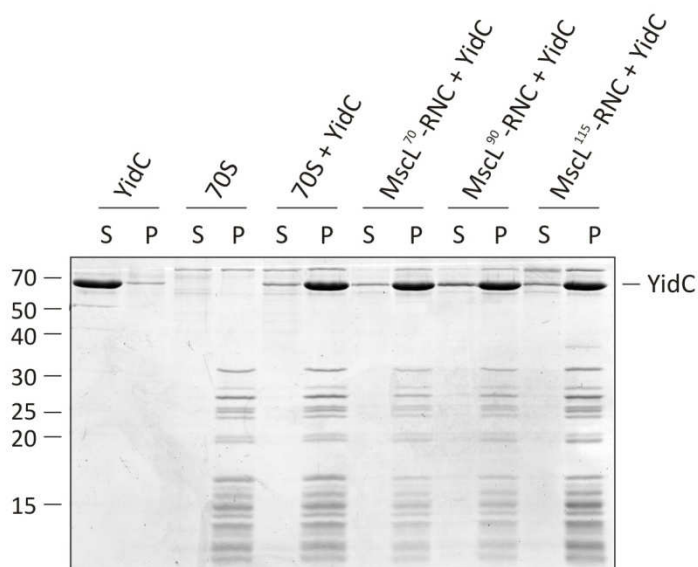
Figure 3.28: Reconstitution assay for comparison of the binding of *E. coli* YidC to 70S ribosomes and different MscL-RNCs, respectively. 70S ribosomes and different MscL-RNCs, respectively, were *in vitro* reconstituted with excess amounts of purified *E. coli* YidC and subjected to centrifugation through a sucrose cushion. The resulting supernatant (S) and pellet (P) fractions were analyzed by SDS-PAGE and subsequent Coomassie-staining. Note that no clear difference in the binding could be detected.

Preliminary low-resolution cryo-EM structures of both the *S. mutans* YidC2-MscL^{115}-RNC complex and the *E. coli* YidC-MscL^{115}-RNC complex were determined using the Spirit microscope. Thereby, it can be shown if the presence of the MscL nascent chain now led to the observation of YidC on the ribosome due to an increased binding specificity.
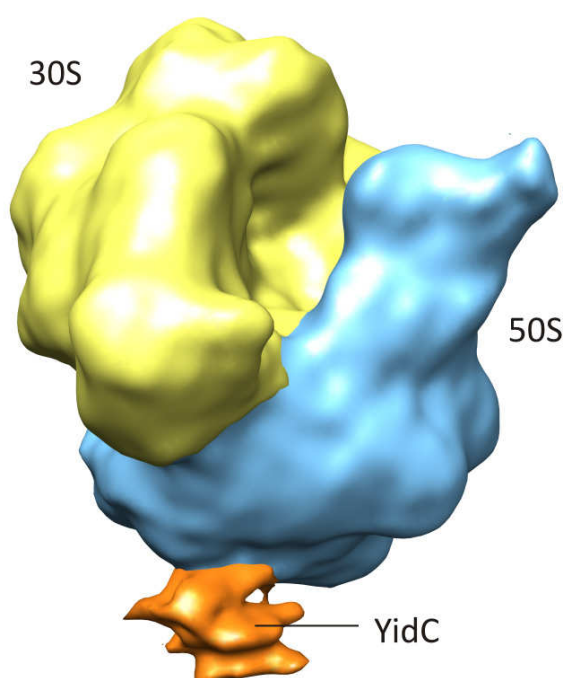
Figure 3.29: Preliminary low-resolution cryo-EM reconstruction of the *E. coli* YidC-MscL^{115}-RNC complex. The small ribosomal subunit is shown in yellow, the large subunit in blue. The extra density that can be attributed to the membrane insertase YidC is shown in orange. The resolution is approximately 25 Å.

An additional density near the ribosomal tunnel exit could be detected in the low-resolution cryo-EM reconstruction of the *E. coli* YidC-MscL[115]-RNC complex (Fig. 3.29) but not in the *S. mutans* YidC2-MscL[115]-RNC complex (data not shown).

3.3.5 Reconstitution of the membrane protein YidC2 into proteoliposomes

In addition to the above described strategy, it was also tried to visualize YidC2 in cryo-EM by incorporating it back into its native membrane environment. The process of the insertion of a purified membrane protein in an artificial lipid membrane is called membrane reconstitution (Geertsma et al., 2008). Besides the possible prevention of flexibility there were still other reasons for the usage of this strategy. (1) Since general membrane properties such as fluidity and permeability and also specific protein-lipid interactions are required for the functioning of most integral membrane proteins (de Kruijff, 1997), a fluid phospholipid environment could be important for the activity of YidC2. (2) Furthermore, it is unknown to what extent the detergent micelle of a solubilized membrane protein contributes to the cryo-EM density (Becker et al., 2009).

The procedure for the reconstitution of YidC2 into proteoliposomes, which was based on a protocol by Geertsma and coworkers (Geertsma et al., 2008), was carried out in four stages (see Section 2.2.8). In the first stage, large, homogeneous, and unilamellar lipid vesicles were prepared from *E. coli* total lipid extract (Avanti Polar Lipids). In the second stage, these preformed liposomes were solubilized by adding increasing amounts of the detergent Triton X-100 to the lipid suspension. To monitor the solubilization process, the optical density of the lipid-detergent suspension was measured at 540 nm as a function of detergent concentration (data not shown). Since for most membrane proteins, the reconstitution has proven to be most efficient at detergent concentrations slightly above the point where liposomes are fully saturated (Geertsma et al., 2008), the purified membrane protein YidC2 was added to the detergent-destabilized liposomes exactly at this point of solubilization (Fig. 3.30A). The fourth and last step of the reconstitution procedure was the slow and complete removal of detergent by adding polystyrene beads (BioBeads®) to the lipid-detergent-protein mixture. This leads to spontaneous formation of liposomes with bilayer membranes in which YidC2 is incorporated (YidC2-proteoliposomes) (Fig. 3.30A). The removal of the detergent through hydrophobic adsorption onto polystyrene beads was chosen because it has been shown to be the most efficient method, especially for detergents with a low critical micelle concentration (CMC), such as the used Triton X-100 (Knol et al., 1998).
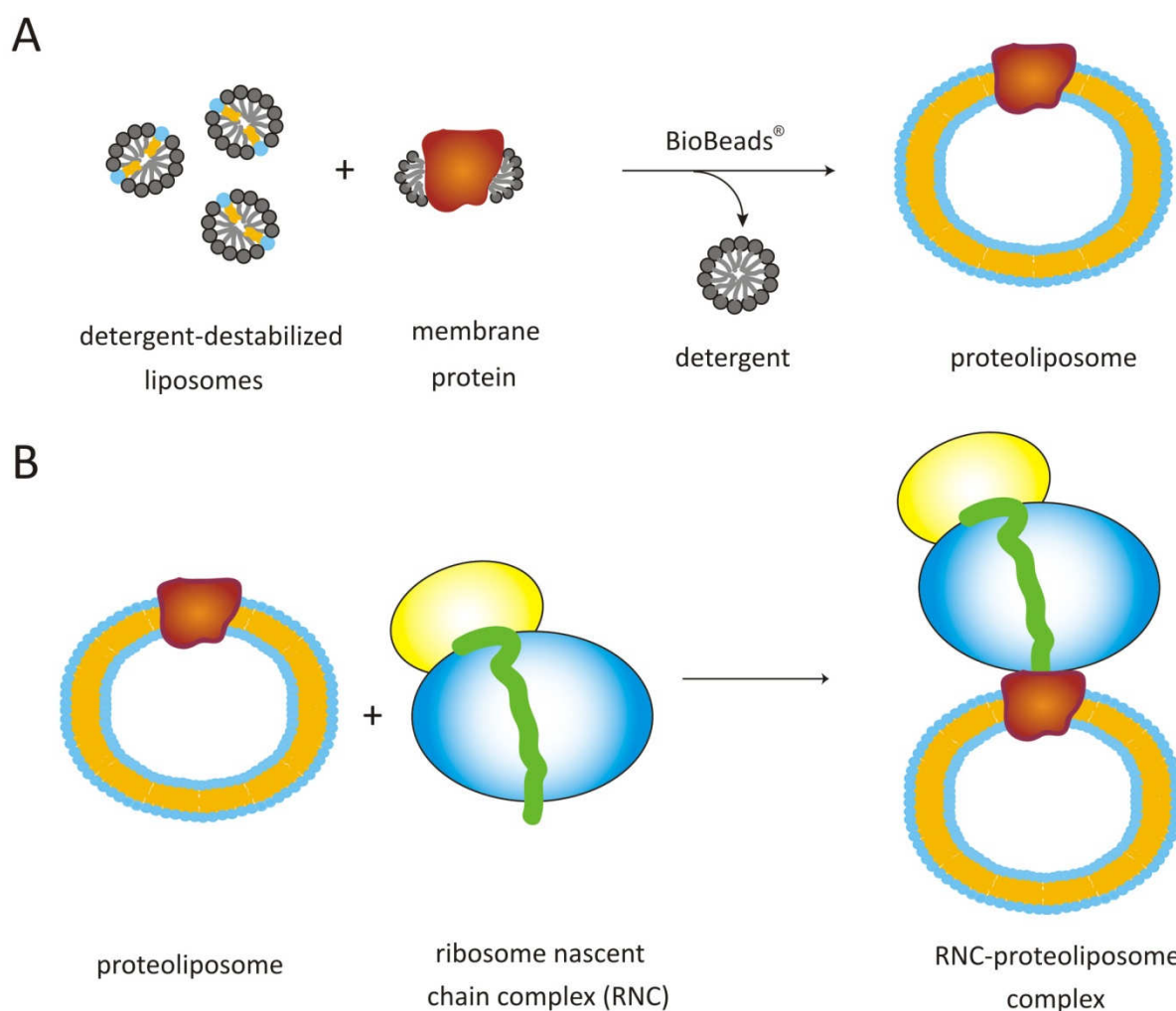
Figure 3.30: Schematic representation of the preparation of a ribosome-proteoliposome-complex. (**A**) For the preparation of proteoliposomes the detergent-solubilized, purified membrane protein is inserted into detergent-destabilized preformed-liposomes. The detergent is then removed through hydrophobic adsorption onto polystyrene beads (BioBeads®), leading to spontaneous formation of proteoliposomes. (**B**) The proteoliposomes are incubated with ribosome nascent chain complexes (RNCs) under appropriate conditions, yielding a RNC-proteoliposome complex which can be analyzed by cryo-EM and single particle reconstruction.

In order to remove nonincorporated and/or aggregated membrane proteins, the reconstituted YidC2-proteoliposomes were subjected to discontinuous flotation gradient centrifugation (Fig. 3.31A). Therefore, the reconstituted sample was first deposited in a 30% sucrose layer and then covered with successive layers of 20, 15, and 10% sucrose solution. During centrifugation, the proteoliposomes float upwards, whereas the nonincorporated membrane proteins stay in the pellet fraction. Subsequent SDS-PAGE analysis (data not shown) as well as negative-stain EM (Fig. 3.31B) of the floated fraction revealed that YidC2 could be incorporated successfully into proteoliposomes.

The YidC2-proteoliposomes were then used for binding experiments with MscL-RNCs in order to finally generate a functional MscL-RNC-YidC2-proteoliposome-complex (Fig. 3.30B) which should then be analyzed by cryo-EM and single particle reconstruction. For this purpose, it will be necessary to have a homogeneous population of YidC2-proteoliposomes with a size of around 250 Å (25 nm) which corresponds roughly to the diameter of the ribosome.
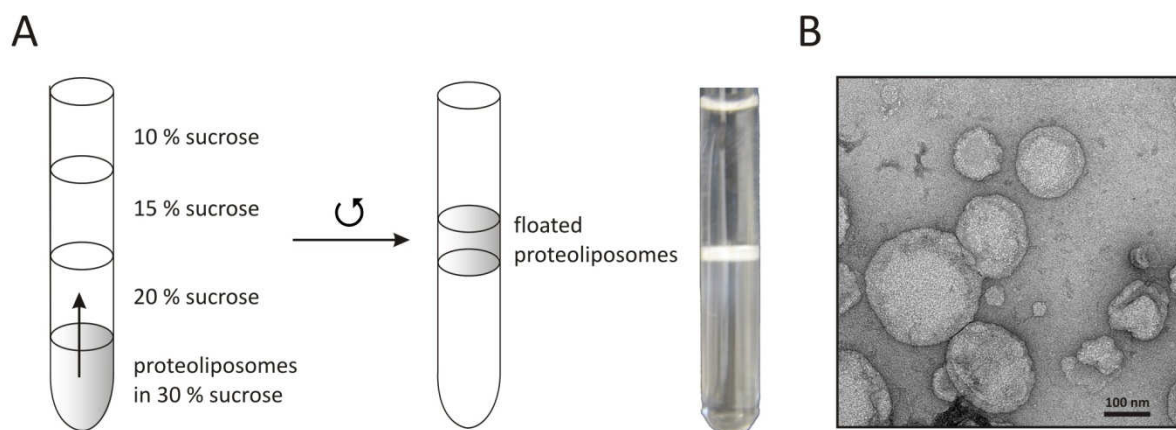
Figure 3.31: Schematic representation of the flotation of proteoliposomes and negative stain analysis of the floated fraction. (**A**) The last step of the proteoliposomes preparation is a discontinuous flotation gradient centrifugation in order to remove nonincorporated and/or aggregated membrane proteins. Thus, the proteoliposomes are deposited in a 30% sucrose layer and covered with lower concentrated sucrose solutions. After centrifugation, the floated proteoliposomes are recognized as white layer in the supernatant. (**B**) Negative stain electron microscopy showing a heterogeneous population of YidC2-proteoliposomes.

3.3.6 Reconstitution of a 70S ribosome-YidC2-proteoliposome complex

For the reconstitution of a functional 70S ribosome-YidC2-proteoliposome complex the appropriate binding conditions had to be determined. The experimental setup of the hence performed reconstitution assays involved the discontinuous flotation gradient centrifugation and was based on a protocol by Birgitta Beatrix (Moller et al., 1998). The components to be tested were mixed in a ribosome binding buffer (RBB) which contained the binding conditions (see Section 2.2.9). After incubation at different temperatures and/or different times, the binding mixture was deposited in a 2.3 M sucrose layer and covered with successive layers of 1.9 M sucrose in RBB and RBB without sucrose (Fig. 3.32A). After subsequent centrifugation, the tube was frozen in liquid nitrogen, cut into a supernatant and a pellet fraction, and then subjected to SDS-PAGE analysis. The proteoliposomes as well as the

ribosomes which are bound to the proteoliposomes float upwards whereas the non-bound ribosomes stay in the pellet fraction.
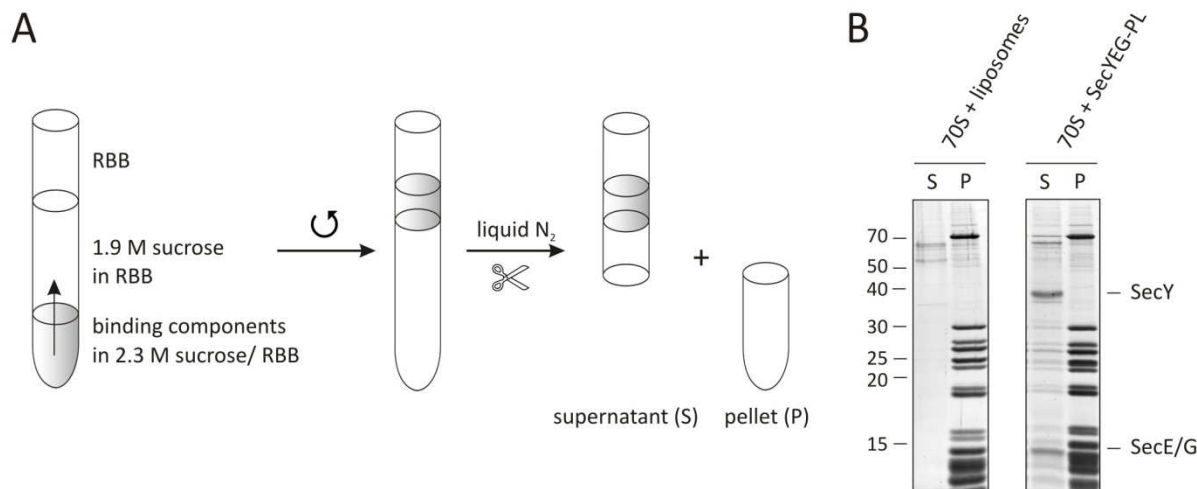
Figure 3.32: Schematic representation of the flotation binding assay and SDS-PAGE analysis of control experiments. (**A**) The binding components are mixed in a ribosome binding buffer (RBB), incubated, and deposited in a 2.3 M sucrose layer which is then covered with successive layers of 1.9 M sucrose in RBB and RBB without sucrose. After centrifugation, the tube is frozen in liquid nitrogen and cut into a supernatant (S) and a pellet (P) fraction. Both, the proteoliposomes and the ribosomes which are bound to the proteoliposomes float upwards whereas the non-bound ribosomes stay in the pellet fraction. (**B**) Liposomes as well as SecYEG-proteoliposomes (SecYEG-PL) were bound to 70S ribosomes and subjected to the flotation binding assay, serving as a negative and positive control, respectively. 70S ribosomes showed specific binding to SecYEG-PL but no unspecific interaction with liposomes.

In order to verify the experimental setup, proteoliposomes containing purified SecYEG (provided by Jens Frauenfeld) were generated and used as a positive control since it is known that SecYEG binds to non-translating 70S ribosomes (Prinz et al., 2000). SDS-PAGE analysis of the performed flotation binding assay showed bands corresponding to the SecYEG-proteoliposomes as well as ribosomal bands in the supernatant fraction (S) (Fig. 3.32B), revealing that as expected 70S ribosomes have bound to the SecYEG-proteoliposomes. To exclude the possibility that ribosomes bind unspecifically to the proteoliposomes, liposomes were prepared in the same way as the proteoliposomes but without addition of a membrane protein. In the SDS-PAGE analysis of the flotation binding assay (Fig. 3.32B) where liposomes were incubated with 70S ribosomes (provided by Daniel Wilson) no ribosomal bands could be detected in the supernatant fraction, showing that the observed flotation of ribosomes strictly depends on the membrane protein integrated into liposomes.

In order to determine at which temperature binding is achieved, YidC2-proteoliposomes were incubated with empty 70S ribosomes for 30 min at 4°C, 21°C, 30°C, and 37°C. SDS-PAGE analysis of the flotation binding assay revealed that strongest binding of YidC2-proteoliposomes to empty ribosomes could be observed at an incubation temperature of 30°C

since here the intensity of the ribosomal bands in the supernatant fraction was much stronger than in the other cases (Fig. 3.33A). Yet another flotation binding assay was performed in which YidC2-proteoliposomes were incubated with 70S ribosomes for a different period of time, ranging from 15 min to 120 min at 30°C. Here, strongest binding could be observed at an incubation time of 90 min (Fig. 3.33B).
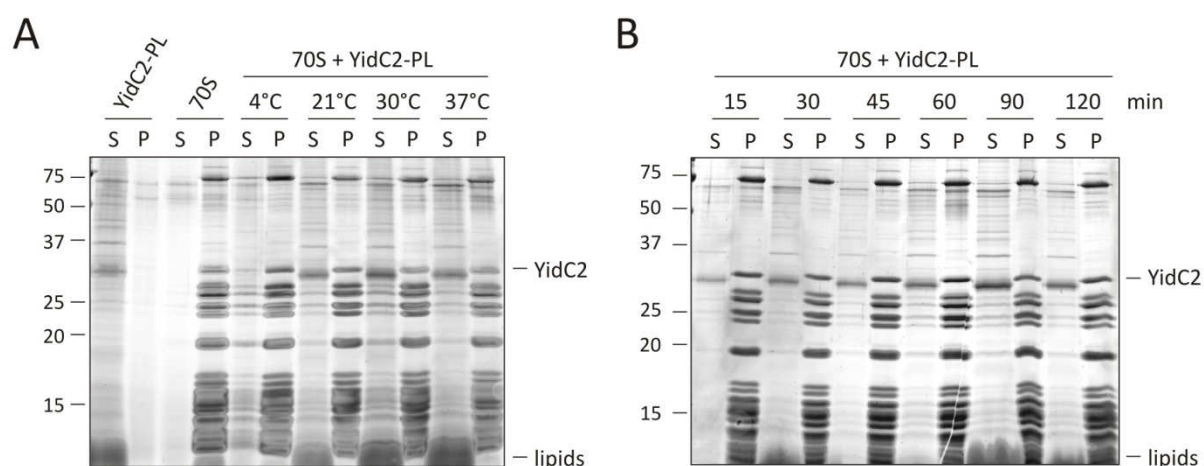
Figure 3.33: Flotation binding assays of YidC2-proteoliposomes to 70S ribosomes using different incubation conditions. YidC2-proteoliposomes (YidC2-PL) were *in vitro* reconstituted with empty 70S ribosomes and subjected to discontinuous flotation gradient centrifugation. The resulting supernatant (S) and pellet (P) fractions were analyzed by SDS-PAGE and subsequent Sypro-Orange staining. (**A**) YidC2-proteoliposomes were incubated with empty 70S ribosomes for 30 min at 4°C, 21°C, 30°C, and 37°C. (**B**) YidC2-proteoliposomes were incubated with empty 70S ribosomes for 15, 30, 45, 60, 90, and 120 min at 30°C. Strongest binding could be achieved with an incubation of 90 min at 30°C.

The best binding conditions, *i.e.* an incubation of 90 min at 30°C, were then used in a flotation binding assay in which the binding of YidC2-proteoliposomes to idle 70S ribosomes was compared to the binding of the proteoliposomes to the different MscL-RNCs. In the SDS-PAGE analysis of the flotation binding assay (Fig. 3.34) no clear difference in the intensity of the ribosomal bands of the floated fraction (S) could be observed. According to this result, the binding of YidC2-proteoliposomes to ribosomes appears to be independently of the presence of a YidC2-specific nascent chain.
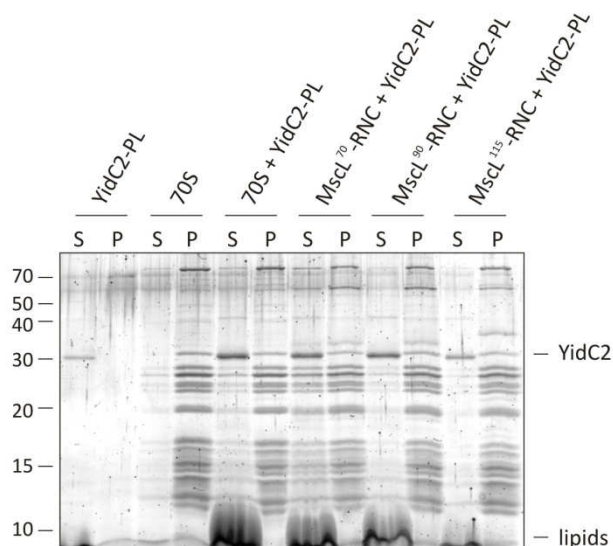
Figure 3.34: Flotation binding assay for comparison of the binding of 70S ribosomes and different MscL-RNCs, respectively, to YidC2-proteoliposomes. YidC2-proteoliposomes (YidC2-PL) were incubated with empty 70S ribosomes and different MscL-RNCs, respectively, for 90 min at 30°C, and then subjected to discontinuous flotation gradient centrifugation. The hence resulting supernatant (S) and pellet (P) fractions were analyzed by SDS-PAGE and subsequent Sypro-Orange staining. Note that no clear difference could be detected.

3.3.7 Attempts for downsizing of the liposomes and YidC2-proteoliposomes

After showning that YidC2-proteoliposomes can be *in vitro* reconstituted with MscL-RNCs, the size of the proteoliposomes was another important factor on the way to the preparation of a functional 70S ribosome-YidC2-proteoliposome complex which can be analyzed by cryo-EM and single particle reconstruction. Since the single particles on an electron microscope grid are embedded in a thin layer of vitreous ice (30-100 nm) (Frank, 2002), the proteoliposomes should have a size of around 25 nm up to 50 nm in diameter. However, analysis of both, a liposome and a proteoliposome preparation by dynamic light scattering (Fig. 3.35A, C) revealed that the size distribution of the lipid vesicles showed a wide variety, ranging from an averaged radius of 50 nm up to 4350 nm. In order to get a homogeneous population of small lipid vesicles both, liposomes and YidC2-proteoliposomes were subjected to several sonication trials in which the duration as well as the intensity were varied. All these different sonication attempts consistently yielded in the same result: the main fraction of the lipid vesicles showed an averaged radius of approximately 200 nm (Fig. 3.35B, D). This means that even though sonication on its own did not lead to a homogeneous population of liposomes with a size of less than 50 nm in diameter, the lipid suspension appeared to be more uniform, and the averaged particle size could also be reduced.
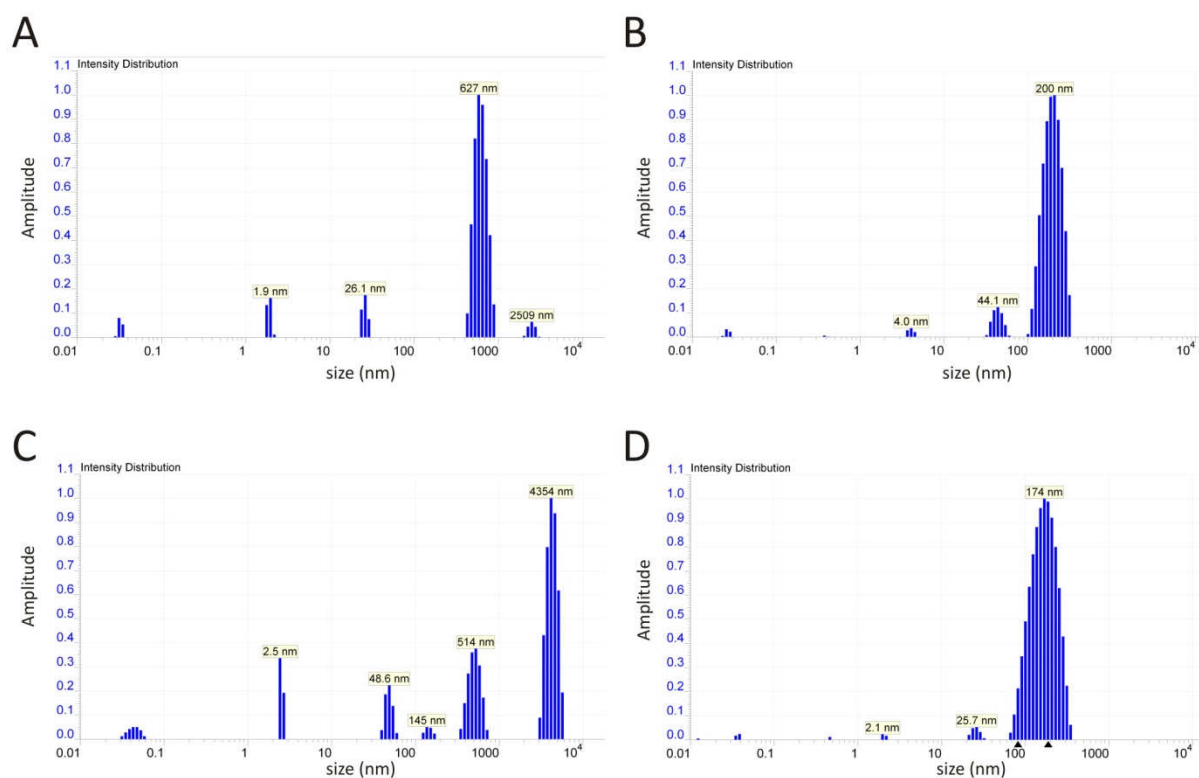
Fig. 3.35: Size distribution profiles of liposomes and YidC2-proteoliposomes before and after sonication. The profiles which show the hydrodynamic radii of the lipid vesicles in nm were determined by dynamic light scattering. (**A**) Size distribution profile of untreated liposomes. (**B**) Size distribution profile of liposomes after sonication. (**C**) Size distribution profile of untreated YidC2-proteoliposomes. (**D**) Size distribution profile of YidC2-proteoliposomes after sonication. In both cases, sonication led to a more homogeneous sample with an averaged particle size of approximately 400 nm in diameter.

Another possibility for downsizing the lipid vesicles was the use of a mini-extruder (Avanti Polar Lipids) where the lipid suspension is pushed through an extruder-membrane with a defined pore size. After the liposomes and proteoliposomes, respectively, achieved an averaged particle size of 400 nm in diameter using sonication, the lipid suspension was pushed for a minimum of eleven times through an extruder-membrane with a pore size of 200 nm. Afterwards, the extruder-membrane was changed to another membrane with a pore size of 100 nm, then 50 nm, and finally 30 nm in order to obtain at best, a homogeneous population of unilamellar lipid vesicles with a size of 30 nm. Since after extrusion the lipid suspension was too diluted to evaluate the size distribution with dynamic light scattering, negative-stain EM was used for analysis. After sonication and extrusion through a 200 nm, 100 nm, 50 nm, and 30 nm extruder-membrane, several small (~ 30 nm) but also many large (~ 200 nm) liposomes (Fig. 3.36A-C) and YidC2-proteoliposomes (Fig. 3.36D-F), respectively, could be detected. Conspicuously, however, was the observation that many of the membrane vesicles show narrow protrusions akin to the tubule formation which is

achieved with reconstituted, HA-tagged Yop1 (Hu et al., 2008). The diameter of the observed tubules (~ 30 nm, Fig. 3.36B) would be suitable for cryo-EM analysis.

Since no difference between liposomes and YidC2-proteoliposomes could be observed in the results of the downsizing trials, the reconstituted membrane protein apparently has no negative influence on the size of the lipid vesicles.
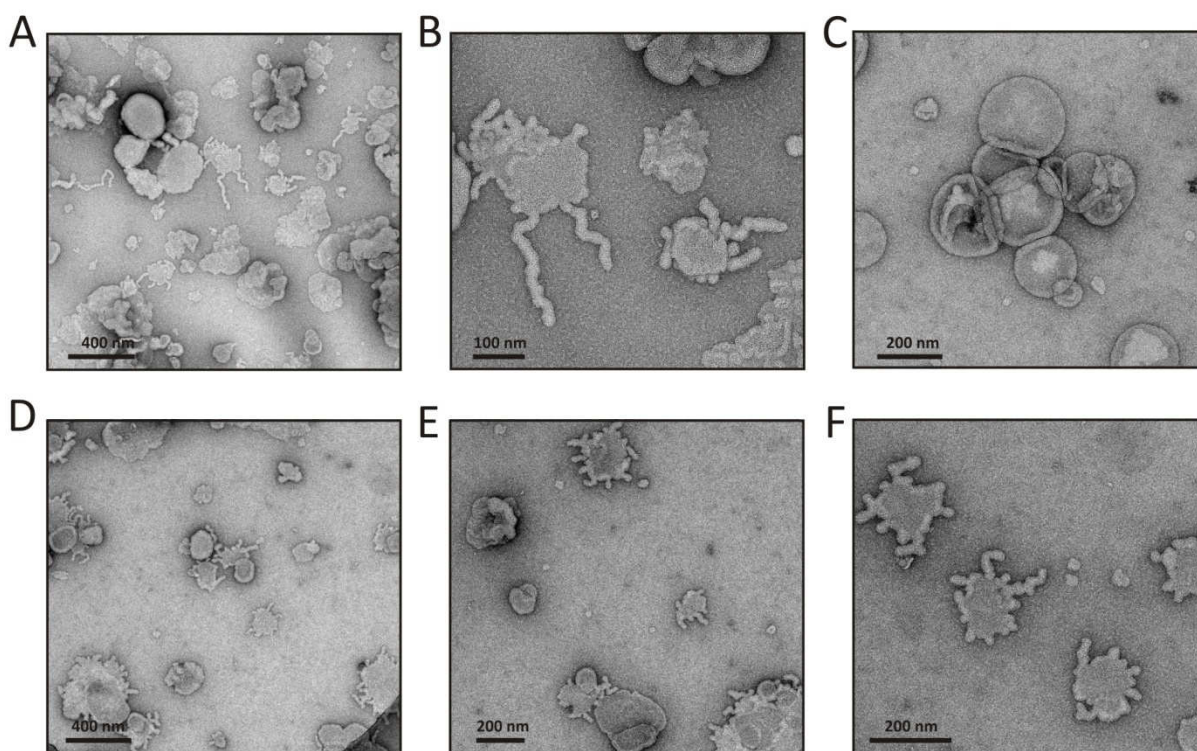
Fig. 3.36: Negative-stain EM images of liposomes and YidC2-proteoliposomes after sonication and extrusion. (**A-C**) EM-images of negative-stained liposomes. (**D-F**) EM-images of negative-stained YidC2-proteoliposomes.

In summary, sonication and subsequent extrusion through a mini-extruder are unsuitable methods for the generation of a homogeneous population of small and uniform YidC2-proteoliposomes, but they led to the formation of narrow tubule-like protrusions which are a good starting point for further attempts.

IV DISCUSSION

In this study, two different aspects of the bacterial ribosome were investigated using cryo-EM and single particle reconstruction as a main technique. In the first part of this thesis, cryo-EM structures of stalled 70S ribosomes were determined and analyzed to better understand the mechanism by which nascent chains can modulate ribosome activity and thus regulate bacterial gene expression. In the second part, the central role of the prokaryotic ribosome in cotranslational insertion of membrane proteins was investigated in order to determine a cryo-EM structure of the membrane protein insertase YidC bound to a translating ribosome.

4.1 Ribosome stalling in prokaryotes

In prokaryotes, amino acids are polymerized into polypeptides in the PTC of the 70S ribosome. The growing nascent peptide chain then moves through the exit tunnel of the large ribosomal subunit before it reaches the extra-ribosomal environment. While most of the polypeptides are thought to transit passively through the exit tunnel, certain nascent chains, such as TnaC and SecM, appear to interact specifically with ribosomal tunnel components, which in turn can modulate the rate of translation (Lu and Deutsch, 2008) or even induce translational stalling (Tenson and Ehrenberg, 2002).

4.1.1 Visualization of the TnaC-70S complex at 5.8 Å resolution

One of the best biochemically characterized examples of nascent chain-dependent ribosome stalling is the expression of the *tna* operon of *E. coli* which encodes tryptophan-metabolizing enzymes. In the presence of inducing levels of tryptophan, the free Trp binds to the ribosome translating the 24-residue long regulatory peptide TnaC and inhibits hydrolysis of the nascent TnaC-tRNA[Pro]. This leads to a stalled ribosomal complex on the *tna* transcript which prevents Rho-mediated transcription termination in the leader region of the operon, thus allowing the transcription of the two downstream structural genes to proceed (Gong and Yanofsky, 2002a). On the basis of comprehensive mutational studies, several features of the amino acid sequence of the TnaC nascent peptide as well as specific nucleotides and amino acids of the *E. coli* 70S ribosome have been identified to be essential for ribosome stalling. However, to further understand the mechanism by which the TnaC leader peptide induces translational stalling,

cryo-EM and single particle reconstruction were used in this study to determine the structure of an *E. coli* 70S ribosome which was stalled during translation of the TnaC leader gene in the presence of free tryptophan (Fig. 3.4C).

The TnaC-70S complex with a resolution of ~ 5.8 Å, based on the FSC 0.5 cut-off criterion (Fig. 3.2B), is currently the highest resolved 70S ribosome using cryo-EM and single particle reconstruction. The currently second highest resolution of a prokaryotic ribosome was the 6.4 Å reconstruction from the *Thermus thermophilus* 70S-tRNA-EF-Tu-GDP-kirromycin complex (Schuette et al., 2009); on the other hand, the highest obtained resolution of an eukaryotic ribosome is the 6.1 Å reconstruction of the 80S RNC-Ssh1 complex (Becker et al., 2009). In general, the resolution value is an important indicator to access the overall quality of a cryo-EM reconstruction. Although the FSC criterion has become the standard quality measure, the issue of the FSC threshold level at which one defines the resolution remains controversial (see (van Heel and Schatz, 2005)). To overcome this problem, the quality of the cryo-EM map of the TnaC-70S complex was also characterized by comparison with filtered X-ray structures of the *E. coli* 70S ribosome (Schuwirth et al., 2005). Thereby, the density map of the TnaC-70S complex mostly resembled the 6 Å resolution model of the X-ray structure (Fig. 3.3) which confirmed the use of the FSC 0.5 cut-off criterion for resolution determination in this case.

Several different factors may have contributed to the high resolution reconstruction of the TnaC-70S complex. One of these factors was most likely the high purity of the sample. The TnaC-stalled 70S ribosomes were gradient-purified and only the monosome fraction of the stalled RNCs was used for grid preparation. Therefore, the sample was biochemically homogeneous, which is an important prerequisite for high resolution cryo-EM structures (Saibil, 2000). In contrast, other RNC preparations do not use gradient-purified ribosomes (Mitra et al., 2005), which results in a mixture of monosomes and polysomes thus leading to a more heterogeneous sample. Furthermore, the ratchet-like rotation of the small subunit relatively to the large subunit, which is usually induced by the binding of EF-G to the pretranslocational ribosome (Valle et al., 2003), was inhibited due to the high occupancy of peptidyl-tRNA (~ 76%) in the ribosomal particles. This also led to an increased conformational homogeneity of the particles. Another possible factor could have been the specimen preparation using the half automated Vitrobot™ system (see materials and methods section) which was most likely performed under optimal conditions, such as the temperature, the humidity, and the procedure itself. The resulting thickness of the ice layer on the EM grid, which has been identified as one of the factors determining the resolution of the

reconstruction (Stagg et al., 2006) was optimal, *i.e.* just thick enough to prevent beam damage of the specimen during electron microscopy, while maintaining a good contrast of the images. Another important factor for the high resolution of the cryo-EM structure was certainly the high number (~ 263,000) of single particles used for the final 3D reconstruction. By the use of even more particles of this quality, the resolution of the final cryo-EM structure possibly could have been even higher.

4.1.2 The TnaC-stalled nascent chain interacts with the ribosomal tunnel

The high quality of the cryo-EM reconstruction of the TnaC-70S complex allowed, for the first time at subnanometer resolution, the visualization of a naturally stalled nascent polypeptide chain in the ribosomal exit tunnel (Fig. 3.4D). In 2005, Mitra and coworkers also claimed that they could visualize density for most of the path of the SecM-stalled nascent polypeptide chain in the ribosomal exit tunnel (Mitra et al., 2006; Mitra et al., 2005). However, the resolution of their cryo-EM reconstruction is with 15 Å much too low to allow further analysis of the underlying stalling mechanism. Recently, another highly-resolved nascent chain, which was published by Thomas Becker and coworkers, could be traced in the exit tunnel of the cryo-EM reconstructions of both, the yeast 80S RNC-Ssh1complex and the mammalian 80S RNC-Sec61 complex (Becker et al., 2009). In contrast to the TnaC-70S complex, the DP120 nascent chains were artificially stalled using truncated mRNA lacking a stop codon.

The TnaC nascent chain represents a strong feature in the cryo-EM reconstruction of the TnaC-70S complex, since even at high contour levels, robust density for the C-terminal half of the nascent chain could be observed which becomes continuous throughout the entirety of the tunnel at lower contour levels (Fig. 3.5). Therefore, a molecular model of all 24 amino acids of the TnaC leader peptide could be fitted into the isolated density using the program Rapper (de Bakker et al., 2006) and MDFF (Trabuco et al., 2008). The fitting resulted in an ensemble of 10 different poly-Ala models which all displayed an extended conformation of the nascent chain with root-mean-square fluctuations (RMSFs) for the Cα atoms smaller than 2 Å (Fig. 4.1). The extended conformation of the TnaC peptide is also in agreement with the observed similarity of the nascent chain to the extended N-terminal region of ribosomal protein L27 (Fig. 3.6). The fact that several models, which are slightly differing in the positions of the Cα atoms, could be fitted into the nascent chain density, reveals the limit of

the 5.8 Å resolution map, *i.e.* it was not possible to fit side chains into the density of the TnaC leader peptide. Therefore, all structural analyses were restricted to the backbone trace.
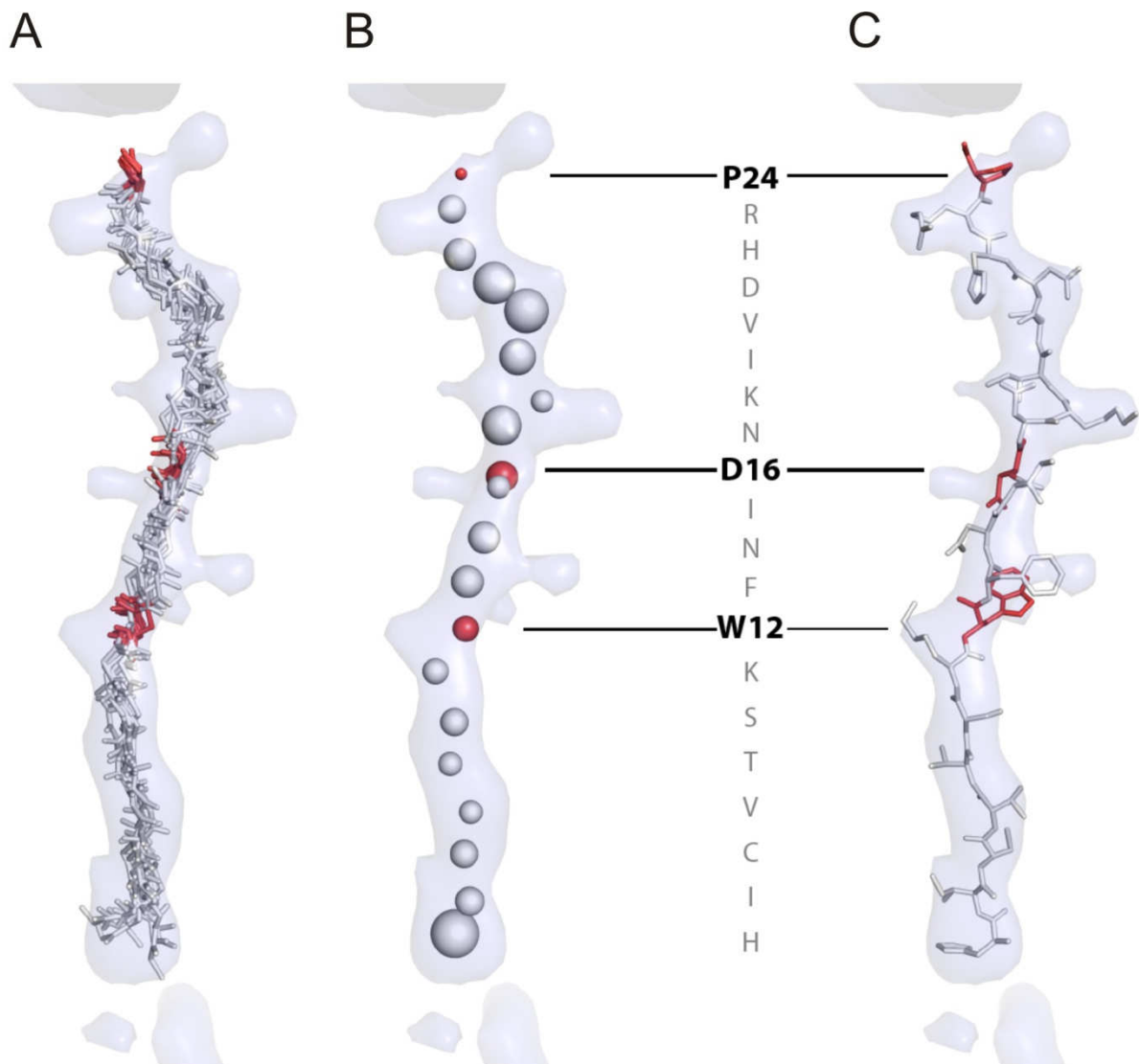
Figure 4.1: Cα atoms representations for an ensemble of 10 different TnaC conformers generated by the program Rapper and refined by MDFF. (**A**) Backbone representation and (**B**) radii of the Cα atoms in (A) corresponding to the root mean squared fluctuations (RMSF) in the Cα positions. (**C**) All-atom representation of one of the ten TnaC conformers, demonstrating the excellent agreement between the cryo-EM density and the generated model.

Genomic comparisons of TnaC amino acid sequences identified Trp[12], Asp[16], and Pro[24] as highly conserved TnaC residues. Replacing these amino acids by other residues has been shown to reduce or even eliminate Trp-mediated induction of *tna* operon expression (Cruz-Vera and Yanofsky, 2008). The cryo-EM reconstruction of the TnaC-stalled 70S complex revealed that these important residues are indeed involved in specific contacts with nucleotides and amino acids that form the peptide exit tunnel in the 50S ribosomal subunit (Fig. 3.7) and also have been shown to be essential for stalling of the TnaC leader peptide

(Cruz-Vera et al., 2005). Thus, the biochemical data which were determined by comprehensive mutational studies and cross-linking analyses could be confirmed by structural analysis of the TnaC stalling complex.

4.1.3 The role of A2602 and U2585 in the TnaC stalling mechanism

The PTC of the ribosome plays a fundamental role in protein synthesis, since it catalyzes both peptide bond formation and peptide release. Inspection of the PTC of the TnaC-stalled 70S ribosome, where hydrolysis of the nascent TnaC-tRNA^{Pro} is inhibited (Gong and Yanofsky, 2002a), revealed that the two most flexible nucleotides of the PTC, A2602 and U2585, are in a fixed conformation.

It has been shown that mutations at position A2602 significantly inhibited the ribosome's ability to promote the catalysis of peptide release (Polacek et al., 2003; Youngman et al., 2004). Recent findings suggest that these severe reductions are most likely the result of a conformationally distorted PTC (Amort et al., 2007). Furthermore, experiments with *E. coli* ribosomes showed that mutations of U2585 also reduced the rate of peptide release, but to a smaller extent (Youngman et al., 2004). Thus, A2602 seems to be one of the main players for the peptide release, with a likely additional contribution of U2585.

The distinct conformation of the nucleotide A2602 observed in the cryo-EM structure of the TnaC-stalled 70S ribosome (Fig. 3.9E) resembles the position that A2602 also adopts when the translation inhibitor sparsomycin is bound at the PTC (Schmeing et al., 2005b). In structural models of the ribosome in translation, the antibiotic sparsomycin was shown to contact the nucleotide A2602 (Hansen et al., 2003; Porse et al., 1999). In addition, the conformation of nucleotides implicated in A-site binding, such as U2584, was affected upon interaction of sparsomycin with the *Deinococcus radiodurans* ribosome (Bashan et al., 2003). Furthermore, it has been shown that the antibiotic puromycin, an analog of RF2 activity, when interacting with the A-site of the *Haloarcula marismortui* ribosome induces specific movements of the nucleotides G2583 to U2585 (Schmeing et al., 2005a). That means that both puromycin and sparsomycin affect the orientation of the nucleotide U2584, which is located in the vicinity of U2585. In the cryo-EM structure of the TnaC-70S complex, the flexible base U2585 might have shifted into a fixed conformation in order to interact with the Pro[24] of the TnaC leader peptide, because a continuous density between the nascent chain and the location of U2585 could be observed (Fig. 3.9C). Since the free Trp can inhibit the binding and action of both antibiotics, it has been suggested that the bound tryptophan alters

the location of A2602, U2584, and U2585 (Cruz-Vera et al., 2007) which is in agreement with the distinct conformations of these nucleotides observed in the cryo-EM reconstruction of the TnaC-70S complex.

The ribosome stalling on the *tnaC* leader transcript is the result of inhibition of RF2-mediated cleavage of the nascent TnaC-peptidyl-tRNA at its UGA stop codon (Gong and Yanofsky, 2002b).   Based on the results of mutational studies, Polacek and coworkers proposed a model in which the class I RF triggers peptide release by reorienting A2602 in the PTC so that it can coordinate and possibly activate a water molecule (Polacek et al., 2003). In this model, the universally conserved GGQ peptide mini-motif of the A-site bound RF functions to promote the conformational change of A2602. The central location of A2602 in the PTC and its structural flexibility are compatible with this proposed role (Bashan et al., 2003; Nissen et al., 2000; Wilson et al., 2005). The repositioning of A2602, which is required for peptide release, can possibly be coordinated with the movement of U2585 (Schmeing et al., 2005b).

In the cryo-EM structure of the TnaC-70S complex it could be shown that the fixed conformations of A2602 and U2585 are incompatible with simultaneous cohabitation of termination release factor 2 (Fig. 3.9F) (Weixlbaumer et al., 2008). This suggest that even though RF2 can still bind to TnaC-stalled 70S ribosomes (Cruz-Vera et al., 2005), the fixed conformation of A2602 and U2585 would prevent the correct positioning of the GGQ peptide mini-motif of the RF within the PTC that is necessary for efficient hydrolysis and release of the nascent chain. Therefore, the inactive conformation of the PTC of TnaC-stalled ribosomes could be explained by the cryo-EM reconstruction of the TnaC-70S complex determined in this study.

4.1.4 Where is the free tryptophan?

The binding of free tryptophan to the ribosome is required for the TnaC-mediated inactivation of the PTC. Although the exact location of the binding site of free Trp is not known, it has been proposed to overlap with that of the antibiotic sparsomycin (Cruz-Vera et al., 2006; Cruz-Vera et al., 2007). This proposal is attractive given the sparsomycin-like conformation of A2602 observed in the PTC of the TnaC-70S complex. Furthermore, the possible stacking of the free Trp between the peptidyl-tRNA and A2602, in a manner analogous to sparsomycin, would explain the fixed conformation of A2602. In addition, it has been shown that when the *tnaC* UGA stop codon is replaced by a tryptophan codon, Trp-tRNA at the ribosomal A-site can substitute for free Trp as inducer and also inhibit hydrolysis of TnaC-

tRNA^{Pro} (Gong and Yanofsky, 2002a). This finding suggests that the free tryptophan molecule binds where the amino-acyl moiety of an A-site tRNA is located at the PTC, which also overlaps with the sparsomycin binding site (Cruz-Vera et al., 2007).

Nevertheless, despite the fact that the purification and cryo-EM analysis of the TnaC-70S complex were carried out in the presence of 2 mM Trp, which was shown to be the most effective Trp concentration in inhibiting puromycin or RF2 action (Cruz-Vera et al., 2006; Cruz-Vera et al., 2005), no additional density that could be attributed to the free Trp molecule could be observed within the sparsomycin-binding site, or in the A-site of the PTC (Fig. 3.9E). The main reason for it is that the resolution of the cryo-EM structure is not sufficient to detect a single tryptophan molecule. In addition, it is not known where exactly it binds, and if the binding is rigid enough for visualization using cryo-EM. Probably, it would be possible to detect the free tryptophan molecule at atomic resolution using X-ray crystallography.

4.1.5 Model for the TnaC relay system

Ribosome recognition of specific features of the TnaC leader peptide results in specific binding of free Trp in the ribosome, inhibiting peptidyl transferase activity. Since residues of the TnaC nascent chain that are essential for ribosome stalling are located far from the PTC, some sort of signal must be propagated from the depths of the tunnel back to the PTC. On the basis of the cryo-EM structure of the TnaC-stalled 70S ribosome and previous biochemical data a model can be proposed where a nascent chain-induced relay of interactions leads to silencing of the PTC (Fig. 4.2).

A total of three non-mutually exclusive possibilities for the TnaC relay system were identified. One possibility is that the signal is relayed back via the nascent chain itself, *i.e.* the interaction between the TnaC nascent chain and the ribosomal peptide exit tunnel induces a specific conformation in the nascent chain that inhibits the PTC activity via a feedback mechanism (Relay R1 in Fig. 4.2B). Since the spacing between Trp^{12}, which is located in the narrow region of the ribosomal exit tunnel, and Pro^{24}, which is located near the active site, is important, an involvement of the nascent peptide itself in the signaling process appears likely (Cruz-Vera et al., 2005; Gong and Yanofsky, 2002a). In addition, Cruz-Vera and coworkers also concluded from their data that the highly conserved residues of the TnaC leader peptide, Trp^{12}, Asp^{16}, and Pro^{24}, probably play an important role in creating a tryptophan binding site in the ribosome where the tryptophan then inhibits the peptidyl transferase reaction (Cruz-Vera and Yanofsky, 2008).
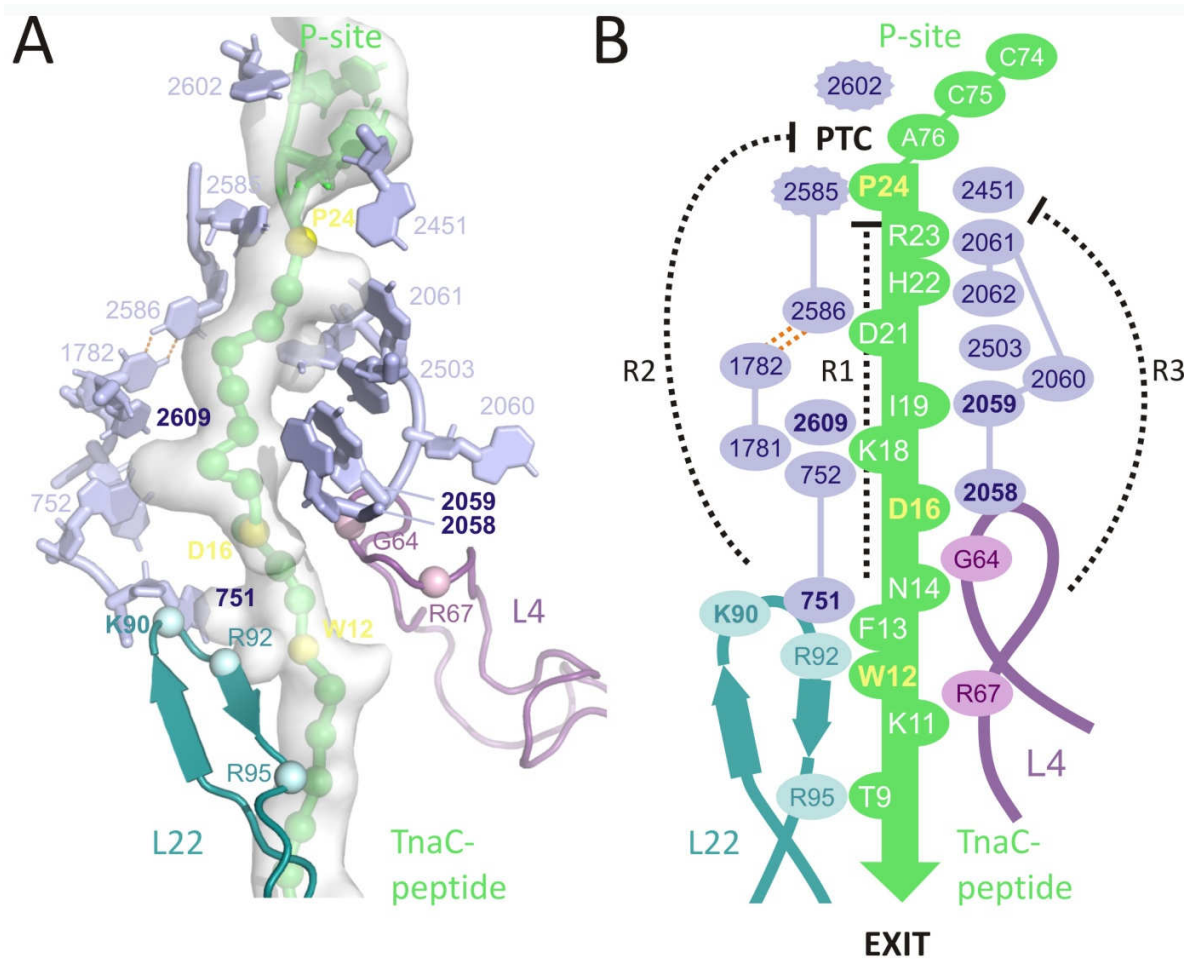
Figure 4.2: Nascent chain-mediated relay of interactions for PTC silencing. (**A**) Ribosomal components (23S rRNA nucleotides, blue; L22, teal; L4, mauve) which are potentially involved in a relay mechanism where interaction of the TnaC nascent chain (green) with the ribosomal tunnel components leads to inactivation of the PTC. Ribosomal components implicated in TnaC stalling are in bold font and approximate positions of TnaC nascent chain residues that are essential for stalling are coloured yellow. The isolated P-site tRNA and nascent chain density is shown as a transparent grey surface. (**B**) Schematic indicating potential relay pathways from the Trp[12] (W12) of the TnaC nascent chain to the PTC, either through the nascent chain itself (R1) or via a network of interconnected 23S rRNA nucleotides (R2 and R3).

Another possibility for the TnaC relay system is that the "stalling signal" is relayed back through a series of conformational changes in the network of ribosomal tunnel components. Interestingly, contacts between the TnaC nascent chain and the ribosomal exit tunnel, which were observed in the cryo-EM reconstruction of the TnaC-70S complex (Fig. 3.7), can be incorporated into one of two possible relay pathways (R2 and R3 in Fig. 4.2B). These relay pathways, encompassing important stalling residues, terminate at nucleotides within the PTC that are crucial for peptidyl transferase and peptidyl-tRNA hydrolysis activity. For example, in Relay 2, Trp[12] of the TnaC leader peptide and Lys[90] of ribosomal protein L22 can be relayed to U2585, via a network of contacts comprising A751-A752, U2609, 1781-1782 to U2586. This relay is in agreement with the assumption, proposed by Cruz-Vera and

coworkers, that Trp[12] of TnaC-tRNA[Pro] alters the position of several nucleotides of 23S rRNA in the ribosomal exit tunnel, thereby contributing in creating a free Trp binding site in the PTC (Cruz-Vera et al., 2006; Cruz-Vera et al., 2005). Similarly, in Relay 3, Asp[16] of the TnaC nascent chain can be linked to A2451 within the PTC through a network consisting of 2058-2059, U2053, 2060-2061. Indeed, it has been shown that ribosomes with mutations of the nucleotides U2585 and A2451, which terminate Relay 2 and 3, respectively, display significant defects in peptidyl-tRNA hydrolysis activity (Green et al., 1997; Youngman et al., 2004) and could therefore play an important role in the TnaC stalling mechanism.

4.1.6 TnaC vs. SecM stalling

In addition to the ribosome stalling on the TnaC leader peptide, several other nascent peptides have been shown to act *in cis*, inhibiting completion of their own synthesis. The 170-amino acid secreted SecM peptide in *E. coli* that regulates the translation of the downstream *secA* gene in response to the secretion status of the cell (Oliver et al., 1998) is another well-characterized example for ribosome stalling in prokaryotes.

During synthesis, the SecM nascent chain induces translation arrest through its C-terminal, 17 amino acids long stalling sequence, which similarly to TnaC also has been shown to interact with ribosomal RNA and protein residues of the peptide exit tunnel near its constriction site (Nakatogawa and Ito, 2002), although the sets of mutants affecting the respective process overlap only partially. In both stalling complexes, a critical tryptophan residue of the stalling peptide, *i.e.* Trp[12] of TnaC and Trp[155] of SecM, may contribute to the recognition of the nascent chain by specific elements of the ribosomal exit tunnel. However, the region of the tunnel involved in SecM recognition seems to be located somewhat farther from the PTC than in the case of the TnaC peptide (Beringer, 2008). This may reflect a difference in the conformation of the peptides leading to the different locations of the parts of the nascent chains which interact with the ribosomal exit tunnel. According to FRET measurements, the stalled SecM peptide assumes some compacted structure, possibly an α-helix (Woolhead et al., 2006), whereas the TnaC nascent chain adapts an extended conformation, as shown in the cryo-EM reconstruction of the TnaC-70S complex (Fig. 3.6).

In contrast to TnaC, the SecM stalling is caused by the inability of the PTC to catalyze peptide bond formation since the critical Pro[166]-tRNA remains at the ribosomal A-site without forming a peptide bond with the peptidyl-tRNA[Gly] located at the P-site (Muto et al., 2006). Here, the nonincorporated Pro[166]-tRNA seems to act as an A-site effector of translation arrest,

similar to the free Trp in the TnaC system (Ito et al., 2010). However, while the intracellular concentration of tryptophan varies according to nutritional conditions, the A-site effector of SecM is genetically encoded, and therefore constitutive and integrated into the intrinsic arrest function of the stalling peptide.

Based on the cryo-EM structure of a SecM-stalled 70S ribosome of ~ 15 Å resolution, Mitra and coworkers proposed a mechanism for elongation arrest by SecM via an internal signal transduction within the ribosome (Mitra et al., 2006). When comparing a refined atomic model for the *E. coli* 70S ribosome with the cryo-EM maps of the SecM-stalled (Mitra et al., 2005) and stalled, prestate (Valle et al., 2003) ribosome complexes, they observed significant conformational changes ($\geq$ 2 Å) of the 23S rRNA bases A2058 and A749-753, which have been shown to be essential for SecM stalling (Nakatogawa and Ito, 2002), and of other important morphological and functional features of the 50S subunit. The conformational changes in the 50S subunit also affected the geometry of the intersubunit bridges and the positioning of the tRNAs, which in turn resulted in a rearrangement of rRNA elements of the 30S subunit (Mitra et al., 2006). On the basis of these observations they suggested that SecM induces a cascade of large-scale conformational changes, which are propagated from the exit tunnel throughout the whole ribosome, most likely resulting in an inhibition of mRNA translocation.

Although the SecM stalling mechanism proposed by Mitra *et al.* might indeed be physiological, one has to be cautious with the molecular interpretation of atomic models fitted into low-resolution cryo-EM maps, where not even secondary structure elements are resolved. Moreover, the observed 2 Å movements of rRNA elements in a 15 Å resolution cryo-EM density are most likely not significant. In any case, the large-scale conformational changes, which are proposed to lead to the inhibition of SecM translation, contrast with the observation in the cryo-EM structure of the TnaC-70S complex where only very modest conformational changes could be detected.

In order to prove or disprove the SecM stalling mechanism suggested by Mitra *et al.* and also to compare it with the TnaC stalling mechanism, a cryo-EM structure of a SecM stalled *E. coli* 70S ribosome with a resolution of 6.2 Å (according to the FSC 0.5 criterion) was determined (Fig. 3.13) using the same RNC purification method as used for the TnaC-70S complex (see Section 2.2.1). In contrast to the TnaC dataset, sorting of the SecM dataset was more challenging since a ratchet-like rotation of the small subunit relatively to the large subunit could be observed. On the one hand, this observation would confirm the conformational changes of the 30S subunit which have been proposed by Mitra *et al.* for the

SecM-stalled ribosome (Mitra et al., 2006). On the other hand, it could also mean that the occupancy of peptidyl-tRNA was too low, since structural and biochemical studies have been shown that when a nascent peptide is covalently bound to the P-site tRNA, the ratchet-like rotation is inhibited even in the presence of EF-G (Valle et al., 2003; Zavialov and Ehrenberg, 2003). This is also in agreement with the situation in the ribosomal exit tunnel of the SecM-70S cryo-EM reconstruction where almost no extra density could be attributed to the SecM nascent peptide at higher contour levels (Fig. 3.16). The main reason for the absence of continuous density for the nascent chain in the peptide exit tunnel could be that the used RNC purification method, which was primarily established for the TnaC-stalled ribosomes, was unsuitable for the preparation of SecM-stalled RNCs. Since the purification of the RNCs took at least two days, it is possible that the SecM-stalled ribosomes are less stable *in vitro* than TnaC-stalled ribosomes, possibly due to the absence of an inducing molecule. One indicator for this explanation is given by the yield of the SecM-stalled RNCs, which was considerably lower than the achieved yield of the TnaC-stalled RNCs.
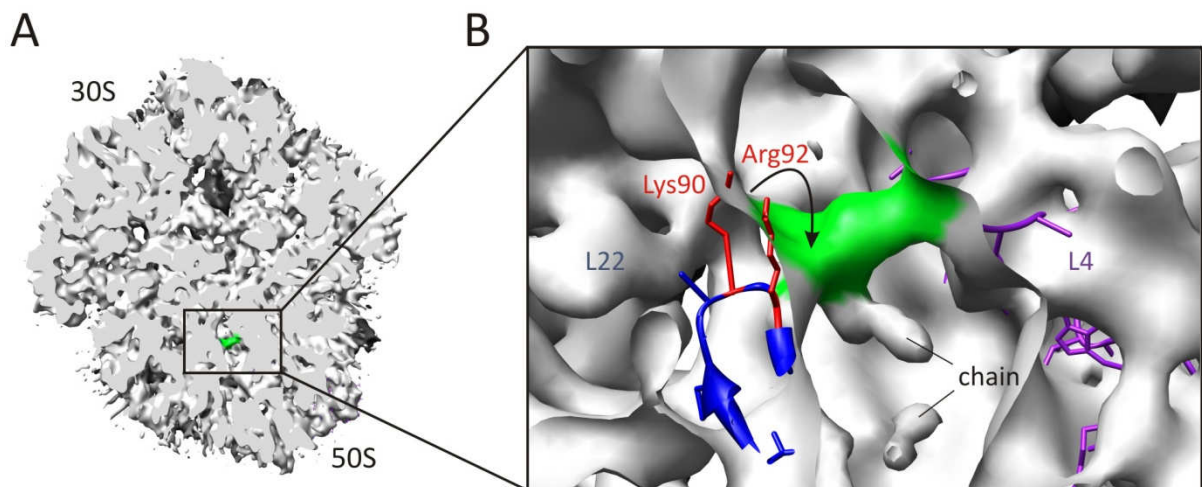
Figure 4.3: Working model for the formation of a connection between ribosomal proteins L22 and L4 in the exit tunnel of the SecM-70S cryo-EM reconstruction. (**A**) Section through the SecM-70S complex (grey) showing a strong density (green) within the ribosomal exit tunnel. (**B**) Enlargement of the tunnel region from (A) to show the bridge (green) connecting ribosomal proteins L22 (blue) and L4 (purple). The residues Lys^{90} and Arg^{92} of L22, which are suggested to flip across the tunnel (indicated by an arrow) in order to prevent further passage of the SecM nascent peptide, are shown in red.

Nevertheless, a strong density within the narrow region of the exit tunnel of the SecM-70S cryo-EM reconstruction could be observed, connecting the β-hairpin loop of L22 with the extended loop of L4 (Fig. 3.17). Berisio and coworkers have previously proposed a working model for the SecM arrest sequence action where SecM may act like the antibiotic TAO,

displacing the β-hairpin region of L22 from the wall and causing it to flip across the tunnel (Berisio et al., 2003). Based on this model and the observations in the SecM-70S complex, it could indeed be possible that specific residues of L22, such as Lys[90] and Arg[92], may shift to interact with ribosomal protein L4, thus blocking the exit tunnel and preventing further passage of the SecM nascent chain (Fig. 4.3). An involvement of the L22 residues Lys[90] and Arg[92] is likely since mutations of the adjacent residues Gly[91] and Ala[93] have been shown to relieve the stalling effect of the SecM nascent peptide (Nakatogawa and Ito, 2002). However, the here suggested SecM stalling mechanism has to be proven by another high-resolution structure of a SecM-stalled 70S ribosome where strong densities for both, an A-site tRNA and the SecM nascent chain are visible. A basis for this could already be established with the purification of SecM-stalled DP120-RNCs where the presence of an A-site tRNA could already be demonstrated by a puromycin assay (Fig. 3.19) as well as by a first low-resolution cryo-EM reconstruction (Fig. 3.20). For the visualization of the SecM nascent chain the dataset needs to be further processed, sorted according to the presence of A- and P-site tRNA, and finally refined to get a high resolution structure of SecM-stalled DP120-RNCs. Until then, the here suggested stalling model remains speculative, but also interesting since such a bridge connecting L22 and L4 could not be observed in the peptide exit tunnel of the TnaC-70S complex.

4.1.7 Conclusions

By structural analysis of two different stalling systems in prokaryotes, TnaC and SecM, it could be shown that the peptide exit tunnel in the large ribosomal subunit is not just a passive conduit for the growing polypeptide chain as originally thought (Ban et al., 2000), but rather an active compartment which seems to recognize and interact with specific amino acid sequences of nascent chains, and thus affecting the structure and function of the ribosome. In addition, the observation that different nascent polypeptide chains, which have little or no sequence conservation, interact with the exit tunnel in a distinct manner and adopt individual conformations (Fig. 3.8) may be important not only for initial folding events in the ribosomal tunnel, as recently shown by Shashi Bhushan *et al.* (Bhushan et al., 2010), but also for diverse nascent chain-mediated regulatory mechanisms (Tenson and Ehrenberg, 2002). The fact that ribosomal mutations that relieve translational arrest in one regulatory system do not necessarily have the same suppression effect in another (Lawrence et al., 2008), shows that the stalling sequences may use different mechanisms to arrest their own translation. Thus,

structures of other prokaryotic stalling systems, such as the membrane integration-monitoring peptide MifM in *Bacillus subtilis* which seems to act in a similar manner as SecM in *E. coli* (Chiba et al., 2009), could provide more mechanistic insights into the different or even same stalling mechanisms used for regulation of bacterial gene expression.

Since sequences that cause translational pausing are also found in eukaryotes, structural analysis of these systems would also be interesting, especially to determine whether they are similar to the prokaryotic stalling mechanisms or to what extent they differ from each other. A stalling system in eukaryotes for example, which is quite similar to the TnaC system in prokaryotes, is the expression of the arginine-specific carbamoyl-phosphatase synthase small subunit in fungi which is regulated by the cellular concentration of arginine (Fang et al., 2004). Here, in the presence of high concentrations of arginine, the nascent arginine attenuator peptide (AAP) stalls the translating ribosome due to the inhibition of translation termination. Determination of a cryo-EM structure of an AAP-stalled 80S ribosome would help to elucidate the underlying stalling mechanism and to compare it with the TnaC-stalled 70S ribosome.

4.2 Characterization of a ribosome-YidC complex

Since membrane proteins represent approximately 20-30% of the proteome in bacteria and are involved in fundamental biological processes, their biogenesis is of vital importance (Xie and Dalbey, 2008). In *E. coli*, two evolutionary conserved pathways have been identified by which membrane proteins are integrated into the cytoplasmic membrane, namely the Sec pathway which is the main pathway for membrane protein insertion, and the YidC-only pathway (see Section 1.4). The shared component of both pathways is the membrane protein insertase YidC which is the prokaryotic member of the conserved YidC/Oxa1/Alb3 protein family (Dalbey and Kuhn, 2004). YidC assists in assembly and folding of membrane proteins in the Sec pathway and also integrates Sec-independent membrane proteins, such as the double membrane-spanning MscL protein into the lipid bilayer (Facey et al., 2007; Serek et al., 2004).

4.2.1 Towards a high resolution structure of a ribosome-YidC complex

In contrast to the extensively studied Sec translocon, where already several cryo-EM and X-ray structures have been determined, the structural information on YidC is limited. For *E. coli*

YidC there is an X-ray structure of the large periplasmic domain (Oliver and Paetzel, 2008; Ravaud et al., 2008), a 10 Å 2D projection map of the membrane-integrated dimer (Lotz et al., 2008), as well as a low-resolution cryo-EM reconstruction where it is in complex with a translating 70S ribosome (Kohler et al., 2009). Although all of these structures provide important insights into the architecture of YidC, they are not sufficient to answer for instance the question whether YidC is indeed an oligomer during insertion of Sec-independent substrates. In order to understand how YidC functions at a molecular level, it is therefore essential to solve the structure of YidC bound to substrate-specific RNCs at high resolution. How important the resolution of a cryo-EM reconstruction for its interpretation is, could be recently demonstrated by the structures of eukaryotic ribosome-Sec61 complexes which were determined at resolutions of ~ 6 Å (Becker et al., 2009). Until then, there was a long-time discussion about the oligomeric state of the Sec complex during cotranslational translocation. On the basis of low-resolution cryo-EM structures it has been suggested that two to four SecY/Sec61 molecules are present to build an active PCC (Beckmann et al., 1997; Beckmann et al., 2001; Menetret et al., 2000; Menetret et al., 2005; Mitra et al., 2005; Morgan et al., 2002), even though the X-ray structure of an archaeal SecYEβ complex led to the interpretation that a single copy of the Sec complex would be already sufficient (Van den Berg et al., 2004). Thomas Becker *et al.* now identified only one copy of the Sec61 complex in their high-resolution structures, and showed that a surrounding detergent/lipid micelle of varying sizes could have been the reason for the misinterpretation of the previous low-resolution cryo-EM structures (Becker et al., 2009).

In this study, *E. coli* YidC and YidC2 from the Gram-positive bacterium *S. mutans* were used for structure determination, since YidC2 contains an extended hydrophilic C-terminal region akin to the positively charged extension of the mitochondrial YidC homologue Oxa1 where this domain has been shown to directly interact with mitochondrial ribosomes (Jia et al., 2003; Szyrach et al., 2003). The usage of *S. mutans* YidC2 was promising since it was assumed that its C-terminus might not only support, but also stabilize the binding to 70S ribosomes, which is an important prerequisite for its visualization via cryo-EM. For the purification of *S. mutans* YidC2 out of *E. coli* membrane vesicles a protocol could successfully be established (see Section 2.2.4). The amount as well as its purity (Fig. 3.21) was sufficient for reconstitution and cryo-EM analysis. Since the yield achieved in homologous expression systems is in general higher than in heterologous systems (Knol et al., 1998), overexpression of YidC2 in *S. mutans* could probably increase the yield of the membrane protein.

The cryo-EM reconstruction of YidC2 in complex with the *E. coli* 70S ribosome revealed that YidC2 could not be visualized when using empty 70S ribosomes (Fig. 3.23) even though a binding was demonstrated in several reconstitution assays (Fig. 3.22). To overcome the likely problems of nonspecific binding and ligand flexibility, the binding affinity of YidC was increased by usage of programmed ribosomes carrying MscL as a YidC-specific nascent chain. MscL is a homopentameric complex in the inner membrane of *E. coli* which consists of two TM-domains and was shown to be targeted to the membrane via the SRP pathway (Facey et al., 2007). The TnaC system, which was analyzed in the first part of this study, could successfully be used for the preparation of TnaC-stalled MscL-RNCs varying in the length of the nascent chains, which represent different MscL insertion intermediates (Fig. 3.26). In spite of the presence of a YidC-specific substrate, a difference in the binding to empty 70S ribosomes could not be detected in the reconstitution assay (Fig. 3.27). Moreover, the preliminary determined low-resolution cryo-EM structure of the YidC2-MscL[115]-RNC complex revealed that it was not possible to visualize *S. mutans* YidC2. The heterologous YidC2-ribosome interaction is probably not only nonspecific but also too flexible for its visualization via cryo-EM. It could also be that YidC2 binds to the ribosome but gets dissociated during grid preparation probably due to a high binding off-rate. Maybe it is possible to determine the structure when using a homologous system, *i.e.* to reconstitute YidC2 with *S. mutans* ribosomes carrying a YidC2-specific nascent chain. This could lead to an increased binding specificity, and therefore to its visualization in cryo-EM.

In contrast to *S. mutans* YidC2, *E. coli* YidC could successfully be visualized in complex with TnaC-stalled Mscl[115]-RNCs in a preliminary determined low-resolution reconstruction (Fig. 3.29). Here, the usage of MscL-RNCs probably was the decisive step for its visualization via cryo-EM. Hence, the foundations are laid for a high-resolution structure of *E. coli* YidC bound to a translating ribosome.

4.2.2 Visualization of YidC2 in the membrane environment

In order to determine to what extent the detergent micelle of the detergent-solubilized membrane protein contributes to the cryo-EM density, a structure of YidC2 in its native membrane environment and in complex with MscL-RNCs is required. Established procedures for membrane protein reconstitution were used for the incorporation of YidC2 back into the membrane environment (Geertsma et al., 2008). In this study, YidC2 could successfully be reconstituted into proteoliposomes using an *E. coli* total lipid extract (see Section 3.3.5).

Furthermore, it could also be shown that the reconstituted YidC2-proteoliposomes bind to both, empty 70S ribosomes and MscL-RNCs varying in the length of the nascent chains (Fig. 3.34).

The biggest challenge, however, turned out to be the size-reduction of the proteoliposomes to a diameter of around 25 nm up to 50 nm. This is an important requirement for cryo-EM analysis, since the particles on a grid are embedded in a thin layer of vitreous ice (30-100 nm) (Frank, 2002). Sonication of the lipid suspension indeed resulted in a more homogeneous population of proteoliposomes but with an average diameter of approximately 400 nm (Fig. 3.35). The subsequent usage of a mini-extruder then led to the formation of several small (~ 30 nm) but also many large (~ 200 nm) lipid vesicles (Fig. 3.36). Therefore, it can be concluded that sonication and extruder alone are not suitable for the generation of a homogeneous population of small proteoliposomes. Conspicuously, however, was the observation, that the size distribution of the proteoliposomes also depended on the concentration of the lipid suspension. The more concentrated it was, the higher was the propensity that the particles fuse into larger vesicles. In contrast, liposome preparations which were highly diluted showed a large portion of smaller particles. However, for sample preparation as well as for cryo-EM analysis it is important that the YidC2-proteoliposomes are relatively concentrated.

4.2.3 Outlook

In order to analyze and interpret the structure of *E. coli* YidC in complex with TnaC-stalled MscL[115]-RNCs at a molecular level, a high-resolution cryo-EM dataset has to be collected and processed until a subnanometer-resolution is achieved. In the case of the visualization of *S. mutans* YidC2 in the membrane environment several possibilities are supposable. To prevent the observed fusion of the YidC2-proteoliposomes, the type of the phospholipids used for the membrane reconstitution could be changed since this is, besides the temperature and the pH, one of the factors that has been shown to play a role in the fusion process of membrane vesicles (Oku and MacDonald, 1983; Siegel, 1993). Another possibility to obtain a homogeneous population of small proteoliposomes is the additional usage of the yeast curvature protein Yop1 during the membrane reconstitution process. Yop1 belongs to a class of integral membrane proteins which are localized exclusively in the endoplasmic reticulum where it seems to function as a curvature-stabilizing protein (Hu et al., 2008). Hu and coworkers could show that purified Yop1 when incorporated into liposomes led to the

formation of small vesicles and tubules with a diameter of ~ 17 nm. Therefore, the co-reconstitution of Yop1 and YidC2 into liposomes could solve the size problem.

Furthermore, YidC2 could also be inserted into soluble nanoscale phospholipid bilayers, termed Nanodiscs (Alami et al., 2007; Bayburt and Sligar, 2003). Jens Frauenfeld has already established a protocol for the preparation of SecYEG-Nanodiscs, and could also successfully determine a high-resolution cryo-EM structure of SecYEG-Nanodiscs bound to translating 70S ribosomes, and therefore visualize the Sec translocon in the membrane environment (unpublished data).

V REFERENCES

Alami, M., K. Dalal, B. Lelj-Garolla, S.G. Sligar, and F. Duong, 2007. Nanodiscs unravel the interaction between the SecYEG channel and its cytosolic partner SecA. EMBO J 26: 1995-2004.

Amort, M., B. Wotzel, K. Bakowska-Zywicka, M.D. Erlacher, R. Micura, and N. Polacek, 2007. An intact ribose moiety at A2602 of 23S rRNA is key to trigger peptidyl-tRNA hydrolysis during translation termination. Nucleic Acids Res 35: 5130-40.

Andersson, H., and G. von Heijne, 1993. Sec dependent and sec independent assembly of E. coli inner membrane proteins: the topological rules depend on chain length. EMBO J 12: 683-91.

Ban, N., P. Nissen, J. Hansen, P.B. Moore, and T.A. Steitz, 2000. The complete atomic structure of the large ribosomal subunit at 2.4 A resolution. Science 289: 905-20.

Bashan, A., I. Agmon, R. Zarivach, F. Schluenzen, J. Harms, R. Berisio, H. Bartels, F. Franceschi, T. Auerbach, H.A. Hansen, E. Kossoy, M. Kessler, and A. Yonath, 2003. Structural basis of the ribosomal machinery for peptide bond formation, translocation, and nascent chain progression. Mol Cell 11: 91-102.

Bauer, M., M. Behrens, K. Esser, G. Michaelis, and E. Pratje, 1994. PET1402, a nuclear gene required for proteolytic processing of cytochrome oxidase subunit 2 in yeast. Mol Gen Genet 245: 272-8.

Bayburt, T.H., and S.G. Sligar, 2003. Self-assembly of single integral membrane proteins into soluble nanoscale phospholipid bilayers. Protein Sci 12: 2476-81.

Beck, K., G. Eisner, D. Trescher, R.E. Dalbey, J. Brunner, and M. Muller, 2001. YidC, an assembly site for polytopic Escherichia coli membrane proteins located in immediate proximity to the SecYE translocon and lipids. EMBO Rep 2: 709-14.

Becker, T., S. Bhushan, A. Jarasch, J.P. Armache, S. Funes, F. Jossinet, J. Gumbart, T. Mielke, O. Berninghausen, K. Schulten, E. Westhof, R. Gilmore, E.C. Mandon, and R. Beckmann, 2009. Structure of monomeric yeast and mammalian Sec61 complexes interacting with the translating ribosome. Science 326: 1369-73.

Beckmann, R., D. Bubeck, R. Grassucci, P. Penczek, A. Verschoor, G. Blobel, and J. Frank, 1997. Alignment of conduits for the nascent polypeptide chain in the ribosome-Sec61 complex. Science 278: 2123-6.

Beckmann, R., C.M. Spahn, N. Eswar, J. Helmers, P.A. Penczek, A. Sali, J. Frank, and G. Blobel, 2001. Architecture of the protein-conducting channel associated with the translating 80S ribosome. Cell 107: 361-72.

Bellafiore, S., P. Ferris, H. Naver, V. Gohre, and J.D. Rochaix, 2002. Loss of Albino3 leads to the specific depletion of the light-harvesting system. Plant Cell 14: 2303-14.

Bender, G.R., S.V. Sutton, and R.E. Marquis, 1986. Acid tolerance, proton permeabilities, and membrane ATPases of oral streptococci. Infect Immun 53: 331-8.

Beringer, M., 2008. Modulating the activity of the peptidyl transferase center of the ribosome. RNA 14: 795-801.

Berisio, R., F. Schluenzen, J. Harms, A. Bashan, T. Auerbach, D. Baram, and A. Yonath, 2003. Structural insight into the role of the ribosomal tunnel in cellular regulation. Nat Struct Biol 10: 366-70.

Berk, V., and J.H. Cate, 2007. Insights into protein biosynthesis from structures of bacterial ribosomes. Curr Opin Struct Biol 17: 302-9.

Berk, V., W. Zhang, R.D. Pai, and J.H. Cate, 2006. Structural basis for mRNA and tRNA positioning on the ribosome. Proc Natl Acad Sci U S A 103: 15830-4.

Bernabeu, C., and J.A. Lake, 1982. Nascent polypeptide chains emerge from the exit domain of the large ribosomal subunit: immune mapping of the nascent chain. Proc Natl Acad Sci U S A 79: 3111-5.

Bernstein, H.D., 2000. The biogenesis and assembly of bacterial membrane proteins. Curr Opin Microbiol 3: 203-9.

Bhushan, S., M. Gartmann, M. Halic, J.P. Armache, A. Jarasch, T. Mielke, O. Berninghausen, D.N. Wilson, and R. Beckmann, 2010. alpha-Helical nascent polypeptide chains visualized within distinct regions of the ribosomal exit tunnel. Nat Struct Mol Biol 17: 313-7.

Bonnefoy, N., F. Chalvet, P. Hamel, P.P. Slonimski, and G. Dujardin, 1994. OXA1, a Saccharomyces cerevisiae nuclear gene whose sequence is conserved from prokaryotes to eukaryotes controls cytochrome oxidase biogenesis. J Mol Biol 239: 201-12.

Botsford, J.L., and R.D. DeMoss, 1971. Catabolite repression of tryptophanase in Escherichia coli. J Bacteriol 105: 303-12.

Butkus, M.E., L.B. Prundeanu, and D.B. Oliver, 2003. Translocon "pulling" of nascent SecM controls the duration of its translational pause and secretion-responsive secA regulation. J Bacteriol 185: 6719-22.

Calhoun, K.A., and J.R. Swartz, 2006. Total amino acid stabilization during cell-free protein synthesis reactions. J Biotechnol 123: 193-203.

Cannon, M., 1968. The puromycin reaction and its inhibition by chloramphenicol. Eur J Biochem 7: 137-45.

Canutescu, A.A., A.A. Shelenkov, and R.L. Dunbrack, Jr., 2003. A graph-theory algorithm for rapid protein side-chain prediction. Protein Sci 12: 2001-14.

Carter, A.P., W.M. Clemons, D.E. Brodersen, R.J. Morgan-Warren, B.T. Wimberly, and V. Ramakrishnan, 2000. Functional insights from the structure of the 30S ribosomal subunit and its interactions with antibiotics. Nature 407: 340-8.

Celebi, N., L. Yi, S.J. Facey, A. Kuhn, and R.E. Dalbey, 2006. Membrane biogenesis of subunit II of cytochrome bo oxidase: contrasting requirements for insertion of N-terminal and C-terminal domains. J Mol Biol 357: 1428-36.

Chen, J.Z., and N. Grigorieff, 2007. SIGNATURE: a single-particle selection system for molecular electron microscopy. J Struct Biol 157: 168-73.

Chen, M., J.C. Samuelson, F. Jiang, M. Muller, A. Kuhn, and R.E. Dalbey, 2002. Direct interaction of YidC with the Sec-independent Pf3 coat protein during its membrane protein insertion. J Biol Chem 277: 7670-5.

Chen, M., K. Xie, J. Yuan, L. Yi, S.J. Facey, N. Pradel, L.F. Wu, A. Kuhn, and R.E. Dalbey, 2005. Involvement of SecDF and YidC in the membrane insertion of M13 procoat mutants. Biochemistry 44: 10741-9.

Chiba, S., A. Lamsa, and K. Pogliano, 2009. A ribosome-nascent chain sensor of membrane protein biogenesis in Bacillus subtilis. EMBO J 28: 3461-75.

Crowther, R.A., 1971. Procedures for three-dimensional reconstruction of spherical viruses by Fourier synthesis from electron micrographs. Philos Trans R Soc Lond B Biol Sci 261: 221-30.

Cruz-Vera, L.R., and C. Yanofsky, 2008. Conserved residues Asp16 and Pro24 of TnaC-tRNAPro participate in tryptophan induction of Tna operon expression. J Bacteriol 190: 4791-7.

Cruz-Vera, L.R., M. Gong, and C. Yanofsky, 2006. Changes produced by bound tryptophan in the ribosome peptidyl transferase center in response to TnaC, a nascent leader peptide. Proc Natl Acad Sci U S A 103: 3598-603.

Cruz-Vera, L.R., S. Rajagopal, C. Squires, and C. Yanofsky, 2005. Features of ribosome-peptidyl-tRNA interactions essential for tryptophan induction of tna operon expression. Mol Cell 19: 333-43.

Cruz-Vera, L.R., A. New, C. Squires, and C. Yanofsky, 2007. Ribosomal features essential for tna operon induction: tryptophan binding at the peptidyl transferase center. J Bacteriol 189: 3140-6.

Dalbey, R.E., and A. Kuhn, 2004. YidC family members are involved in the membrane insertion, lateral integration, folding, and assembly of membrane proteins. J Cell Biol 166: 769-74.

de Bakker, P.I., N. Furnham, T.L. Blundell, and M.A. DePristo, 2006. Conformer generation under restraints. Curr Opin Struct Biol 16: 160-5.

de Gier, J.W., P.A. Scotti, A. Saaf, Q.A. Valent, A. Kuhn, J. Luirink, and G. von Heijne, 1998. Differential use of the signal recognition particle translocase targeting pathway for inner membrane protein assembly in Escherichia coli. Proc Natl Acad Sci U S A 95: 14646-51.

de Kruijff, B., 1997. Lipid polymorphism and biomembrane function. Curr Opin Chem Biol 1: 564-9.

Deeley, M.C., and C. Yanofsky, 1981. Nucleotide sequence of the structural gene for tryptophanase of Escherichia coli K-12. J Bacteriol 147: 787-96.

Dong, Y., S.R. Palmer, A. Hasona, S. Nagamori, H.R. Kaback, R.E. Dalbey, and L.J. Brady, 2008. Functional overlap but lack of complete cross-complementation of Streptococcus mutans and Escherichia coli YidC orthologs. J Bacteriol 190: 2458-69.

Doudna, J.A., and T.R. Cech, 2002. The chemical repertoire of natural ribozymes. Nature 418: 222-8.

Driessen, A.J., and N. Nouwen, 2008. Protein translocation across the bacterial cytoplasmic membrane. Annu Rev Biochem 77: 643-67.

Dubochet, J., A.W. McDowall, B. Menge, E.N. Schmid, and K.G. Lickfeld, 1983. Electron microscopy of frozen-hydrated bacteria. J Bacteriol 155: 381-90.

Edwards, R.M., and M.D. Yudkin, 1982. Location of the gene for the low-affinity tryptophan-specific permease of Escherichia coli. Biochem J 204: 617-9.

Emsley, P., and K. Cowtan, 2004. Coot: model-building tools for molecular graphics. Acta Crystallogr D Biol Crystallogr 60: 2126-32.

Erlacher, M.D., and N. Polacek, 2008. Ribosomal catalysis: the evolution of mechanistic concepts for peptide bond formation and peptidyl-tRNA hydrolysis. RNA Biol 5: 5-12.

Facey, S.J., S.A. Neugebauer, S. Krauss, and A. Kuhn, 2007. The mechanosensitive channel protein MscL is targeted by the SRP to the novel YidC membrane insertion pathway of Escherichia coli. J Mol Biol 365: 995-1004.

Fang, P., C.C. Spevak, C. Wu, and M.S. Sachs, 2004. A nascent polypeptide domain that can regulate translation elongation. Proc Natl Acad Sci U S A 101: 4059-64.

Frank, J., 2002. Single-particle imaging of macromolecules by cryo-electron microscopy. Annu Rev Biophys Biomol Struct 31: 303-19.

Frank, J., M. Radermacher, P. Penczek, J. Zhu, Y. Li, M. Ladjadj, and A. Leith, 1996. SPIDER and WEB: processing and visualization of images in 3D electron microscopy and related fields. J Struct Biol 116: 190-9.

Frank, J., J. Zhu, P. Penczek, Y. Li, S. Srivastava, A. Verschoor, M. Radermacher, R. Grassucci, R.K. Lata, and R.K. Agrawal, 1995. A model of protein synthesis based on cryo-electron microscopy of the E. coli ribosome. Nature 376: 441-4.

Funes, S., F.E. Nargang, W. Neupert, and J.M. Herrmann, 2004. The Oxa2 protein of Neurospora crassa plays a critical role in the biogenesis of cytochrome oxidase and

defines a ubiquitous subbranch of the Oxa1/YidC/Alb3 protein family. Mol Biol Cell 15: 1853-61.

Funes, S., A. Hasona, H. Bauerschmitt, C. Grubbauer, F. Kauff, R. Collins, P.J. Crowley, S.R. Palmer, L.J. Brady, and J.M. Herrmann, 2009. Independent gene duplications of the YidC/Oxa/Alb3 family enabled a specialized cotranslational function. Proc Natl Acad Sci U S A 106: 6656-61.

Gabashvili, I.S., S.T. Gregory, M. Valle, R. Grassucci, M. Worbs, M.C. Wahl, A.E. Dahlberg, and J. Frank, 2001. The polypeptide tunnel system in the ribosome and its gating in erythromycin resistance mutants of L4 and L22. Mol Cell 8: 181-8.

Geertsma, E.R., N.A. Nik Mahmood, G.K. Schuurman-Wolters, and B. Poolman, 2008. Membrane reconstitution of ABC transporters and assays of translocator function. Nat Protoc 3: 256-66.

Geller, B.L., and W. Wickner, 1985. M13 procoat inserts into liposomes in the absence of other membrane proteins. J Biol Chem 260: 13281-5.

Gong, F., and C. Yanofsky, 2001. Reproducing tna operon regulation in vitro in an S-30 system. Tryptophan induction inhibits cleavage of TnaC peptidyl-tRNA. J Biol Chem 276: 1974-83.

Gong, F., and C. Yanofsky, 2002a. Instruction of translating ribosome by nascent peptide. Science 297: 1864-7.

Gong, F., and C. Yanofsky, 2002b. Analysis of tryptophanase operon expression in vitro: accumulation of TnaC-peptidyl-tRNA in a release factor 2-depleted S-30 extract prevents Rho factor action, simulating induction. J Biol Chem 277: 17095-100.

Gong, F., K. Ito, Y. Nakamura, and C. Yanofsky, 2001. The mechanism of tryptophan induction of tryptophanase operon expression: tryptophan inhibits release factor-mediated cleavage of TnaC-peptidyl-tRNA(Pro). Proc Natl Acad Sci U S A 98: 8997-9001.

Gong, M., L.R. Cruz-Vera, and C. Yanofsky, 2007. Ribosome recycling factor and release factor 3 action promotes TnaC-peptidyl-tRNA Dropoff and relieves ribosome stalling during tryptophan induction of tna operon expression in Escherichia coli. J Bacteriol 189: 3147-55.

Green, R., R.R. Samaha, and H.F. Noller, 1997. Mutations at nucleotides G2251 and U2585 of 23 S rRNA perturb the peptidyl transferase center of the ribosome. J Mol Biol 266: 40-50.

Gryczan, T.J., G. Grandi, J. Hahn, R. Grandi, and D. Dubnau, 1980. Conformational alteration of mRNA structure and the posttranscriptional regulation of erythromycin-induced drug resistance. Nucleic Acids Res 8: 6081-97.

Gualerzi, C.O., and C.L. Pon, 1990. Initiation of mRNA translation in prokaryotes. Biochemistry 29: 5881-9.

Halic, M., M. Blau, T. Becker, T. Mielke, M.R. Pool, K. Wild, I. Sinning, and R. Beckmann, 2006. Following the signal sequence from ribosomal tunnel exit to signal recognition particle. Nature 444: 507-11.

Hampl, H., H. Schulze, and K.H. Nierhaus, 1981. Ribosomal components from Escherichia coli 50 S subunits involved in the reconstitution of peptidyltransferase activity. J Biol Chem 256: 2284-8.

Hansen, J.L., P.B. Moore, and T.A. Steitz, 2003. Structures of five antibiotics bound at the peptidyl transferase center of the large ribosomal subunit. J Mol Biol 330: 1061-75.

Harms, J., F. Schluenzen, R. Zarivach, A. Bashan, S. Gat, I. Agmon, H. Bartels, F. Franceschi, and A. Yonath, 2001. High resolution structure of the large ribosomal subunit from a mesophilic eubacterium. Cell 107: 679-88.

Hasona, A., P.J. Crowley, C.M. Levesque, R.W. Mair, D.G. Cvitkovitch, A.S. Bleiweis, and L.J. Brady, 2005. Streptococcal viability and diminished stress tolerance in mutants

lacking the signal recognition particle pathway or YidC2. Proc Natl Acad Sci U S A 102: 17466-71.

Herskovits, A.A., A. Seluanov, R. Rajsbaum, C.M. ten Hagen-Jongman, T. Henrichs, E.S. Bochkareva, G.J. Phillips, F.J. Probst, T. Nakae, M. Ehrmann, J. Luirink, and E. Bibi, 2001. Evidence for coupling of membrane targeting and function of the signal recognition particle (SRP) receptor FtsY. EMBO Rep 2: 1040-6.

Horinouchi, S., and B. Weisblum, 1980. Posttranscriptional modification of mRNA conformation: mechanism that regulates erythromycin-induced resistance. Proc Natl Acad Sci U S A 77: 7079-83.

Houben, E.N., P.A. Scotti, Q.A. Valent, J. Brunner, J.L. de Gier, B. Oudega, and J. Luirink, 2000. Nascent Lep inserts into the Escherichia coli inner membrane in the vicinity of YidC, SecY and SecA. FEBS Lett 476: 229-33.

Hu, J., Y. Shibata, C. Voss, T. Shemesh, Z. Li, M. Coughlin, M.M. Kozlov, T.A. Rapoport, and W.A. Prinz, 2008. Membrane proteins of the endoplasmic reticulum induce high-curvature tubules. Science 319: 1247-50.

Humphrey, W., A. Dalke, and K. Schulten, 1996. VMD: visual molecular dynamics. J Mol Graph 14: 33-8, 27-8.

Ito, K., S. Chiba, and K. Pogliano, 2010. Divergent stalling sequences sense and control cellular physiology. Biochem Biophys Res Commun 393: 1-5.

Jewett, M.C., and J.R. Swartz, 2004. Mimicking the Escherichia coli cytoplasmic environment activates long-lived and efficient cell-free protein synthesis. Biotechnol Bioeng 86: 19-26.

Jia, L., M. Dienhart, M. Schramp, M. McCauley, K. Hell, and R.A. Stuart, 2003. Yeast Oxa1 interacts with mitochondrial ribosomes: the importance of the C-terminal region of Oxa1. EMBO J 22: 6438-47.

Jiang, F., M. Chen, L. Yi, J.W. de Gier, A. Kuhn, and R.E. Dalbey, 2003. Defining the regions of Escherichia coli YidC that contribute to activity. J Biol Chem 278: 48965-72.

Jiang, F., L. Yi, M. Moore, M. Chen, T. Rohl, K.J. Van Wijk, J.W. De Gier, R. Henry, and R.E. Dalbey, 2002. Chloroplast YidC homolog Albino3 can functionally complement the bacterial YidC depletion strain and promote membrane insertion of both bacterial and chloroplast thylakoid proteins. J Biol Chem 277: 19281-8.

Jossinet, F., and E. Westhof, 2005. Sequence to Structure (S2S): display, manipulate and interconnect RNA data from sequence to structure. Bioinformatics 21: 3320-1.

Kang, S.H., T.J. Oh, R.G. Kim, T.J. Kang, S.H. Hwang, E.Y. Lee, and C.Y. Choi, 2000. An efficient cell-free protein synthesis system using periplasmic phosphatase-removed S30 extract. J Microbiol Methods 43: 91-6.

Karimi, R., M.Y. Pavlov, R.H. Buckingham, and M. Ehrenberg, 1999. Novel roles for classical factors at the interface between translation termination and initiation. Mol Cell 3: 601-9.

Katunin, V.I., G.W. Muth, S.A. Strobel, W. Wintermeyer, and M.V. Rodnina, 2002. Important contribution to catalysis of peptide bond formation by a single ionizing group within the ribosome. Mol Cell 10: 339-46.

Khaitovich, P., A.S. Mankin, R. Green, L. Lancaster, and H.F. Noller, 1999. Characterization of functionally active subribosomal particles from Thermus aquaticus. Proc Natl Acad Sci U S A 96: 85-90.

Kiefer, D., and A. Kuhn, 2007. YidC as an essential and multifunctional component in membrane protein assembly. Int Rev Cytol 259: 113-38.

Klein, D.J., P.B. Moore, and T.A. Steitz, 2004. The roles of ribosomal proteins in the structure assembly, and evolution of the large ribosomal subunit. J Mol Biol 340: 141-77.

Knol, J., K. Sjollema, and B. Poolman, 1998. Detergent-mediated reconstitution of membrane proteins. Biochemistry 37: 16410-5.

Kohler, R., D. Boehringer, B. Greber, R. Bingel-Erlenmeyer, I. Collinson, C. Schaffitzel, and N. Ban, 2009. YidC and Oxa1 form dimeric insertion pores on the translating ribosome. Mol Cell 34: 344-53.

Kol, S., N. Nouwen, and A.J. Driessen, 2008. Mechanisms of YidC-mediated insertion and assembly of multimeric membrane protein complexes. J Biol Chem 283: 31269-73.

Kosolapov, A., and C. Deutsch, 2009. Tertiary interactions within the ribosomal exit tunnel. Nat Struct Mol Biol 16: 405-11.

Kossel, H., 1970. Purification and properties of peptidyl-tRNA hydrolase from Escherichia coli. Biochim Biophys Acta 204: 191-202.

Kramer, G., D. Boehringer, N. Ban, and B. Bukau, 2009. The ribosome as a platform for co-translational processing, folding and targeting of newly synthesized proteins. Nat Struct Mol Biol 16: 589-97.

Kuhn, A., R. Stuart, R. Henry, and R.E. Dalbey, 2003. The Alb3/Oxa1/YidC protein family: membrane-localized chaperones facilitating membrane protein insertion? Trends Cell Biol 13: 510-6.

Laemmli, U.K., 1970. Cleavage of structural proteins during the assembly of the head of bacteriophage T4. Nature 227: 680-5.

Lake, J.A., and L. Kahan, 1975. Ribosomal proteins S5, S11, S13 and S19 localized by electron microscopy of antibody-labeled subunits. J Mol Biol 99: 631-44.

Laurberg, M., H. Asahara, A. Korostelev, J. Zhu, S. Trakhanov, and H.F. Noller, 2008. Structural basis for translation termination on the 70S ribosome. Nature 454: 852-7.

Lawrence, M.G., L. Lindahl, and J.M. Zengel, 2008. Effects on translation pausing of alterations in protein and RNA components of the ribosome exit tunnel. J Bacteriol 190: 5862-9.

Lee, P.A., D. Tullman-Ercek, and G. Georgiou, 2006. The bacterial twin-arginine translocation pathway. Annu Rev Microbiol 60: 373-95.

Lepault, J., F.P. Booy, and J. Dubochet, 1983. Electron microscopy of frozen biological suspensions. J Microsc 129: 89-102.

Liu, D.V., J.F. Zawada, and J.R. Swartz, 2005. Streamlining Escherichia coli S30 extract preparation for economical cell-free protein synthesis. Biotechnol Prog 21: 460-5.

Lotz, M., W. Haase, W. Kuhlbrandt, and I. Collinson, 2008. Projection structure of yidC: a conserved mediator of membrane protein assembly. J Mol Biol 375: 901-7.

Lu, J., and C. Deutsch, 2005. Folding zones inside the ribosomal exit tunnel. Nat Struct Mol Biol 12: 1123-9.

Lu, J., and C. Deutsch, 2008. Electrostatics in the ribosomal tunnel modulate chain elongation rates. J Mol Biol 384: 73-86.

Luirink, J., T. Samuelsson, and J.W. de Gier, 2001. YidC/Oxa1p/Alb3: evolutionarily conserved mediators of membrane protein assembly. FEBS Lett 501: 1-5.

Luirink, J., G. von Heijne, E. Houben, and J.W. de Gier, 2005. Biogenesis of inner membrane proteins in Escherichia coli. Annu Rev Microbiol 59: 329-55.

Malkin, L.I., and A. Rich, 1967. Partial resistance of nascent polypeptide chains to proteolytic digestion due to ribosomal shielding. J Mol Biol 26: 329-46.

McNicholas, P., R. Salavati, and D. Oliver, 1997. Dual regulation of Escherichia coli secA translation by distinct upstream elements. J Mol Biol 265: 128-41.

Menetret, J.F., A. Neuhof, D.G. Morgan, K. Plath, M. Radermacher, T.A. Rapoport, and C.W. Akey, 2000. The structure of ribosome-channel complexes engaged in protein translocation. Mol Cell 6: 1219-32.

Menetret, J.F., R.S. Hegde, S.U. Heinrich, P. Chandramouli, S.J. Ludtke, T.A. Rapoport, and C.W. Akey, 2005. Architecture of the ribosome-channel complex derived from native membranes. J Mol Biol 348: 445-57.

Menninger, J.R., 1976. Peptidyl transfer RNA dissociates during protein synthesis from ribosomes of Escherichia coli. J Biol Chem 251: 3392-8.

Milligan, R.A., and P.N. Unwin, 1982. In vitro crystallization of ribosomes from chick embryos. J Cell Biol 95: 648-53.

Mindell, J.A., and N. Grigorieff, 2003. Accurate determination of local defocus and specimen tilt in electron microscopy. J Struct Biol 142: 334-47.

Mitra, K., C. Schaffitzel, F. Fabiola, M.S. Chapman, N. Ban, and J. Frank, 2006. Elongation arrest by SecM via a cascade of ribosomal RNA rearrangements. Mol Cell 22: 533-43.

Mitra, K., C. Schaffitzel, T. Shaikh, F. Tama, S. Jenni, C.L. Brooks, 3rd, N. Ban, and J. Frank, 2005. Structure of the E. coli protein-conducting channel bound to a translating ribosome. Nature 438: 318-24.

Moller, I., M. Jung, B. Beatrix, R. Levy, G. Kreibich, R. Zimmermann, M. Wiedmann, and B. Lauring, 1998. A general mechanism for regulation of access to the translocon: competition for a membrane attachment site on ribosomes. Proc Natl Acad Sci U S A 95: 13425-30.

Moore, M., M.S. Harrison, E.C. Peterson, and R. Henry, 2000. Chloroplast Oxa1p homolog albino3 is required for post-translational integration of the light harvesting chlorophyll-binding protein into thylakoid membranes. J Biol Chem 275: 1529-32.

Morgan, D.G., J.F. Menetret, A. Neuhof, T.A. Rapoport, and C.W. Akey, 2002. Structure of the mammalian ribosome-channel complex at 17A resolution. J Mol Biol 324: 871-86.

Murakami, A., H. Nakatogawa, and K. Ito, 2004. Translation arrest of SecM is essential for the basal and regulated expression of SecA. Proc Natl Acad Sci U S A 101: 12330-5.

Muto, H., H. Nakatogawa, and K. Ito, 2006. Genetically encoded but nonpolypeptide prolyl-tRNA functions in the A site for SecM-mediated ribosomal stall. Mol Cell 22: 545-52.

Nakatogawa, H., and K. Ito, 2001. Secretion monitor, SecM, undergoes self-translation arrest in the cytosol. Mol Cell 7: 185-92.

Nakatogawa, H., and K. Ito, 2002. The ribosomal exit tunnel functions as a discriminating gate. Cell 108: 629-36.

Nakatogawa, H., and K. Ito, 2004. Intraribosomal regulation of expression and fate of proteins. Chembiochem 5: 48-51.

Nakatogawa, H., A. Murakami, and K. Ito, 2004. Control of SecA and SecM translation by protein secretion. Curr Opin Microbiol 7: 145-50.

Narayanan, C.S., and D. Dubnau, 1985. Evidence for the translational attenuation model: ribosome-binding studies and structural analysis with an in vitro run-off transcript of ermC. Nucleic Acids Res 13: 7307-26.

Neumann-Haefelin, C., U. Schafer, M. Muller, and H.G. Koch, 2000. SRP-dependent co-translational targeting and SecA-dependent translocation analyzed as individual steps in the export of a bacterial protein. EMBO J 19: 6419-26.

Nissen, P., J. Hansen, N. Ban, P.B. Moore, and T.A. Steitz, 2000. The structural basis of ribosome activity in peptide bond synthesis. Science 289: 920-30.

Nouwen, N., and A.J. Driessen, 2002. SecDFyajC forms a heterotetrameric complex with YidC. Mol Microbiol 44: 1397-405.

Ogle, J.M., D.E. Brodersen, W.M. Clemons, Jr., M.J. Tarry, A.P. Carter, and V. Ramakrishnan, 2001. Recognition of cognate transfer RNA by the 30S ribosomal subunit. Science 292: 897-902.

Oku, N., and R.C. MacDonald, 1983. Solubilization of phospholipids by chaotropic ion solutions. J Biol Chem 258: 8733-8.

Oliver, D., J. Norman, and S. Sarker, 1998. Regulation of Escherichia coli secA by cellular protein secretion proficiency requires an intact gene X signal sequence and an active translocon. J Bacteriol 180: 5240-2.

Oliver, D.B., and J. Beckwith, 1982. Regulation of a membrane component required for protein secretion in Escherichia coli. Cell 30: 311-9.

Oliver, D.C., and M. Paetzel, 2008. Crystal structure of the major periplasmic domain of the bacterial membrane protein assembly facilitator YidC. J Biol Chem 283: 5208-16.

Palade, G.E., 1955. A small particulate component of the cytoplasm. J Biophys Biochem Cytol 1: 59-68.

Penczek, P.A., R.A. Grassucci, and J. Frank, 1994. The ribosome at improved resolution: new techniques for merging and orientation refinement in 3D cryo-electron microscopy of biological particles. Ultramicroscopy 53: 251-70.

Penczek, P.A., J. Zhu, and J. Frank, 1996. A common-lines based method for determining orientations for N > 3 particle projections simultaneously. Ultramicroscopy 63: 205-18.

Peranen, J., M. Rikkonen, M. Hyvonen, and L. Kaariainen, 1996. T7 vectors with modified T7lac promoter for expression of proteins in Escherichia coli. Anal Biochem 236: 371-3.

Petry, S., D.E. Brodersen, F.V.t. Murphy, C.M. Dunham, M. Selmer, M.J. Tarry, A.C. Kelley, and V. Ramakrishnan, 2005. Crystal structures of the ribosome in complex with release factors RF1 and RF2 bound to a cognate stop codon. Cell 123: 1255-66.

Pettersen, E.F., T.D. Goddard, C.C. Huang, G.S. Couch, D.M. Greenblatt, E.C. Meng, and T.E. Ferrin, 2004. UCSF Chimera--a visualization system for exploratory research and analysis. J Comput Chem 25: 1605-12.

Picking, W.D., W.L. Picking, O.W. Odom, and B. Hardesty, 1992. Fluorescence characterization of the environment encountered by nascent polyalanine and polyserine as they exit Escherichia coli ribosomes during translation. Biochemistry 31: 2368-75.

Pogliano, J.A., and J. Beckwith, 1994. SecD and SecF facilitate protein export in Escherichia coli. EMBO J 13: 554-61.

Polacek, N., and A.S. Mankin, 2005. The ribosomal peptidyl transferase center: structure, function, evolution, inhibition. Crit Rev Biochem Mol Biol 40: 285-311.

Polacek, N., M.J. Gomez, K. Ito, L. Xiong, Y. Nakamura, and A. Mankin, 2003. The critical role of the universally conserved A2602 of 23S ribosomal RNA in the release of the nascent peptide during translation termination. Mol Cell 11: 103-12.

Poritz, M.A., H.D. Bernstein, K. Strub, D. Zopf, H. Wilhelm, and P. Walter, 1990. An E. coli ribonucleoprotein containing 4.5S RNA resembles mammalian signal recognition particle. Science 250: 1111-7.

Porse, B.T., S.V. Kirillov, M.J. Awayez, H.C. Ottenheijm, and R.A. Garrett, 1999. Direct crosslinking of the antitumor antibiotic sparsomycin, and its derivatives, to A2602 in the peptidyl transferase center of 23S-like rRNA within ribosome-tRNA complexes. Proc Natl Acad Sci U S A 96: 9003-8.

Preuss, M., M. Ott, S. Funes, J. Luirink, and J.M. Herrmann, 2005. Evolution of mitochondrial oxa proteins from bacterial YidC. Inherited and acquired functions of a conserved protein insertion machinery. J Biol Chem 280: 13004-11.

Prinz, A., C. Behrens, T.A. Rapoport, E. Hartmann, and K.U. Kalies, 2000. Evolutionarily conserved binding of ribosomes to the translocation channel via the large ribosomal RNA. EMBO J 19: 1900-6.

Radermacher, M., T. Wagenknecht, A. Verschoor, and J. Frank, 1986. A new 3-D reconstruction scheme applied to the 50S ribosomal subunit of E. coli. J Microsc 141: RP1-2.

Ramakrishnan, V., 2002. Ribosome structure and the mechanism of translation. Cell 108: 557-72.

Ramu, H., A. Mankin, and N. Vazquez-Laslop, 2009. Programmed drug-dependent ribosome stalling. Mol Microbiol 71: 811-24.

Ravaud, S., G. Stjepanovic, K. Wild, and I. Sinning, 2008. The crystal structure of the periplasmic domain of the Escherichia coli membrane protein insertase YidC contains a substrate binding cleft. J Biol Chem 283: 9350-8.

Ren, D., L.A. Bedzyk, R.W. Ye, S.M. Thomas, and T.K. Wood, 2004. Stationary-phase quorum-sensing signals affect autoinducer-2 and gene expression in Escherichia coli. Appl Environ Microbiol 70: 2038-43.

Roberts, R.B., 1958. Microsomal particles and protein synthesis. A symposium. Microsomal particles and protein synthesis. A symposium: x+168p. Illus.

Roseman, A.M., 2003. Particle finding in electron micrographs using a fast local correlation algorithm. Ultramicroscopy 94: 225-36.

Ruprecht, J., and J. Nield, 2001. Determining the structure of biological macromolecules by transmission electron microscopy, single particle analysis and 3D reconstruction. Prog Biophys Mol Biol 75: 121-64.

Saibil, H.R., 2000. Macromolecular structure determination by cryo-electron microscopy. Acta Crystallogr D Biol Crystallogr 56: 1215-22.

Samuelson, J.C., M. Chen, F. Jiang, I. Moller, M. Wiedmann, A. Kuhn, G.J. Phillips, and R.E. Dalbey, 2000. YidC mediates membrane protein insertion in bacteria. Nature 406: 637-41.

Sarker, S., K.E. Rudd, and D. Oliver, 2000. Revised translation start site for secM defines an atypical signal peptide that regulates Escherichia coli secA expression. J Bacteriol 182: 5592-5.

Schaffitzel, C., and N. Ban, 2007. Reprint of "Generation of ribosome nascent chain complexes for structural and functional studies" [J. Struct. Biol. 158 (2007) 463-471]. J Struct Biol 159: 302-10.

Schluenzen, F., A. Tocilj, R. Zarivach, J. Harms, M. Gluehmann, D. Janell, A. Bashan, H. Bartels, I. Agmon, F. Franceschi, and A. Yonath, 2000. Structure of functionally activated small ribosomal subunit at 3.3 angstroms resolution. Cell 102: 615-23.

Schmeing, T.M., K.S. Huang, S.A. Strobel, and T.A. Steitz, 2005a. An induced-fit mechanism to promote peptide bond formation and exclude hydrolysis of peptidyl-tRNA. Nature 438: 520-4.

Schmeing, T.M., K.S. Huang, D.E. Kitchen, S.A. Strobel, and T.A. Steitz, 2005b. Structural insights into the roles of water and the 2' hydroxyl of the P site tRNA in the peptidyl transferase reaction. Mol Cell 20: 437-48.

Schmidt, M.G., and D.B. Oliver, 1989. SecA protein autogenously represses its own translation during normal protein secretion in Escherichia coli. J Bacteriol 171: 643-9.

Schmidt, M.G., E.E. Rollo, J. Grodberg, and D.B. Oliver, 1988. Nucleotide sequence of the secA gene and secA(Ts) mutations preventing protein export in Escherichia coli. J Bacteriol 170: 3404-14.

Schuette, J.C., F.V.t. Murphy, A.C. Kelley, J.R. Weir, J. Giesebrecht, S.R. Connell, J. Loerke, T. Mielke, W. Zhang, P.A. Penczek, V. Ramakrishnan, and C.M. Spahn, 2009. GTPase activation of elongation factor EF-Tu by the ribosome during decoding. EMBO J 28: 755-65.

Schuwirth, B.S., M.A. Borovinskaya, C.W. Hau, W. Zhang, A. Vila-Sanjurjo, J.M. Holton, and J.H. Cate, 2005. Structures of the bacterial ribosome at 3.5 A resolution. Science 310: 827-34.

Scolnick, E., R. Tompkins, T. Caskey, and M. Nirenberg, 1968. Release factors differing in specificity for terminator codons. Proc Natl Acad Sci U S A 61: 768-74.

Scotti, P.A., M.L. Urbanus, J. Brunner, J.W. de Gier, G. von Heijne, C. van der Does, A.J. Driessen, B. Oudega, and J. Luirink, 2000. YidC, the Escherichia coli homologue of mitochondrial Oxa1p, is a component of the Sec translocase. EMBO J 19: 542-9.

Selmer, M., C.M. Dunham, F.V.t. Murphy, A. Weixlbaumer, S. Petry, A.C. Kelley, J.R. Weir, and V. Ramakrishnan, 2006. Structure of the 70S ribosome complexed with mRNA and tRNA. Science 313: 1935-42.

Serek, J., G. Bauer-Manz, G. Struhalla, L. van den Berg, D. Kiefer, R. Dalbey, and A. Kuhn, 2004. Escherichia coli YidC is a membrane insertase for Sec-independent proteins. EMBO J 23: 294-301.

Shan, S.O., and P. Walter, 2005. Molecular crosstalk between the nucleotide specificity determinant of the SRP GTPase and the SRP receptor. Biochemistry 44: 6214-22.

Siegel, D.P., 1993. Energetics of intermediates in membrane fusion: comparison of stalk and inverted micellar intermediate mechanisms. Biophys J 65: 2124-40.

Stagg, S.M., G.C. Lander, J. Pulokas, D. Fellmann, A. Cheng, J.D. Quispe, S.P. Mallick, R.M. Avila, B. Carragher, and C.S. Potter, 2006. Automated cryoEM data acquisition and analysis of 284742 particles of GroEL. J Struct Biol 155: 470-81.

Stark, H., F. Zemlin, and C. Boettcher, 1996. Electron radiation damage to protein crystals of bacteriorhodopsin at different temperatures. Ultramicroscopy 63: 75-79.

Steitz, T.A., 2008. A structural understanding of the dynamic ribosome machine. Nat Rev Mol Cell Biol 9: 242-53.

Stewart, V., and C. Yanofsky, 1985. Evidence for transcription antitermination control of tryptophanase operon expression in Escherichia coli K-12. J Bacteriol 164: 731-40.

Stewart, V., R. Landick, and C. Yanofsky, 1986. Rho-dependent transcription termination in the tryptophanase operon leader region of Escherichia coli K-12. J Bacteriol 166: 217-23.

Stuart, R.A., and W. Neupert, 2000. Making membranes in bacteria. Nature 406: 575, 577.

Szyrach, G., M. Ott, N. Bonnefoy, W. Neupert, and J.M. Herrmann, 2003. Ribosome binding to the Oxa1 complex facilitates co-translational protein insertion in mitochondria. EMBO J 22: 6448-57.

Tenson, T., and M. Ehrenberg, 2002. Regulatory nascent peptides in the ribosomal tunnel. Cell 108: 591-4.

Trabuco, L.G., E. Villa, K. Mitra, J. Frank, and K. Schulten, 2008. Flexible fitting of atomic structures into electron microscopy maps using molecular dynamics. Structure 16: 673-83.

Tugarinov, V., W.Y. Choy, V.Y. Orekhov, and L.E. Kay, 2005. Solution NMR-derived global fold of a monomeric 82-kDa enzyme. Proc Natl Acad Sci U S A 102: 622-7.

Urbanus, M.L., P.A. Scotti, L. Froderberg, A. Saaf, J.W. de Gier, J. Brunner, J.C. Samuelson, R.E. Dalbey, B. Oudega, and J. Luirink, 2001. Sec-dependent membrane protein insertion: sequential interaction of nascent FtsQ with SecY and YidC. EMBO Rep 2: 524-9.

Valle, M., A. Zavialov, J. Sengupta, U. Rawat, M. Ehrenberg, and J. Frank, 2003. Locking and unlocking of ribosomal motions. Cell 114: 123-34.

van Bloois, E., G.J. Haan, J.W. de Gier, B. Oudega, and J. Luirink, 2006. Distinct requirements for translocation of the N-tail and C-tail of the Escherichia coli inner membrane protein CyoA. J Biol Chem 281: 10002-9.

van Bloois, E., S. Nagamori, G. Koningstein, R.S. Ullers, M. Preuss, B. Oudega, N. Harms, H.R. Kaback, J.M. Herrmann, and J. Luirink, 2005. The Sec-independent function of Escherichia coli YidC is evolutionary-conserved and essential. J Biol Chem 280: 12996-3003.

Van den Berg, B., W.M. Clemons, Jr., I. Collinson, Y. Modis, E. Hartmann, S.C. Harrison, and T.A. Rapoport, 2004. X-ray structure of a protein-conducting channel. Nature 427: 36-44.

van der Does, C., T. den Blaauwen, J.G. de Wit, E.H. Manting, N.A. Groot, P. Fekkes, and A.J. Driessen, 1996. SecA is an intrinsic subunit of the Escherichia coli preprotein translocase and exposes its carboxyl terminus to the periplasm. Mol Microbiol 22: 619-29.

van Heel, M., and M. Schatz, 2005. Fourier shell correlation threshold criteria. J Struct Biol 151: 250-62.

Vazquez-Laslop, N., C. Thum, and A.S. Mankin, 2008. Molecular mechanism of drug-dependent ribosome stalling. Mol Cell 30: 190-202.

Villa, E., J. Sengupta, L.G. Trabuco, J. LeBarron, W.T. Baxter, T.R. Shaikh, R.A. Grassucci, P. Nissen, M. Ehrenberg, K. Schulten, and J. Frank, 2009. Ribosome-induced changes in elongation factor Tu conformation control GTP hydrolysis. Proc Natl Acad Sci U S A 106: 1063-8.

Voss, N.R., M. Gerstein, T.A. Steitz, and P.B. Moore, 2006. The geometry of the ribosomal polypeptide exit tunnel. J Mol Biol 360: 893-906.

Wagenknecht, T., R. Grassucci, and J. Frank, 1988. Electron microscopy and computer image averaging of ice-embedded large ribosomal subunits from Escherichia coli. J Mol Biol 199: 137-47.

Weisblum, B., 1995. Insights into erythromycin action from studies of its activity as inducer of resistance. Antimicrob Agents Chemother 39: 797-805.

Weixlbaumer, A., H. Jin, C. Neubauer, R.M. Voorhees, S. Petry, A.C. Kelley, and V. Ramakrishnan, 2008. Insights into translational termination from the structure of RF2 bound to the ribosome. Science 322: 953-6.

Wilson, D.N., F. Schluenzen, J.M. Harms, T. Yoshida, T. Ohkubo, R. Albrecht, J. Buerger, Y. Kobayashi, and P. Fucini, 2005. X-ray crystallography study on ribosome recycling: the mechanism of binding and action of RRF on the 50S ribosomal subunit. EMBO J 24: 251-60.

Wimberly, B.T., D.E. Brodersen, W.M. Clemons, Jr., R.J. Morgan-Warren, A.P. Carter, C. Vonrhein, T. Hartsch, and V. Ramakrishnan, 2000. Structure of the 30S ribosomal subunit. Nature 407: 327-39.

Winzer, K., K.R. Hardie, and P. Williams, 2002. Bacterial cell-to-cell communication: sorry, can't talk now - gone to lunch! Curr Opin Microbiol 5: 216-22.

Woolhead, C.A., P.J. McCormick, and A.E. Johnson, 2004. Nascent membrane and secretory proteins differ in FRET-detected folding far inside the ribosome and in their exposure to ribosomal proteins. Cell 116: 725-36.

Woolhead, C.A., A.E. Johnson, and H.D. Bernstein, 2006. Translation arrest requires two-way communication between a nascent polypeptide and the ribosome. Mol Cell 22: 587-98.

Xie, K., and R.E. Dalbey, 2008. Inserting proteins into the bacterial cytoplasmic membrane using the Sec and YidC translocases. Nat Rev Microbiol 6: 234-44.

Xie, K., D. Kiefer, G. Nagler, R.E. Dalbey, and A. Kuhn, 2006. Different regions of the nonconserved large periplasmic domain of Escherichia coli YidC are involved in the SecF interaction and membrane insertase activity. Biochemistry 45: 13401-8.

Yang, R., L.R. Cruz-Vera, and C. Yanofsky, 2009. 23S rRNA nucleotides in the peptidyl transferase center are essential for tryptophanase operon induction. J Bacteriol 191: 3445-50.

Yanofsky, C., 2007. RNA-based regulation of genes of tryptophan synthesis and degradation, in bacteria. RNA 13: 1141-54.

Yen, M.R., K.T. Harley, Y.H. Tseng, and M.H. Saier, Jr., 2001. Phylogenetic and structural analyses of the oxa1 family of protein translocases. FEMS Microbiol Lett 204: 223-31.

Yi, L., F. Jiang, M. Chen, B. Cain, A. Bolhuis, and R.E. Dalbey, 2003. YidC is strictly required for membrane insertion of subunits a and c of the F(1)F(0)ATP synthase and SecE of the SecYEG translocase. Biochemistry 42: 10537-44.

Yoshizawa, S., D. Fourmy, and J.D. Puglisi, 1999. Recognition of the codon-anticodon helix by ribosomal RNA. Science 285: 1722-5.

Youngman, E.M., M.E. McDonald, and R. Green, 2008. Peptide release on the ribosome: mechanism and implications for translational control. Annu Rev Microbiol 62: 353-73.

Youngman, E.M., J.L. Brunelle, A.B. Kochaniak, and R. Green, 2004. The active site of the ribosome is composed of two layers of conserved nucleotides with distinct roles in peptide bond formation and peptide release. Cell 117: 589-99.

Yusupov, M.M., G.Z. Yusupova, A. Baucom, K. Lieberman, T.N. Earnest, J.H. Cate, and H.F. Noller, 2001. Crystal structure of the ribosome at 5.5 A resolution. Science 292: 883-96.

Zavialov, A.V., and M. Ehrenberg, 2003. Peptidyl-tRNA regulates the GTPase activity of translation factors. Cell 114: 113-22.

Zavialov, A.V., L. Mora, R.H. Buckingham, and M. Ehrenberg, 2002. Release of peptide promoted by the GGQ motif of class 1 release factors regulates the GTPase activity of RF3. Mol Cell 10: 789-98.

Zhang, Y.J., H.F. Tian, and J.F. Wen, 2009. The evolution of YidC/Oxa/Alb3 family in the three domains of life: a phylogenomic analysis. BMC Evol Biol 9: 137.

VI ABBREVIATIONS

A-site	acceptor-site of the ribosome
aa-tRNA	aminoacyl-tRNA
ATP	adenosine triphosphate
C-terminal	carboxy-terminal
cbp	calmodulin-binding peptide
CTF	contrast transfer function
cryo-EM	cryo-electron microscopy
Da	dalton
DDM	dodecylmaltoside
DNA	deoxyribonucleic acid
DTT	dithiothreitol
E-site	exit-site of the ribosome
E. coli	*Escherichia coli*
EF	elongation factor
EDTA	ethylenediaminotetraacetic acid
EGTA	ethylene glycol tetraacetic acid
FRET	Förster resonance energy transfer
FSC	fourier shell correlation
GTP	guanosine triphosphat
HA	hemagglutinin
HEPES	4-(2-hydroxyethyl)-1-piperazineethanesulfonic acid
IF	initiation factor
IMP	inner membrane protein
IPTG	isopropyl-β-D-thiogalactoside
IVT	*in vitro* translation
LMV	large multi-lamellar vesicle
LUV	large unilamellar vesicle
mRNA	messenger ribonucleic acid
MV	membrane vesicles
N-terminal	amino-terminal
OD	optical density
P-site	peptidyl-site of the ribosome

PAGE	polyacrylamide gelelectrophoresis
PCC	protein-conducting channel
PCR	polymerase chain reaction
PMSF	phenylmethylsulfonyl fluoride
PTC	peptidyl transferase center
RF	release factor
RNA	ribonucleic acid
RNC	ribosome nascent chain
RRF	ribosome recycling factor
rRNA	ribosomal ribonucleic acid
RT	room temperature
S	sedimentation coefficient (Svedberg)
SDS	sodium dodecyl sulfate
S. mutans	*Streptococcus mutans*
SNR	signal-to-noise ratio
SRP	signal recognition particle
SUV	small unilamellar vesicle
TAE	Tris-acetate-EDTA buffer
TBS	Tris-buffered saline
TCA	trichlor acetic acid
TM	transmembrane
tRNA	transfer ribonucleic acid

ACKNOWLEDGEMENT

I would like to thank everybody, who supported me during my PhD time and made this work possible:

First of all, I would like to express my deep gratitude to Prof. Dr. Roland Beckmann for giving me the opportunity to be the first female member in his group and to work on fascinating and also challenging projects in an excellent research environment at the Gene Center. I am grateful for his ideas and constant support over the years, for providing great lab equipment and working conditions. Especially, I want to thank him for giving me the opportunity of "assisted living" and continuation of my work during the badly time after my accident.

This PhD work would not have been thinkable without the successful collaboration with Axel Innis in the TnaC project. I am really grateful for this and also want to thank him for sharing his knowledge about RNC preparations. In this context, I would also like to thank Daniel Wilson for his enormous help with TnaC data analysis and preparation of "final" figures. I really enjoyed the collaboration with you, Daniel, especially when we were struggling with the isolation of cryo-EM densities.

I want to thank all members of the Beckmann group not only for their contribution to have a fantastic time in the past four years but also for their indefatigable helpfulness. Especially, I want to thank…Marco for his enormous help with data processing and for keeping our "Brandenburger" dialect alive…Eli and Sole for their patience to answer millions of questions and for their help in the lab and beyond…Jens for being my "lipid" fellow sufferer and for his incredible funny singing interludes which always cheered me up when lab work was too frustrating…Christoph for being my Photoshop-specialist and the only dependable lunch partner…Alex and Jean-Paul for making movies and for their help with computer problems…Thomas for his help with data processing…Andreas for showing me the "Axel-method" of RNC preparation…Heidi and Joanna for keeping the lab up and running and for the nice talks about life in general…Charlotte and Otto for their help and the funny time in front of the microscope, especially when we observed lipid vesicles masked as ticks on the grid…Birgitta for her help and advice and for her support in the hospital at the worst day in my life…Shashi for sharing his knowledge about RNC preparations and for his help.

I want to thank my practical and bachelor students Caro, Sebastian and Andreas for their help in the lab.

I am grateful to Prof. Dr. Andreas Kuhn from the University of Hohenheim and Prof. Dr. Johannes M. Herrmann from the University of Kaiserslautern for providing plasmids used for generation of MscL constructs and purification of *S. mutans* YidC2, respectively. I would also like to thank Stephanie Ravaud from the Sinning laboratory at the University of Heidelberg for providing purified *E. coli* YidC and sharing her knowledge about its purification.

Furthermore, I would also like to thank Thorsten and Jörg from the EM-facility in Berlin for their patience, their help with data collection, for solving problems with the microscope even during the night, and for the nice coffee breaks.

In addition, I want to thank the whole Wilson, Strässer and former Jansen group for creating a nice working atmosphere, for helpful advice and frequent exchange of knowledge and material. Especially, I am grateful to Lina for always being ready to listen.

Schließlich möchte ich mich noch ganz herzlich bei meinen Eltern bedanken, dass sie mich über die vielen Jahre meiner Ausbildung immer unterstützt haben. Vielen Dank, Thomas, dass Du immer für mich da bist. Deine Unterstützung und Liebe haben mir die Kraft gegeben, mein Ziel nie aus den Augen zu verlieren. Danke, dass Du mir das Wertvollste in meinem Leben geschenkt hast, unsere kleine Tochter Colleen.

CURRICULUM VITAE

PERSONAL DATA:

Name	Birgit Seidelt
Date of birth	09.07.1978
Place of birth	Strausberg, Germany
Citizenship	German
Marital status	Single, 1 daughter

EDUCATION:

2006-2010	PhD thesis at the Gene Center of the Ludwig-Maximilians-University Munich in the laboratory of Prof. Dr. Roland Beckmann
2006	Diploma thesis in the laboratory of Dr. Roland Beckmann, Berlin "Untersuchungen am aktiven 70S Ribosom-SecYEG-Komplex"
2001-2006	Studies of Biochemistry, Free University Berlin
1998-2001	Apprenticeship as physiotherapist at the Charité Berlin
1991-1998	Grammar school, Theodor-Fontane Gymnasium, Strausberg

PUBLICATION:

Seidelt, B.*, Innis, C.A.*, Wilson, D.W., Gartmann, M., Armache, J., Villa, E., Trabuco, L.G., Becker, T., Mielke, T., Schulten, K., Steitz, T.A., Beckmann, R. (2009). Structural Insight into Nascent Polypeptide Chain-Mediated Translational Stalling. Science 326: 1412-15. (* These authors contributed equally to this work)